UNIVERSITÀ DI MODENA E REGGIO EMILIA

Dottorato di ricerca in Neuroscienze

in convenzione con l'Università di Parma

Ciclo XXXIV

Neuronal mechanisms for the processing of executed and observed actions in monkey pre-supplementary motor cortex

Candidato: Davide Albertini

Relatore: Prof. Luca Bonini

Coordinatore del Corso di Dottorato: Prof. Michele Zoli

Abstract

The pre-supplementary motor area F6 is thought to contribute to both motor and executive functions, particularly linked with upper limbs, thereby playing a fundamental role in linking cognition and action. Nonetheless, the high number and variety of experimental conditions and tasks with which area F6 has been investigated have prevented reaching a comprehensive understanding of its functional specificities relative to other nodes of the cortical motor system.

To tackle this problem, we investigated the anatomo-functional organization of area F6 with anatomical techniques and neurophysiological approaches previously employed to investigate action execution and observation in other cortical motor areas. In this way, we first demonstrated that F6 shows a gradient of connectional and functional properties along its rostro-caudal axis, suggesting that its heterogeneity may partially account for the plethora of functions ascribed to area F6 as a whole. Next, we comparatively investigated the specific role of F6 relative to other cortical areas involved in action execution and observation. During execution, our findings showed that F6 provides an earlier signal about the upcoming motor actions and reaches earlier its peak of activity relative to other premotor or parietal areas. During observation, it becomes active later and with a greater contribution of suppressed neuronal responses relative to other areas, especially the ventral premotor area F5, which appears to be a leading node in the processing of other's action. Finally, we assessed the specificity for biological actions of action observation responses; we demonstrated that, in area F6 as in other premotor areas, biological and nonbiological observed movements produce highly similar neural dynamics and rely on largely shared neural codes, which in turn remarkably differ from those associated with executed actions.

These findings, together with previous evidence, support the view that largely shared neural mechanisms and substrates underlie the motor processing of objects, contextual cues and observed actions in area F6, suggesting that a basic property of this area consists in a multimodal recruitment of motor representations afforded by a variety of stimuli in the outside world. This unitary and simple coding principle may be shared by a variety of different processes, enabling to explain the manifold of functional properties and roles attributed to F6.

Riassunto

Si ritiene che l'area pre-supplementare motoria F6 contribuisca sia a funzioni motorie che esecutive, legate in particolare agli arti superiori, giocando così un ruolo fondamentale nel collegare cognizione e azione. Tuttavia, l'elevato numero e la varietà delle condizioni e paradigmi sperimentali con cui l'area F6 è stata studiata hanno impedito di raggiungere una comprensione completa delle sue specificità funzionali rispetto ad altri nodi del sistema motorio corticale.

Per affrontare questo problema, abbiamo studiato l'organizzazione anatomo-funzionale dell'area F6 con tecniche anatomiche e approcci neurofisiologici precedentemente impiegati per studiare l'esecuzione e l'osservazione delle azioni in altre aree motorie corticali. In questo modo, abbiamo prima dimostrato che F6 mostra un gradiente di proprietà di connessione e funzionali lungo l'asse rostro-caudale, suggerendo che la sua eterogeneità può parzialmente spiegare la pletora di funzioni attribuite all'area F6 nel suo complesso. Successivamente, abbiamo indagato comparativamente il ruolo specifico di F6 rispetto ad altre aree corticali coinvolte nell'esecuzione e nell'osservazione delle azioni. Durante l'esecuzione, i nostri risultati mostrano come F6 fornisca un segnale precoce sulle prossime azioni motorie e raggiunga prima il suo picco di attività rispetto ad altre aree premotorie o parietali. Durante l'osservazione, si attiva più tardi e con un maggior contributo di risposte neuronali soppresse rispetto ad altre aree, specialmente l'area premotoria ventrale F5, che sembra essere un nodo principale nell'elaborazione dell'azione altrui. Infine, abbiamo valutato la specificità per le azioni biologiche delle risposte di osservazione dell'azione; abbiamo dimostrato che, nell'area F6 come in altre aree premotorie, i movimenti biologici e non biologici osservati producono dinamiche neurali molto simili e si basano su codici neurali ampiamente condivisi, che a loro volta differiscono notevolmente da quelli associati alle azioni eseguite.

Questi risultati, insieme a precedenti evidenze, supportano l'idea che meccanismi e substrati neurali largamente condivisi siano alla base dell'elaborazione motoria di oggetti, segnali contestuali e azioni osservate nell'area F6, suggerendo che una proprietà di base di quest'area consista nel reclutamento multimodale delle rappresentazioni motorie evocate da una varietà di stimoli nel mondo esterno. Questo principio di codifica unitario e semplice può essere condiviso da una varietà di processi diversi, permettendo di spiegare la molteplicità di proprietà funzionali e ruoli attribuiti a F6.

Authors' note

This thesis is based upon three studies published during my PhD:

1) "*Connectional gradients underlie functional transitions in monkey pre-supplementary motor area*", published in *Progress in Neurobiology* in 2020, of which I am co-first author (https://doi.org/10.1016/j.pneurobio.2019.101699).

2) "*Local and system mechanisms for action execution and observation in parietal and premotor cortices*", published in *Current Biology* in 2021, of which I am co-first author (https://doi.org/10.1016/j.cub.2021.04.034).

3) "*Largely shared neural codes for biological and nonbiological observed movements but not for executed actions in monkey premotor areas*", published in *Journal of Neurophysiology* in 2021, of which I am first author (https://doi.org/10.1152/jn.00296.2021).

Please note that, for the sake of readability, the supplementary figures cited in the text are shown in the appendix at the end of the thesis.

Table of Contents

1 GENERAL INTRODUCTION

The pre-supplementary motor area (pre-SMA) of the primates' cerebral cortex lies in the medial wall, rostrally to the primary and supplementary motor areas in the precentral cortex. It is considered to be a premotor region but relative to more caudal premotor areas, it plays a role during complex and more-cognitive situations (see[1]). The manifold situations in which the pre-SMA becomes activated in human fMRI studies[2] have dramatically increased the list of putative functions ascribed to it, making difficult to understand its real functional relevance.

The human pre-SMA corresponds to area F6 of the macaque monkeys([1,3–5], Figure 1.1A), in which unparalleled spatial and temporal resolution provided by single neuron recordings allow us to directly probe the local computational mechanisms and the underlying anatomy. Shedding light on the computational principles of monkey F6 we achieve an additional tool for understanding the likely more complex functions of the human pre-SMA.

1.1 THE PRE-SUPPLEMENTARY MOTOR AREA F6

Cytoarchitectonically, area F6 is defined as an agranular cortex. Nonetheless, it exhibits intermediate features between the strictly agranular supplementary motor area F3, caudally, and the dysgranular prefrontal area 8B, rostrally[6,7]. Receptor-expression maps show that the distribution of AMPA, kainite and oxotremorine receptors exhibit similarly smooth rather than abrupt changes across area F3, F6 and 8B[8].

From the anatomical point of view, it is strongly connected with the other premotor areas[9], especially the rostral ones (Figure 1.1B), but not with the primary motor area F1 and the spinal cord[9,10]. Instead, it exhibits richer connections with the prefrontal cortex, especially the dorsolateral prefrontal area 46[9], with a pattern of prefrontal connections that resembles that of area 8B (see[11]). Area F6 is also tightly linked with area 24 of the cingulate cortex, especially with its rostral part (area 24c, [9,12]). Lastly, despite some connections with area PFG[9], the connectivity with parietal regions is thought to be generally weak and distributed along the inferior and medial part of the parietal lobule. By virtue of its connectivity pattern, area F6 is a hub where information about objects locations, temporal planning of actions, and motivation, is integrated and used for action selection and initiation, thereby playing the previously hypothesized role in linking cognition and action[1].

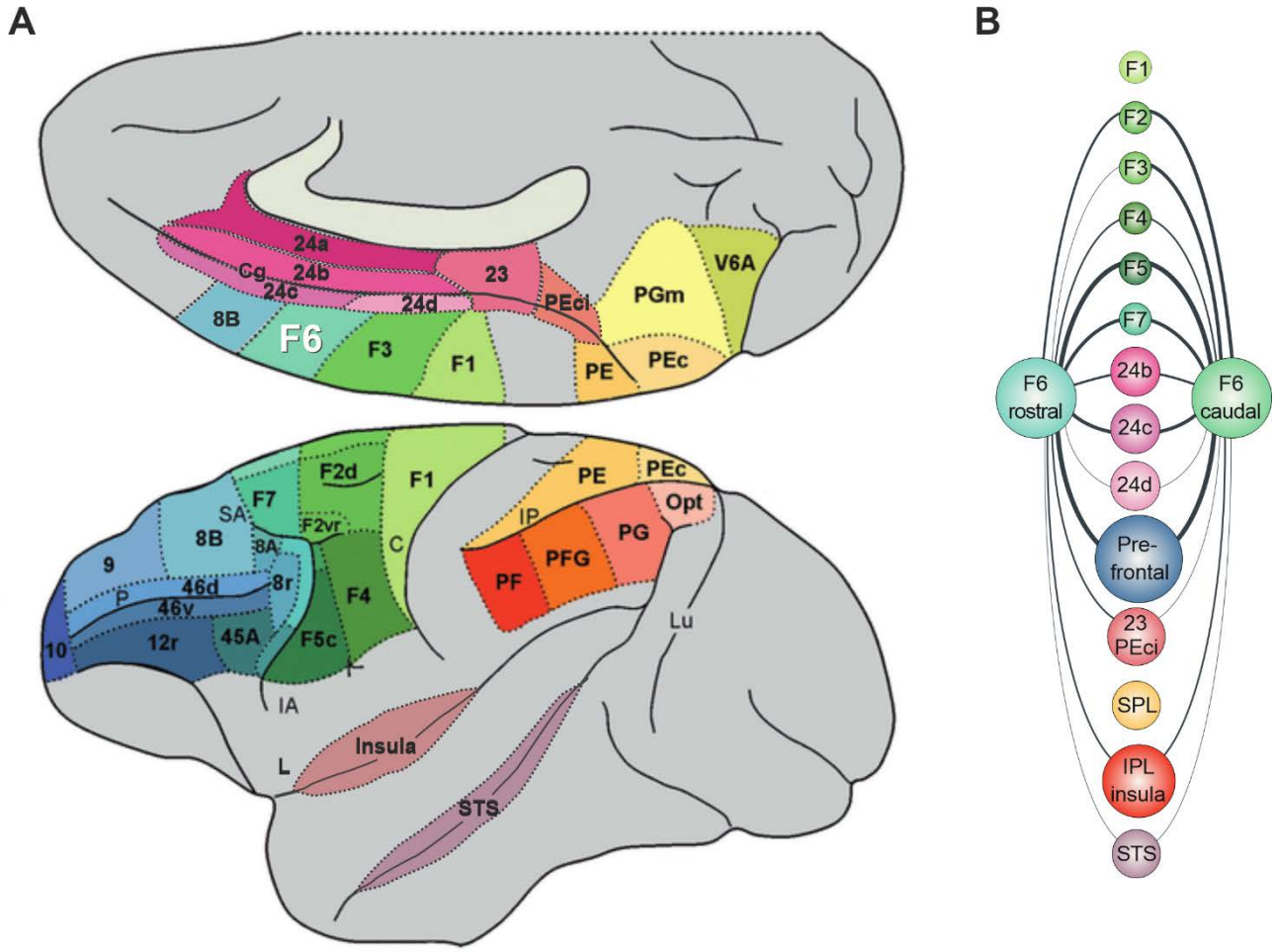

Figure 1.1. Anatomical location and connectivity pattern of area F6. (A) Macaque's brain template showing the anatomical location of area F6 and the surrounding cortical areas. Modified from ref[13]. **(B)** Diagram of cortical connectivity of the rostral and caudal portions of area F6. Modified with permission from ref[1].

1.2 THE FUNCTIONAL PROPERTIES OF AREA F6

The pioneering studies on the functional properties of area F6 primarily assessed its role in movement generation. Unlike other premotor areas, it is difficult to elicit motor responses by electrically stimulating area F6 with standard intensity, and only with higher current some upper limb movements can be evoked([3,14–16], Figure 1.2), consistently with the lack of direct corticospinal connections and of direct projections to F1. The electrically-triggered movements in area F6 are generally slow, complex, and easier to be elicited if the animal was already moving a certain body part. This arm representation in area F6 borders caudally with an oro-facial representation that is on the boundary between cytoarchitectonically and functionally identified areas F6 and F3[3,15,17], the latter being more electrically excitable and directly linked with the primary motor cortex and the

spinal cord. Rostrally, the electrical excitability further decreases, with the ear/eye region of area 8B[18] being even less excitable than area F6[19].

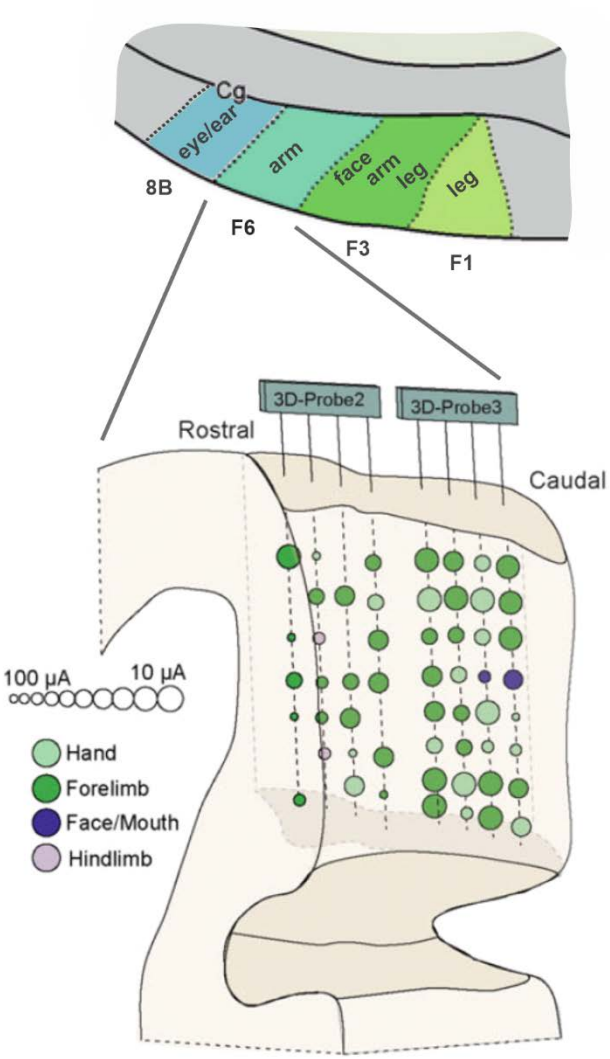

Figure 1.2. Somatotopy and electrical excitability of area F6. Above: schematic of the somatotopy of area F6 and its neighbor areas along the rostro-caudal axis. Modified from ref[13]. Below: thresholds of electrical excitability and nature of evoked movements within area F6. Modified from ref[16]. Differences in both somatotopy and electrical excitability concentrate along the rostro-caudal axis.

At the single neuron level, F6 displays a variety of responses in the plethora of different conditions, from simple passive stimulations to more complex tasks, in which it has been tested. Tanji and colleagues investigated the passive sensory responses of F6 and F3 neurons by moving objects within the monkey's visual field and by touching the monkey in several body parts[20]. Relative to F3 neurons, which showed somatosensory responses when the upper body was stimulated, those of area F6 exhibited virtually no somatosensory response but were generally more often activated by visual stimuli. Similar results were found in another study encompassing area F6 and 8B, where 8B neurons were found unresponsive to both tactile and visual stimulations[19]. Concerning the complex tasks in which the single neuron responses of area F6 have been investigated, these can be grouped into the following categories: those in which the monkey 1) executed single reaching or reaching-grasping movements[4,16,20–22] or 2) executed sequences of actions[15,23,24], 3) estimated time intervals[25–30], 4) switching between movements/rules/tasks[20,31], or 5) engaged in a social interaction[32–35].

During single reach-to-grasp actions, most of F6 neurons become active during the pre-movement phase[4,16,20–22]. Single-neuron and population time-courses indicate that F6 neurons mostly increase their firing rate after the presentation of the target and maintain or progressively

increase their discharge until around movement onset[4,16]. Here, the F6 population activity seems to peak earlier than that of other premotor areas[16], in agreement with a proposed role of F6 in specifying when to act[13]. At the same time, the studies of Bonini and colleagues highlighted that the "visual" activity to presented objects found in area F6 has a strictly pragmatic nature and it is influenced by the possibility of the animal to act on the object. Indeed, if the monkey is instructed not to grasp the object, or the target is presented behind a transparent barrier[16] or located outside the monkey's reaching space[34], the visual response is dramatically lowered. The functional properties of area F6 substantially differ from those of area F3, whose neurons show virtually no discharge at the target presentation and become active only slightly before movement onset. The selectivity for the specific object to be grasped appears to be lower in F6 than in F3[21], although the fraction of object-tuned neurons (26%) is still comparable with that of F5, the premotor area acknowledged to be crucial for grasping (41%[16]). In sum, in the context of reaching-grasping F6 neurons appear to encode "when", "whether" and, to some extent, also "how" to act: visuospatial, contextual, and likely motivational factors might be integrated in this area and if the appropriate conditions are met the movement initiates.

Area F6 seems to play an important role in coding action sequences, both when performed consecutively[15] or separated by a waiting time[23,24,36]. Tanji and colleagues trained monkeys to perform three different instructed movements (push, pull, and turn of a manipulandum) in different orders, and separated by a waiting time. About 40% of the task-related neurons were selective for the specific rank-order (e.g., the third action in the sequence). About 25% of them were selective for the time intervals between the single actions (e.g., a neuron firing selectively after the completion of a pull if this was followed by a turn). Finally, 15% of the neurons were selective for specific sequences (e.g., at the push but only if the sequence was push-pull-turn), or for specific actions (e.g., the push). By contrast, neurons of area F3 in the same task were more selective for the time interval (~40%) but less for the rank-order (~20%), indicating a major commitment of area F6 in the rank-order representation[24]. Concerning the response timing, F6 neurons typically displayed a preparatory activity and an abrupt suppression after movement onset whereas F3 neurons peaked closer to movement onsets, consistent with what we observed for single reach-grasp movements. Furthermore, if F6 (but not F3) is inactivated with muscimol the animal shows a visible impairment in the ability to begin each of the three actions due to a deficit in memory retrieval of the correct sequence, whereas sequences guided by visual cues are executed normally[17].

Hikosaka and coworkers investigated the role of area F6 in the execution of multiple reaching movements directed to different spatial locations[15]. From a panel of 16 LEDs monkeys had to press, in a specific order, 2 of them. When the first sequence ("set") was learned, another sequence was presented until a final "hyperset" formed by five different sets was learned. About 30% of task-related neurons discharged when the monkeys were learning a new sequence and at the beginning of the correct sequence performance but were weakly activated during its execution once the monkeys had mastered the hyperset. In area F3, fewer neurons were task-related (20%) and equally shared between those activated during the learning phase and those activated during the execution of the learned sequence.

Several studies ascribed to area F6 the role of estimating time intervals[25–30]. Tanji and colleagues trained monkeys to determine waiting periods of three different durations (2, 4 or 8 seconds) by pressing and then releasing a key after the corresponding estimated delay[25]. F6 neurons typically showed either an interval-dependent decay of activity starting after the cue onset (37.5% of task-related neurons, Figure 1.3A-C), or an interval-dependent buildup activity starting after the cue onset and culminating just before the key-release (62.5%, Figure 1.3B-D). By contrast, in area F3 task-related neurons activated by the visual cue were virtually absent (3%) and they showed exclusively buildup preparatory activity (97%). In addition, while F3 hosts only neurons whose activity magnitude varied monotonically according to the length of the specified time interval (2s < 4s < 8s or 8s < 4s < 2s), F6 hosted also several neurons modulated by the specific length of the time intervals. Thus, in agreement with a recent study[27], F6 appears to decode temporal information in the form of categorical signals.

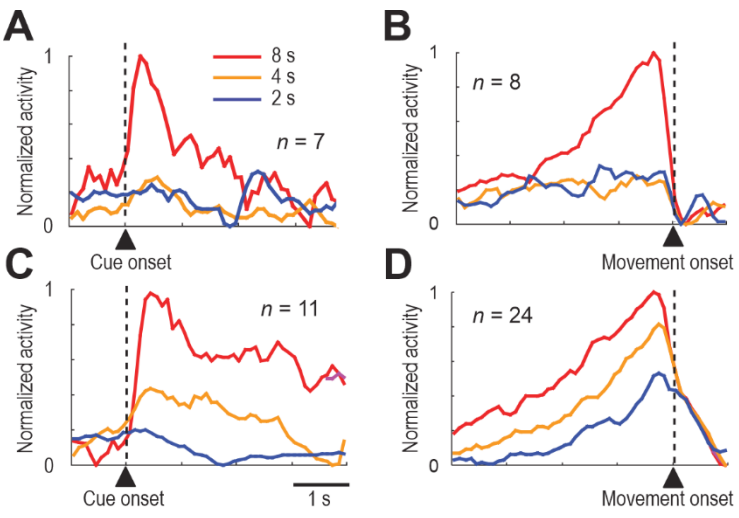

Figure 1.3. Population activity of time-specific and time-graded F6 neurons. (A) Decay activity specific to the 8-s time interval. **(B)** Buildup activity specific to the 8-s time interval. **(C)** Decay activity with magnitude increasing with the corresponding time-interval. **(D)** Buildup activity with magnitudes increasing with the corresponding time-interval. Modified with permission from ref[25].

Merchant and colleagues trained monkeys to press a button repetitively with a constant time

interval between presses that matched the rhythm of a target auditory or visual cue[26,37], whose frequency could be varied. They recorded neural activity from the mesial premotor cortex (encompassing F6 and F3) and found many task-related neurons with a characteristic ramping activity before button press time, which could be further grouped into three categories. One-third of cells were classified as "motor", because they showed a ramping activity starting a fixed time (~400ms) before each button press, independently from the target time interval (Figure 1.4A). Other ramping neurons (~20%), reached their peak of activity at a similar time before button press but exhibited earlier ramp onset for longer time intervals; they were called "relative-timing" cells because they appear to signal how much time is left before button pressing in the task sequence (Figure 1.4B). When the activity is aligned to the previous button press in the sequence, a sizeable group of neurons (~45%) showed an increase followed by a decrease in firing rate, whose amplitude depends on the target time interval; they were called "absolute-timing" neurons because, through the duration of the activation period, they seem to encode the elapsed time since the previous movement (Figure 1.4C). A subgroup of them (~40%), additionally shows an increase in the magnitude of the ramps' peak as a function of target interval and were thus called "time-accumulator" neurons (Figure 1.4D). These findings indicate that the capacity to synchronize with auditory or visual signals and the ability to maintain an internal tempo might depend on neural activity patterns associated with elapsed and remaining time for movement execution.

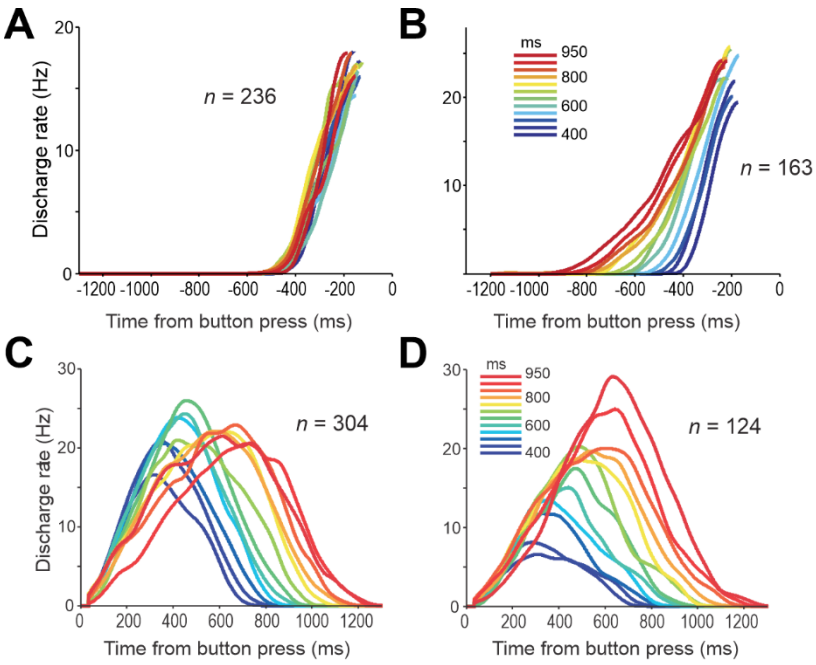

Figure 1.4. Population activity of time-related neurons. (A) Population activity of motor neurons before button press. **(B)** Population activity of relative-timing neurons before button press. **(C)** Population activity of absolute-timing neurons after button press. **(D)** Population activity of time-accumulator neurons after button press. Modified from ref[26].

Globally, the studies discussed so far showed that F6 neurons strongly contribute to the process of retrieving temporal instructions from visual cues, to signal the initiation of action in a time-selective manner, and to track the passing of time.

There is compelling evidence for a role of area F6 in changing hand and eye motor plans or switching between tasks and/or rules[20,31]. In the paradigm devised by Matsuzaka and Tanji[20] monkeys were trained to reach and press either a right or left key, depending on which one was previously illuminated. These standard trials were interleaved with "switch trials" where instead of the illuminated target, a cue sound signaled the animal to press the target which was not pressed in the previous trial. About 30% of task-related neurons of area F6 (and only 7% of area F3) exhibited activity changes after the onset of the auditory cue and before action execution, thus encoding trial switching. Crucially, when these neurons did not fire the monkey subsequently failed to change the reaching direction. In the study of Isoda and Hikosaka[31], monkeys had to gaze at one of two possible targets, located to the left or right of the fixation point, which had the same color of the cue at the fixation point. For several trials the color of the central cue was kept constant, and then it changed unpredictably. About 30% of the recorded F6 neurons showed activity changes ~150ms after central cue onset during switch trials but not during non-switch trials, well within the critical time window available for influencing the behavior (Figure 1.5). Indeed, electrical stimulation of the pre-SMA increased the rejection of the automatic incorrect responses in favor of slower correct responses. In a go/no-go control task, the authors found that switch-related neurons also activated during saccade inhibition or facilitation, in a mechanism that appears to first suppress the automatic unwanted saccade and then boosting the desired action. In support of these findings, a lesion of the medial premotor cortex impairs monkeys' ability to change between two actions, the action rewarded in the previous day (e.g., pulling a handle) and the currently rewarded one (e.g., turning the handle)[38]. Lesioned monkeys took more time to update the action not because they did not know when to move or for motivational factors, but due to the lack of a signal instructing them what action perform.

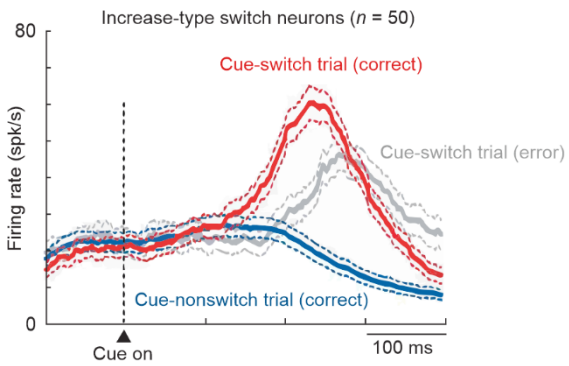

Figure 1.5. Population activity of switch neurons. Population activity (mean ± s.d.) for all increase-type switch neurons (50 out of 55 switch neurons), aligned with cue onset. There was greater discharge when the monkey correctly switched (red trace) than when it made an error and did not switch (grey trace) or during non-switch trials (blue trace). Modified with permission from ref[31].

Thus, area F6 appears to play a crucial role in switching from automatic actions to volitionally controlled actions, necessary for correctly updating learned motor plans to sudden changes.

1.2.1 THE FUNCTIONAL PROPERTIES OF F6 IN ACTION EXECUTION AND OBSERVATION

The involvement of area F6 in coordinating social interactions have been investigated relatively recently. The seminal work of Isoda and colleagues[32] reported the existence of neurons (11% of the recorded ones) firing both when the monkey reaches one of two possible targets and when it observes another monkey performing the same task, thus satisfying the definition of "mirror neurons"[39]. In addition, an even larger population of neurons responded selectively for the other's action (16%), with one third of them also selective for the target position during action observation. Similar results were found by Genovesio and colleagues, who reported that 22% of F6 neurons selectively encode the target position of a reaching performed by another agent even before the actual movement was performed, and another 10% encoded the target position in both execution and observation trials[35]. In comparison, area 8B hosted more neurons encoding other's target position, whereas F3 hosted more neurons selectively encoding self's target position[35]. Along the same line, a recent work of Bonini and coworkers[34] investigated the properties of F6 neurons during the execution of reaching-grasping actions and the observation of other's action, classifying neurons as self-type, other-type, and self/other type (Figure 1.6A). Next, the authors assessed the decoding accuracy of the Go/No-Go condition and target object type in a time-resolved manner using the activity of the whole neuronal population, from the target presentation to the self/other's action execution phases (Figure 1.6B). They found that the neural responses elicited by the presentation of the target object are mostly shared between self and other whereas during the movement phase the neural responses associated with self's action and other's action differ substantially (Figure 1.6B). In an additional condition where monkeys observe an action performed in their extrapersonal space, the self-other similarity further decreases[34]. In sum, these studies indicate that, besides playing a role in executing one's own actions, area F6 is also critically involved in the representation of other's actions and their targets, which may be crucial for effective social interactions.

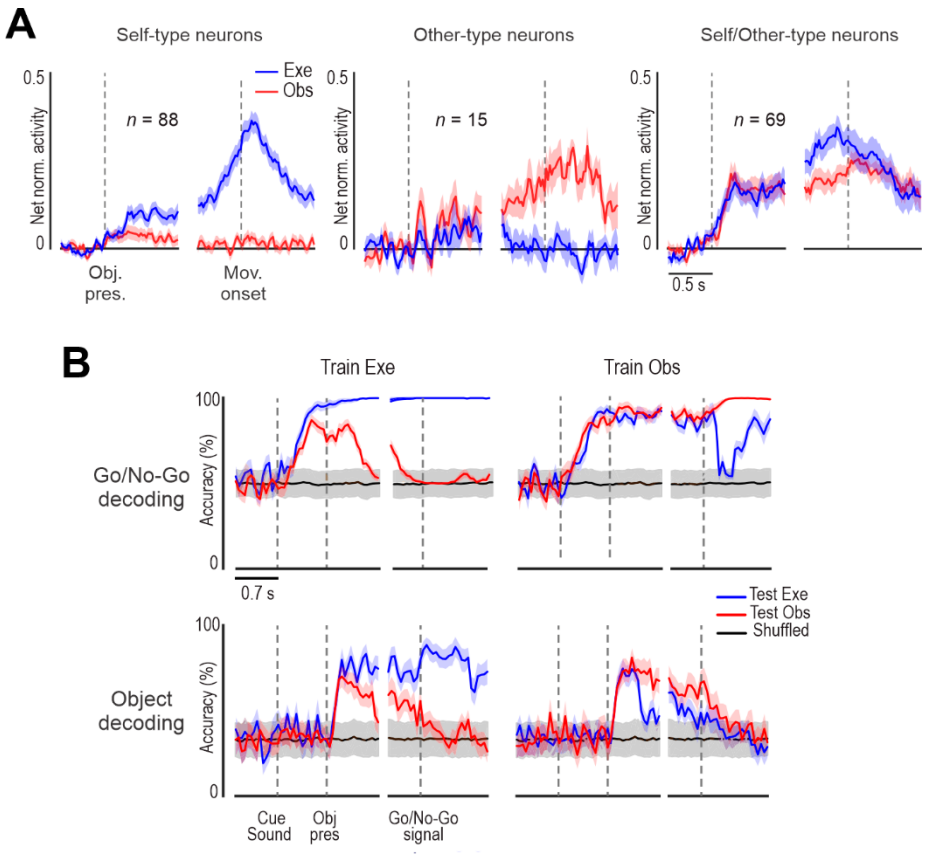

Figure 1.6. Population activity and self-other generalization during execution and observation. (A) Population activity of neurons modulated by one's own action (Self-type neurons), by the other's action (Other-type neurons), or both (Self/Other-type neurons). **(B)** Above: Go/No-Go classification accuracy during execution and observation tasks using the whole neuronal dataset. The decoder generalizes well only during the object presentation phase, whereas it does not during the movement phase. Below: Object classification accuracy during execution and observation tasks. The decoder generalizes during the object presentation phase, whereas its performance decays as one approaches the movement phase. Modified from ref[34].

The functional heterogeneity described so far should make it clear that we are still far from a comprehensive understanding of the fundamental neural mechanisms underlying F6 functioning. In this respect, we identified three main gaps in the current knowledge: first, looking for a unique computational principle capable to explain all the putative functions ascribed to F6 might lead to a dead end, because there may exist gradual functional changes along F6 which could account for the plethora of functions ascribed to it[1]; we followed this line and probed the functional and anatomical properties of area F6 along its rostro-caudal axis, which has been shown to be the direction of the largest changes in electrical excitability and somatotopy transitions[16,17,24].

A second gap involves the paucity of works comparing the neural properties of F6 with those of other anatomically-connected areas with the same set of tasks, which is crucial to identify the specific contribution of each node to the investigated function. We tackled this issues by comparing

the functional properties of area F6 with those of the ventral premotor area F5 and of the anterior intraparietal area (AIP), two cortical areas known to be involved in processing executed and observed actions[40,41].

Third, the apparent plurality of F6 functions may in fact reflect a plurality of aspects shared by a single function; for instance, the evidence that the same neurons in the pre-SMA reflect both task switching and response inhibition/facilitation[31] might indicate that some apparently different functions could rely on the same computational principle[1]. We applied this line of thought to our data and assessed whether action observation responses exhibited by area F6 are in fact specific for biological actions or if, instead, both biological and nonbiological observed actions recruit the same neural codes.

2 CONNECTIONAL GRADIENTS UNDERLIE FUNCTIONAL TRANSITIONS IN MONKEY PRE-SUPPLEMENTARY MOTOR AREA

The pre-supplementary motor area F6 is involved in a variety of functions in multiple domains, from planning/withholding goal-directed actions in space to rule-based cognitive processes and social interactions. Yet, the neural machinery underlying this functional heterogeneity remains unclear. Here, we measured local population dynamics in different rostro-caudal sites of cytoarchitectonically verified area F6 in two monkeys during spatial, contextual, and motor processes, both in individual and social conditions. Then, we correlated multimodal population tuning with local anatomical connectivity revealed by neural tracer injections into the functionally characterized sites. We found stronger tuning for object position relative to the monkey in the rostral portion of area F6 than in its caudal part, which in turn exhibits stronger tuning to self and other's (observed) action. Functional specificities were associated with a rostro-caudal transition in connectivity strength from lateral prefrontal cortex, pregenual anterior cingulate cortex and associative striatum (rostrally), to dorso-ventral premotor areas and the motor putamen (caudally). These findings suggest that the functional heterogeneity of the pre-supplementary area F6 is accounted for by gradual transitions in functional properties grounded on local cortico-cortical and cortico-striatal connectional specificities.

2.1 INTRODUCTION

The pre-SMA (called F6 in the monkey, see[3,7]) lies in the mesial wall of the cerebral hemispheres, rostrally to the supplementary motor area[4,5]. It receives inputs from prefrontal and cingulate cortex and sends projections to parieto-dependent areas of the dorsal and ventral premotor cortex[42–44], hence being optimally placed for "linking cognition to action"[1], and to act as a hub for processes related with motor intentionality[45]. Its involvement in a so wide set of functions, ranging from planning of goal-directed actions in space to rule-based cognitive processes and social interactions, makes it "the most frequently activated region" in human brain imaging studies[2].

Indeed, pioneering neurophysiological studies with ethological techniques in the monkey suggested that area F6 plays a role in the preparation of reaching–grasping arm movements and in their release when appropriate conditions are set[21]. Subsequent studies showed that this area is also involved in higher-order control[31,46], including updating of motor plans[23], selecting effector-independent actions[47], organizing and learning complex motor sequences[36,48], and planning or controlling reaching-grasping actions[16]. Recent studies also indicate that F6 plays a role in social

behavior and is part of a brain network dedicated to the processing of social interactions[49]. In this regard, single neuron evidence indicates that F6 neurons can exhibit remarkable selectivity for self- and/or others' actions[32,34], others' future choices[35], and even for observed objects depending on whether they constitute potential targets for self and/or others' action[34]. In the light of these findings, it should not be surprising that the neural mechanisms underlying the functional heterogeneity of the pre-supplementary motor cortex remain largely unclear. Nonetheless, two main hypotheses have been proposed concerning its anatomo-functional organization: 1) F6 is a unitary, essentially homogeneous, anatomo-functional area (e.g.[44]), which underlies a specific but still unclear functional signature, or 2) it indexes a variety of functional properties linked with gradual rostro-caudal transitions in local connectional specificities[1].

In the present study, we addressed these questions by combining neurophysiological and neuroanatomical techniques in macaque monkeys. First, we characterized local population dynamics in different rostro-caudal sites of area F6 in two monkeys using a large set of tasks and conditions recently employed in separate single neuron experiments[16,34]. We found stronger tuning of rostral area F6 to the distance of target objects from the monkey relative to the caudal one, which in turn exhibits stronger tuning to one's own executed action and to observed actions performed by others. Then, we injected neural tracers into each functionally characterized site, revealing a rostro-caudal transition in connectivity strength with lateral prefrontal, pregenual anterior cingulate cortex and striatum/anterior putamen preferentially linked with rostral area F6, whereas dorso-ventral premotor areas and the caudal putamen mostly connected with its caudal part. Our findings favor the idea that area F6 indexes a multiplicity of functions by gradual transitions in local connectional specificities rather than subserving a unique and homogeneous functional signature.

2.2 METHODS

Experiments were carried out on two purpose-bred, socially housed male macaque monkeys (Mk1, Macaca nemestrina, 9 kg, and Mk2, Macaca mulatta, 7 kg). Before recordings, monkeys were habituated to sit in a primate chair and to interact with the experimenters. Then, they were trained to perform the visuomotor tasks described below using the hand contralateral to the hemisphere to be recorded. When the training was completed, a head fixation system was implanted under general anesthesia (ketamine hydrochloride, 5 mg/kg, i.m., and medetomidine hydrochloride, 0.1 mg/kg, i.m.), followed by postsurgical pain medications (see[50] for details). Two arrays of linear silicon probes

were implanted in area F6 of each monkey at two different antero-posterior positions of the left (Mk1) or right (Mk2) hemisphere. At the end of the recordings, the probes were removed and antero-retrograde neural tracers were injected, in correspondence with the position previously occupied by each of the explanted probes. All experimental protocols complied with the European law on the humane care and use of laboratory animals (directives 86/609/EEC, 2003/65/CE, and 2010/63/EU), were authorized by the Italian Ministry of Health (D.M. 294/2012-C, 11/12/2012 and 48/2016-PR, 20/01/2016), and were approved by the Veterinarian Animal Care and Use Committee of the University of Parma (Prot. 78/12, 17/07/2012 and Prot. 91/OPBA/2015).

Apparatus and behavioral paradigm

Both monkeys were trained to perform an Execution task (Fig 1A, EXE) as well as to observe the same task performed by an experimenter in their peripersonal (Fig. 1A, OBSp) and extrapersonal (Fig. 1A, OBSe) space. These tasks have been described in details in previous works (see[16,34]).

Briefly, during EXE, the monkey was seated on a primate chair in front of a box, divided horizontally into 2 sectors by a half-mirror where a spot of light (fixation point) was projected in the exact position of the center of mass of the not-yet-visible target object. The objects (a ring, a small cone, and a big cone) afforded three different grip types (hook grip, side grip, whole-hand prehension). They were presented randomly, one at a time, at a reaching distance from monkey's hand starting position. The task included two basic conditions (Go and No-Go), and each trial was preceded by a variable (from 1 to 1.5 s) inter-trial period.

1. *Go condition* (Figure 2.1B). The fixation point was presented and the monkey was required to start fixating it within 1.2 s. Fixation onset resulted in the presentation of a cue sound (high tone, 1200 Hz), which instructed the monkey to grasp the subsequently presented object (Go cue). After 0.8 s one of the objects became visible. Then, after a variable time lag (0.8–1.2 s), the sound ceased (Go signal), and the monkey had to reach, grasp, and pull (for 0.8 s) the object within 1.2 s to get a fixed amount of juice reward (automatically delivered). During another set of trials (grasping in the dark) the light was switched off automatically with the Go signal and the monkey performed the action in complete darkness.
2. *No-Go condition* (Figure 2.1B). The sequence of task events in this condition was the same as in the Go condition but a different cue sound (low tone, 300 Hz) instructed the monkey to remain still and fixate the object for 1.2 s in order to receive the reward.

The same sequence of events described for EXE also applied to OBSp and OBSe. The task phases were automatically controlled and monitored by LabView-based software, enabling the interruption of the trial if the monkey broke fixation, made an incorrect movement, or did not respect the task temporal constraints. In all these cases, no reward was delivered. Failed trials were repeated until at 10 trials were collected for each condition.

Recording Techniques

Neuronal recordings were obtained from 4 multi-shaft 3D arrays of linear silicon probes with 8 recording sites per shaft and 2 parallel modules of 4 shafts per probe (64 channels per probe). The recording sites were spaced by 500 µm, along the 8 mm shank with a rectangular section of 80 µm (width) x 100 µm (thick). Each shaft was spaced by 550 µm from the adjacent one, and each 4-shaft module was spaced apart from the other by 350 µm (see Figure 7 in[51]). These probes were implanted for previous studies[16,34], and details on the methodology of probe fabrication, assembly and implantation have been described elsewhere[52–54]. The signal was amplified and sampled at 40 kHz with a 16-channel Omniplex recording system (Plexon). Different sets of 16 channels were recorded only one time during separate sessions in different days. All signal analyses were performed off-line with fully automated software (MountainSort[55], available online at *https://github.com/magland/mountainlab*), considering both single- and multi-unit activity (referred to as "units", see[56] for details on spike sorting procedures). Furthermore, to exclude that possible artifacts were counted as spikes, we automatically inspected all waveforms of all isolated units and retained, for each one, only those waveforms that did not exceed ±3 SD from the average waveform in all data points (for each unit, about 10% of the spikes were removed in this procedure).

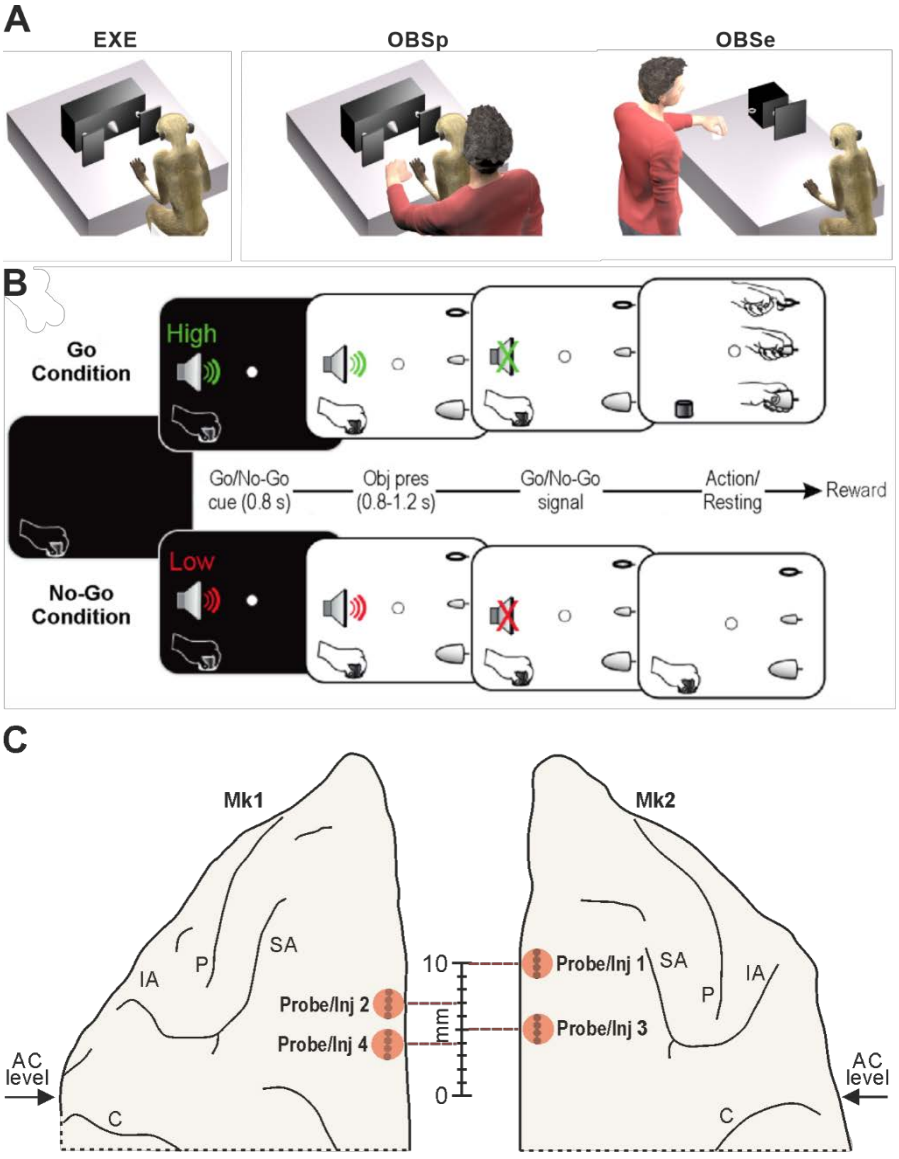

Figure 2.1. Behavioral tasks and investigated regions. (A) Schematic representation of the three tasks: execution (EXE), observation in the monkey's peripersonal (OBSp) and extrapersonal (OBSe) space. **(B)** Temporal sequence of task events. **(C)** Recorded and injected sites. The gray dots illustrate the anatomical location of each probe's shafts and the red shaded circles indicate the location of the core of injection sites relative to the implanted probes. Anatomical position of the injections is defined relative to their distance from the anterior commissure (AC). The scale of Mk2 applies also to Mk1. Abbreviations: C, central sulcus; IA, inferior arcuate sulcus; P, principal sulcus; SA, superior arcuate sulcus.

Recording of behavioral events and definition of the epochs of interest

Contact sensitive devices (Crist Instruments) were used to detect when the monkey (grounded) touched the metal surface of the starting position or one of the target objects. To signal the onset and tonic phase of object pulling, an additional device was connected to the switch located behind each object. Custom-made LabView-based software was used to monitor the monkey's performance and to control the presentation of auditory and visual cues (see for details[57]). Eye position was monitored in parallel with neuronal activity with an eye tracking system[34]: the monkey was required to maintain its gaze on the fixation point (tolerance radius 5°) throughout the task. Off-line analysis of electromyographic activity of proximal and distal forelimb muscles during EXE, OBSp and OBSe has been previously described in both monkeys[34], and allowed us to exclude the possible presence of preparatory motor activity during No-Go trials, observation trials and baseline epochs.

Based on the available events and leveraging the same structure shared by all tasks, we focused the analyses on 4 main epochs, identical across tasks: 1) baseline (500 ms before cue sound onset), 2) cue sound (from 100 to 600 ms after sound onset), 3) object presentation (from 100 to 600 ms after light onset) and 4) Go/No-Go signal (from the end of the cue sound to 1000 ms after this event).

Analyses of the neuronal activity

Sliding window ANOVA

The spiking activity of each unit in all the available trials was compared across conditions (Go/No-Go, objects, Light/Dark) with one-way repeated measures ANOVAs ($p < 0.05$, uncorrected) in 200 ms bins, advanced in steps of 20 ms for the entire period of interest relative to 1) object presentation (from -1300 to 700 ms) and 2) Go/No-Go signal (from -300 to 1200 ms). In the analyses of Go/No-Go and light/dark conditions the trials with the different objects were collapsed, whereas in the analyses of object tuning ANOVAs were carried out within Go and No-Go conditions, separately. The bin-by-bin percentage of significantly tuned units was smoothed with a 60 ms Gaussian kernel to improve visualization. To identify when and for how long the percentage of tuned units was different between subpopulations (rostro-caudal or dorso-ventral) in each monkey, we used bin-by-bin sliding chi-square tests ($p < 0.05$, uncorrected).

Principal Component Analysis (PCA)

Trial-averaged firing rates of each unit were calculated from -1800 to +1600 ms relative to Go/No-Go signal for all conditions and tasks. The spiking activity was first binned in 20 ms time windows and the resulting firing rates were subsequently smoothed with a 200 ms Gaussian kernel. Then, for each unit, the smoothed firing rates were first divided by the maximum firing rate across all conditions and tasks, and then the overall average firing rate was subtracted bin-by-bin to obtain the normalized firing rate. After this pre-processing, we considered the normalized firing rates as an *N*-dimensional neural population state space. Since the amplitude of a generic population vector with respect to any arbitrary baseline grows as $\sqrt{N}$ (the mean line segment length in an *N*-dimensional cube grows as $\sqrt{N}$, see[58]), we normalized each firing rate dividing it for $\sqrt{N}$ to compare reliably PCA projections of different subpopulations even if they were made up of a different number of units. Then, PCA was performed including all conditions (i.e. Go/No-Go, object, light/dark) and tasks (EXE, OBSp, OBSe). For each condition and in each task, we then projected the corresponding full-dimensional neural trajectory onto the plane of the first two PCs (the projections of different objects were remarkably

similar and were thus averaged) obtaining a two-dimensional curve that describes the evolution of the population state along the trial for that particular task and condition. To mark the time corresponding to specific task events (i.e. start of trial, object presentation, Go/No-Go signal, pulling, reward) along the trajectories, we calculated their mean time relative to the Go/No-Go signal of each condition.

Hierarchical cluster analysis

To evidence the possible relationship among neural representation of tasks and conditions we performed a hierarchical cluster analysis. Given a certain neural population of N units, firing rates of all units were calculated binning the spiking activity and averaging it across trials. We created a firing rate matrix F with N rows and $c \cdot t$ columns (where c is the number of conditions and t the number of time points per condition within the epoch of interest). Then, we computed the Mahalanobis linkage distances (Matlab function: manova1) between the activities in the N-dimensional state space of all possible pairs of conditions in the epoch of interest. Since the Mahalanobis distance between any pair of arbitrarily selected conditions increases linearly as a function of the number of units in the population (see Figure S2.1), the resulting matrix of distances was normalized dividing it by N. Finally, normalized distance matrix was used to create a hierarchical cluster tree based on the average linkage criterion (Matlab function: manovacluster), presenting the cluster solutions in the form of dendrograms. While building the dendrograms, we sorted the leafs within a branch on the basis of their average distance to nearest branches (Matlab function: optimalleaforder).

Measures of local relevance of functional properties

To isolate and quantify the rostro-caudal functional changes within F6, we computed the Mahalanobis distance in the neural state space of each probe between all levels of specific factors in selected epochs. Specifically, we considered the factors 1) task context, 2) Go/No-Go and 3) Object/grip. Out of the 27 resulting combinations (see Figure S2.6), seven of them allowed us to isolate specific "functional dimensions", as follows.

1. *Object position*. Mahalanobis distance between EXE and OBSe (regardless of the type of object and Go/No-Go condition), during object presentation epoch. Note that a similar measure could be obtained by contrasting OBSp (where, however, another agent is present close to the monkey) and OBSe, which indeed produce similar results (Figure S2.6).

2. *Experimenter position*. Mahalanobis distance between OBSp and OBSe during baseline, when the monkey is aware of the presence of another agent located either far from or near it but no other confound is present.
3. *Agent*. Mahalanobis distance between EXE and OBSp (involving the same space sector) during baseline (no additional confound), when the monkey knows who will act because the tasks are run in blocks.
4. *Object/Grip*. Mahalanobis distance between all possible pairs of objects (averaged) in the Go condition of EXE during the period ranging from object presentation to the end of the Go/No-Go signal epoch.
5. *Go/No-Go condition in OBSe*. Mahalanobis distance between Go and No-Go conditions in OBSe during Go/No-Go signal epoch, when the observed action occurs.
6. *Go/No-Go condition in OBSp*. Mahalanobis distance between Go and No-Go conditions in OBSp during Go/No-Go signal epoch, when the observed action occurs.
7. *Go/No-Go condition in EXE*. Mahalanobis distance between Go and No-Go conditions in EXE during Go/No-Go signal epoch, when the action is performed.

To test statistically the significance of observed rostro-caudal differences in the selected functional dimensions we applied a subsampling procedure. For each dimension, we randomly subsampled without replacement the *N* units recorded from each probe by selecting $M=N^{2/3}$ units and re-calculating the Mahalanobis distance on this data set: we run this procedure 1000 times and calculated the standard deviation (multiplied by $\sqrt{M/N}$ in order to consider the different size of the subsample with respect to the whole population) of the resulting distribution, taken as standard error. Finally, to test whether the Mahalanobis distances associated to a given functional dimension differed across probes, we applied two-tails Z-tests comparing all pairs of probes.

Tracers' injections and histological procedures

At the end of the recordings, the two probes implanted in each animal were removed and an antero-retrograde neural tracer was injected at the center of the spot previously occupied by each explanted probe. During a surgery under anesthesia (Ketamine, 5mg/kg i.m. and Medetomidine, 0.08–0.1 mg/kg i.m.), neural tracers were slowly pressure injected at the desired depth through a Hamilton microsyringe (Reno, NV, USA). In the left hemisphere of Mk1 we injected Colera Toxin Subunit B conjugated with Alexa 488 (CTB-g, 1% in phosphate-buffered saline; Molecular Probes) and dextran

conjugated with tetramethylrhodamine (Fluoro-Ruby, [FR], 10000 MW, 10% in 0.1 M phosphate buffer, pH 7.4; Invitrogen-Molecular Probes). In the right hemisphere of Mk2 we injected dextran conjugated with lucifer yellow (Lucifer Yellow Dextrane [LYD], 10000 MW, 10% in 0.1 M phosphate buffer, pH 7.4; Life Technologies) and FR. After an appropriate survival period for tracer's transport (about 14-21 days), each animal was deeply anesthetized with an overdose of sodium thiopental and perfused through the left cardiac ventricle with saline, 3.5% paraformaldehyde, and 5% glycerol in this order, prepared in phosphate buffer 0.1 M, pH 7.4. Each brain was then blocked coronally on a stereotaxic apparatus, removed from the skull, photographed, and placed in 10% buffered glycerol for 4 days. Finally, each brain was cut frozen into coronal sections of 60 µm thickness and one section of each five was processed to visualize CTB-g, LYD, and FR using the following labeling protocol. After inactivation by the endogenous peroxidase (methanol: hydrogenperoxide = 4:1), selected sections were incubated for 72 h at 4°C in a primary antibody solution (0.3% Triton and 5% normal goat serum in phosphate buffer solution [PBS]) of rabbit anti-FR or rabbit anti-LY (1:3000; Life Technologies) or rabbit anti-Alexa 488 (1:15000, Life Technologies). Then, they were incubated for 1 h in biotinylated secondary antibody solution (1:200, Vector Laboratories, Burlingame, CA, USA; 0.3% Triton and 5% normal goat serum in PBS). Finally, CTB-g, LYD, and FR labeling was visualized using the Vectastain ABC kit (Vector) and the Vector SG peroxidase substrate kit (SK-4700, Vector) or 3,3'-diaminobenzidine (DAB) as a chromogen. In this latter case the reaction product was intensified with cobalt chloride and nickel ammonium sulfate. For both monkeys, one section of each five was stained using the Nissl method (thionin, 0.1% in 0.1M acetate buffer, ph 3.7).

The locations of the electrode tracks and of the injection sites were assessed under an optical microscope in Nissl-stained sections and then plotted and digitized together with the outer and inner borders of the cerebral cortex using a computer-based charting system (for the details of the procedure, see[32]). The antero-posterior locations of the probes are defined relative to their distance from the anterior commissure (AC) and have been numbered from 1 to 4: the same numbering was adopted to classify the corresponding injection (Figure 2.1C). The histologically identified location of the probes is shown on photomicrographs of each injected hemisphere (Figure S2.2 and S2.3).

Identification and quantification of cortico-cortical and cortico-striatal labeled neurons

The distribution of retrograde cortical labeling was plotted and counted in sections spaced 600 µm apart from each other, together with the outer and inner cortical borders, using the afore mentioned computer based charting system. Data from individual sections were also imported into dedicated

software allowing us to create 3D reconstructions of the hemispheres from individual histological sections containing labeled cells. The criteria and maps adopted for attributing the labeling to different brain regions were the same adopted in previous studies (for details see[56,59]). Concerning cortico-cortical projections, we counted all the labeled cells excluding those of area F6 and expressed the cortical afferents to the injected spot of F6 in terms of percentage of labeled neurons found in a given cortical region relative to the total number of labeled cells. Statistical analysis was performed with a chi-square test, comparing the number of neurons observed in each anatomical territory with the value expected if the proportion of observed neurons was uniform across injections at different antero-posterior positions. In addition, to identify the injections-territory combinations mostly contributing to the effect, we computed the adjusted standardized cell residuals (see Table S1).

The projections to the striatum are typically organized in patches of very dense labeled terminals, surrounded by less densely labeled zones: these were designated as "focal" and "diffuse" projections, respectively[60]. The striatal projections were clearly visible even at relatively low magnification under bright field illumination. Thus, to obtain faithful reproductions of the labeling distribution, the projections were visualized by extracting the labeling from digitalized photographs taken with a ×10 objective (see[61–63]. Specifically, using Adobe Photoshop (Adobe Systems Incorporated, San Jose, CA, USA) the outlines of the basal ganglia and of adjacent structures were delineated in each photograph on a separate layer. Then, striatal projection fields were selected and converted into a black-and-white image applying a threshold appropriate to extract the labeling, stained in black or blue, from the lighter background. Comparison with the original image ensured that the labeling was accurately extracted and no false positives were included in the image (for further details of this procedure see Figure 2 of[61]). For a quantitative assessment of the focal projections in the striatum we subdivided it in three different territories: the caudate, the anterior putamen (i.e. the sector anterior to the AC, also designated as "associative" putamen) and the posterior putamen (i.e. the sector posterior to the AC, also designated as "skeletomotor" putamen). Then, we quantified the density of the focal projections in each of these three striatal subdivisions as follows. We quantified the surface of the striatum labeled by focal projections in sections spaced 900 µm, using the measure function of the Nis-element software (Nikon Instruments Inc.). Then, we expressed the density of the focal projections in the anterior putamen, the motor putamen, and the caudate as a percentage of the surface labeled in each of these subdivisions relative to the total striatal surface labeled.

2.3 RESULTS

Neuronal activity was recorded from four cortical sites at distinct rostro-caudal positions along area F6 of the two monkeys (Figure 2.1C), spanning the entire extent of the cytoarchitectonically verified area F6 (Figure S2.2 and S2.3). We extracted both multi- and single unit activity, here defined as "units" (see Methods) and used all of them in order to better approximate the unbiased sampling of the tracing study subsequently performed on the physiologically characterized sites. We isolated 291 units, of which 100 (34.4%) were classified as single units.

Non-uniform distribution of neuronal tuning properties along the rostro-caudal extent of F6

We isolated 112 units from probe 1 (of which 39 single units), 49 from probe 2 (19 single units), 82 from probe 3 (24 single units) and 48 from probe 4 (18 single units), with a similar percentage of single units isolated from each probe (ranging from 29.3% in probe 3 to 38.8% in probe 2). Then, we compared rostral and caudal subpopulations in each monkey focusing on the factors most prominently represented in the whole data set (Figure S2.4A), namely: Go/No-Go condition, task context (EXE, OBSp, OBSe) and task epoch (baseline, cue sound, object presentation, Go/No-Go signal).

Time-resolved repeated measures ANOVA (Figure 2.2) revealed that, in both monkeys, the caudal probes show the strongest Go/No-Go tuning in EXE and, in case of Mk2, even in OBSp and OBSe. It is worth to note that units recorded from all probes in both monkeys display different Go/No-Go tuning during the cue period (from cue sound onset to the Go/No-Go signal), with greater tuning in OBSp than in OBSe, particularly in Mk1. Furthermore, the percentage of tuned units progressively increases from baseline to action execution epoch in EXE and OBSp throughout the entire task-unfolding period, especially at the most caudal probe of Mk1. Similarly, object tuning (Figure S2.4B) is slightly stronger and more sustained from visual presentation of the target to Go-signal at the caudal probe of Mk1, but it is constrained to the monkey's peripersonal space, as it is absent in OBSe. Importantly, the above described differences appear to be specific for the rostro-caudal direction: indeed, when comparing the tuning properties of the same units grouped based on their dorsal/ventral location (regardless of their rostro-caudal position), we did not find any relevant difference (Figure S2.4C).

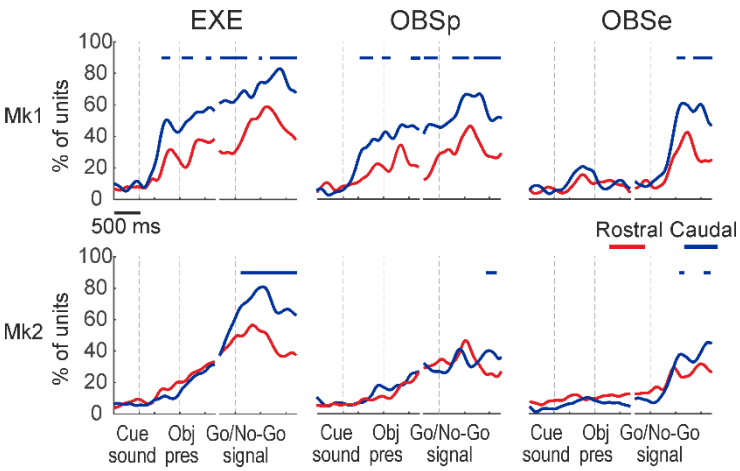

Figure 2.2. Tuning properties of units recorded from probes located in different rostro-caudal positions in area F6. Percentage of units with significant tuning for Go/No-Go condition in (from left to right) EXE, OBSp and OBSe. The percentage is expressed relative to the total number of units recorded from the rostral and the caudal probe within each monkey. Colored lines above each plot indicate the time bins where the fraction of tuned units is significantly different between the rostral and the caudal probe (χ^2 $p < 0.05$, uncorrected).

Next, we directly investigated the neural population dynamics underlying the encoding of task- and/or condition-specific features in F6 by considering the firing rates of all units recorded from each probe as an *N*-dimensional neural state space and performing PCA over these firing rates (see Material and Methods). For each task and condition, we projected the corresponding *N*-dimensional (trial-averaged) neural trajectory onto the plane of the first two PCs, which accounted for a percentage of total variance ranging from 34.7% (probe 2) to 47.8% (probe 3). The resulting two-dimensional trajectories for each probe (Figure 2.3) progress from the start of the trial (colored dots), through object presentation (light bulb), Go/No-Go signal (speaker), object pulling (human and monkey hands) and final reward (blue drop). The starting points and initial trajectories associated with different tasks appear to be clustered differently along the rostro-caudal axis, with greater similarity between EXE and OBSp relative to OBSe, rostrally, and the two OBS tasks relative to EXE, caudally (see Figure 2.5 for statistical comparisons). These initial states are followed by two trends emerging during task unfolding in the subpopulations' dynamics along the rostro-caudal axis, which are consistent in both monkeys: 1) an increase in the amplitude of EXE and 2) an increased similarity between the trajectories of the two OBS conditions.

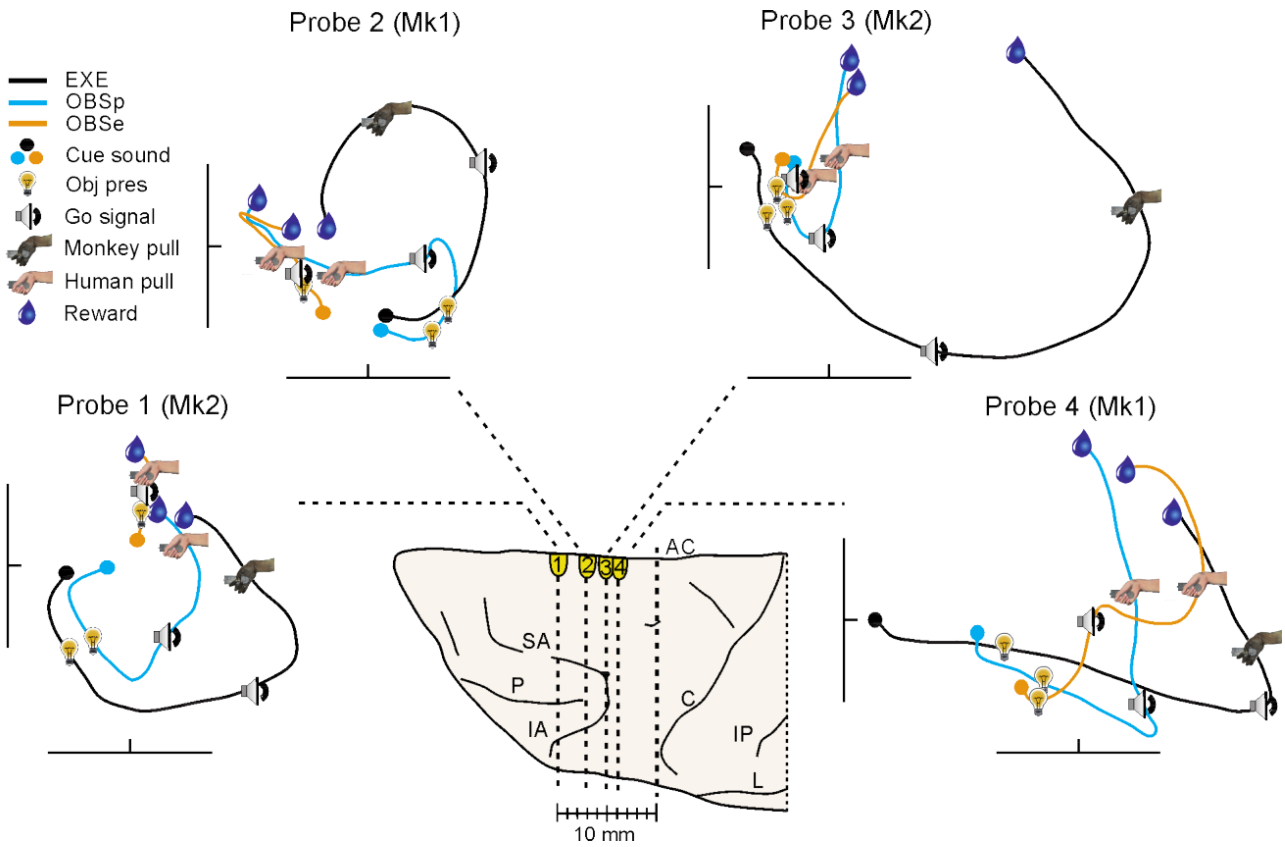

Figure 2.3. Local population dynamics along the rostro-caudal extent of area F6. Projection of the neural population response (object averaged) of each probe in the plane defined by the first two principal components during tasks unfolding in the Go conditions of EXE, OBSp and OBSe (see Figure S2.5 for analysis of No-Go and grasping-in-the-dark conditions). Each trace represents the projection of the full trial-length activity aligned to Go/No-Go signal. Symbols identify the averaged position of task events along the trial. L, lateral sulcus; IP, intraparietal sulcus; other abbreviations as in Figure 2.1.

Finally, we performed a hierarchical cluster analysis by computing the Mahalanobis distances (see Methods) between each pair of conditions of interest (Go/No-Go conditions in all task contexts) in the complete neural state space and presenting the clusters solutions for different epochs as dendrograms (Figure 2.4). During baseline epoch (Figure 2.4A), the linkage distances among tasks (run in blocks and hence known to the monkey) are greater than those between Go/No-Go conditions within each task (unknown to the monkey before cue sound presentation). In particular, population activity of the two most rostral probes clearly separates task contexts depending on the (near/far) space in which the agent will act. This segregation vanishes moving caudally, where it is replaced by an increasingly clear-cut separation of execution relative to observation tasks (probes 3 and 4), regardless of the space sector in which the observation task is carried out. After cue sound onset (Figure 2.4B), all subpopulations consistently segregate the tasks occurring in the monkeys' peripersonal space (EXE and OBSp) from OBSe. Subsequently, during object presentation (Figure

2.4C), the overall separation between Go and No-Go conditions increases, and the hierarchical trees undergo local reorganizations, with rostral probes showing a more marked separation between near and far spaces, to which the caudal probe add separation between agents (self/other). Following Go/No-Go signal (Figure 2.4D), the various subpopulations exhibit the same general structure of the hierarchical tree, in which monkey's action execution segregates with respects to all the remaining conditions.

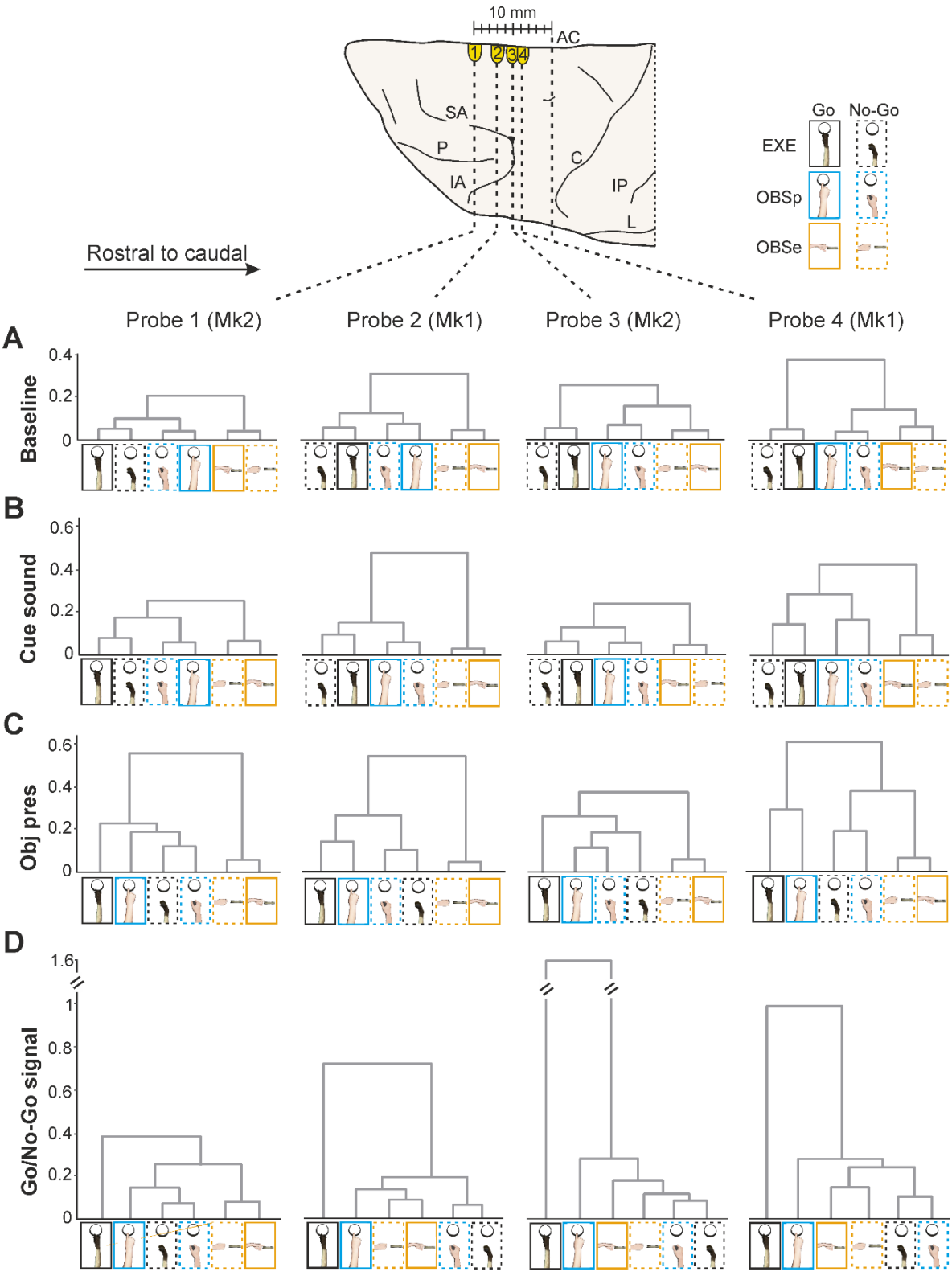

Figure 2.4. Neural distances between conditions during specific epochs of the tasks. Dendrograms illustrate the neural distances between conditions during specific epochs (from A to D) of the tasks. Vertical axes indicate Mahalanobis distances between tasks and conditions. Color codes are the same adopted in Figure 2.3.

The neurophysiological results reveal that area F6 population activity provides information, unevenly distributed along the rostro-caudal extent of the area, about 1) *who is about to act* in a given context (agent-related information), 2) *distance of objects* relative to the monkey (spatial information) and 3) *whether and how the subject will act* (motor information). As a final step, we used Mahalanobis distances in the full-dimensional state space to quantify the local relevance for each of the main functional dimensions (see Methods) emerged from the previous analyses (Figure 2.5). Although all the functional dimensions are represented in all the explored sites, there are clear incremental gradients in the relevance of each dimension along the rostro-caudal (i.e., action execution, agent tuning, observation near and far, object/grip selectivity) and caudo-rostral (i.e., object or experimenter position) direction of area F6.

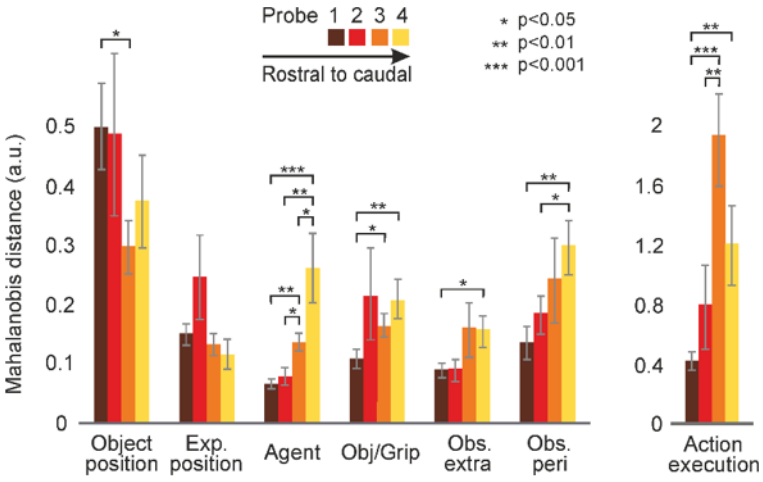

Figure 2.5. Functional gradients within F6. Rostro-caudal changes in F6 functional properties, evaluated by computing the neural (Mahalanobis) distance between conditions (see Methods) based on population activity of each probe (in color code). Histograms represent the population tuning for 1) Object position, 2) Experimenter position, 3) Agent, 4) Object/Grip, 5) Go/No-Go condition in OBSe (Obs extra), 6) Go/No-Go condition in OBSp (Obs Peri), and 7) Go/No-Go condition in EXE (Action execution). Standard errors have been obtained by applying a subsampling procedure and a Z-test has been used to statistically assess significant differences among probes (see Methods).

Next, we addressed whether the local functional specificities here observed can be linked with differential local connectivity patterns.

Cortical afferences and striatal projections of functionally-characterized spots of F6

At end of the neurophysiological experiments, probes were explanted, and antero-retrograde tracers were injected in correspondence of the position of each probe (Figure 2.1C). The injections encompass a territory of area F6 ranging, along the antero-posterior axis, from 10 mm rostral to the anterior commissure (AC) in case of injection 1 (corresponding to probe 1) to 4 mm rostral to AC in case of injection 4 (corresponding to probe 4). All the injection sites were completely confined within the cortical grey matter and involved the entire extent of the mesial surface.

All the injections displayed the general connectional fingerprint expected for area F6[3,43], consisting in robust connections with frontal lobe regions (i.e., premotor areas from F2 to F7, cingulate cortex and dorsolateral prefrontal areas) and weak connections with parietal areas (including inferior and superior parietal lobule and mesial parietal areas) (see Figure 2.6 and S2.8). The connectivity pattern of F6 injected sectors also showed clear-cut specificities, which reflect the antero-posterior location of the injection site (Figure 2.6A). In particular, we observed two main and opposite connectivity gradients, represented by increasingly strong connections with prefrontal (mainly dorsal) areas moving towards the rostral area F6 and increasingly robust connections with premotor and motor cingulate areas moving toward the caudal portion of F6. In the parietal cortex, a relatively stronger labeling was observed after the two more caudal injections in the operculum and in the rostral part of the inferior parietal lobule. Furthermore, denser labeling was observed in medial parietal areas PGm and 31 as well as in posterior parietal area V6A following the most rostral injection (Figure 2.6B, S2.7 and S2.8). Chi-square tests and adjusted standardized cell residuals analysis showed that the quantitative anatomical differences here observed are statistically significant for almost all the territories here considered (see Table S1).

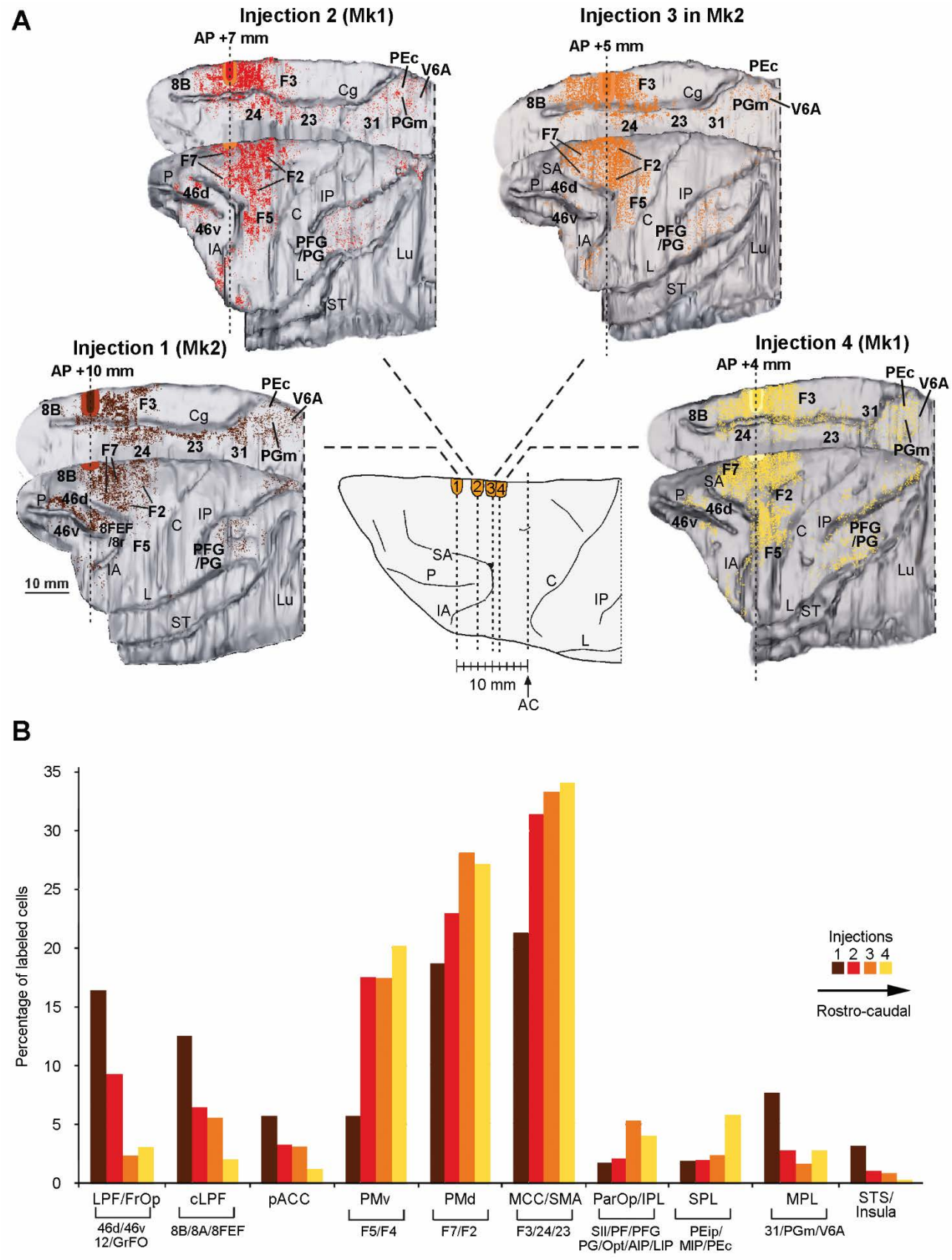

Figure 2.6. Anatomical connectivity of F6 sectors located at different antero-posterior positions. (A) Three dimensional anatomical reconstructions illustrating the distribution of labeled cells after injections in four different spots of F6 at different antero-posterior positions. The labeling is shown in dorsolateral and medial

views of the injected hemispheres: each dot corresponds to one labeled neuron. The location of each injection is shown as a filled area. Dashed lines indicate the position of the injection site (0 corresponds to the anterior commissure). To facilitate the comparison, all the lateral views of the brain are shown as a left hemisphere and the mesial views as a right hemisphere. The 2D reconstruction in the center is a composite view of all the injection sites, shown as red circles, mapped on a template hemisphere. **(B)** Histograms illustrating the percentage of labeled cells in the various cortical regions following each injection (in color code). The areas (listed under the histogram) are grouped based on anatomo-functional similarity. Abbreviations: ACC, anterior cingulate cortex; Cg, cingulate sulcus; cLPC, caudal lateral prefrontal cortex; FrOp, frontal operculum; IP, intraparietal sulcus; IPL, inferior parietal lobule; LPC, lateral prefrontal cortex; Lu, lunate sulcus; MCC, mesial motor cortex; MPL, medial parietal lobule; ParOp, parietal operculum; PMd, dorsal premotor cortex; PMv, premotor cortex; PPC; posterior parietal cortex; SMA, supplementary motor area; SPL, superior parietal lobule; ST, superior temporal sulcus. Other abbreviations as in Figure 2.1.

Since all the tracers injected in this study were antero-retrograde, we could also investigate the distribution of anterograde labeling in the striatum following each injection in area F6 (Figure 2.7). The labeling densely involved the territory of the putamen caudal to the AC, deemed to correspond to the hand- and arm-related motor sector[64,65], as well as the one rostral to the AC, often classified as associative[66,67]. The striatal projections of F6, likewise the cortico-cortical ones, showed a clear rostro-caudal gradient depending on the antero-posterior position of the injected site (Figure 2.7A). Specifically, moving from caudal to rostral injection sites in F6, we observed an increase in the labeled terminals within the "associative" putamen as well as in the caudate territories, whereas moving from rostral to caudal injection sites we observed an increase in the cortico-striatal projections ending in the "motor" sector of the putamen (Figure 2.7B).

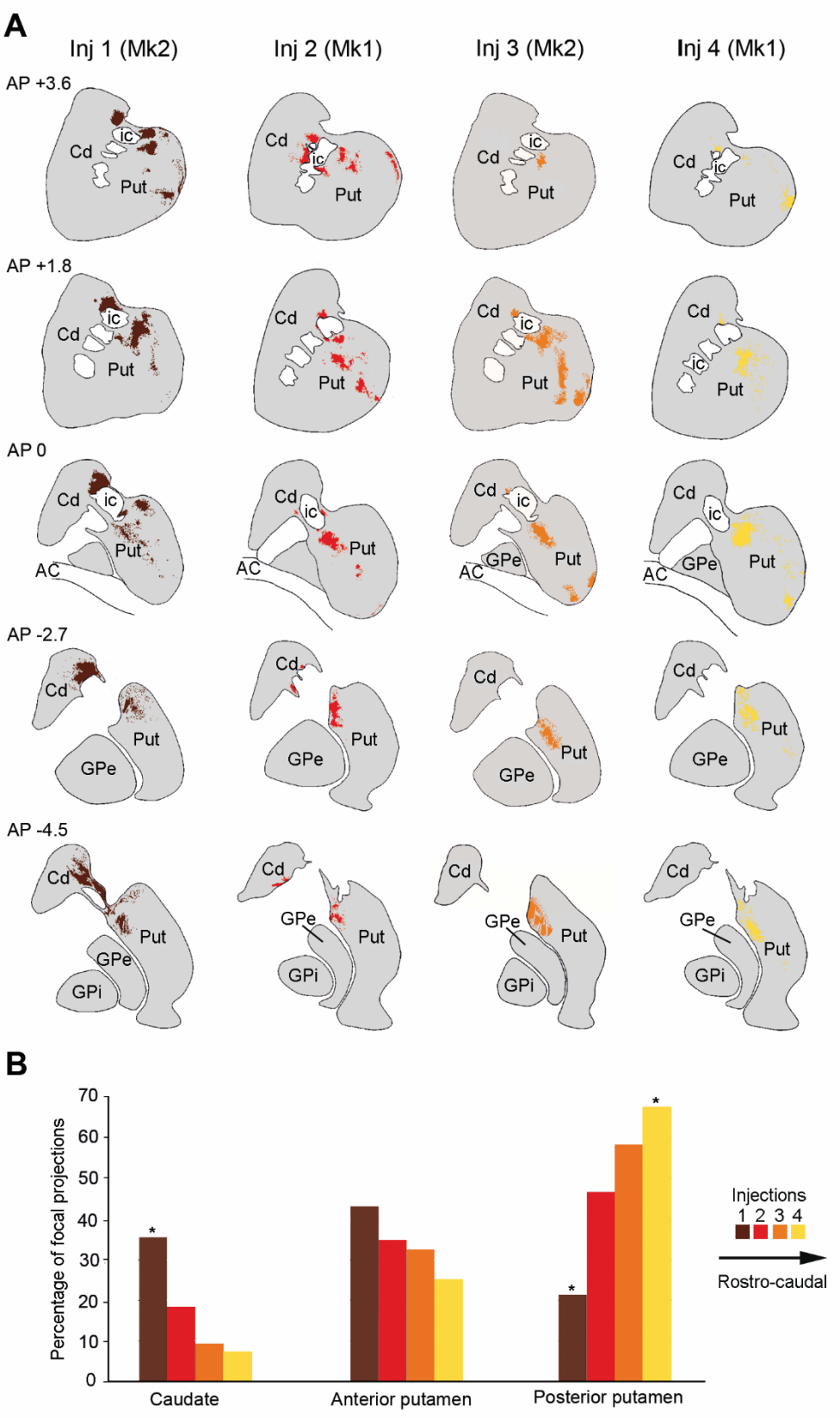

Figure 2.7. Striatal projections of F6 sectors located at different antero-posterior positions. (A) Drawings of coronal sections taken at different rostro-caudal positions along the striatum (in row) showing the distribution of the anterograde labeling following injections into different F6 sectors (in column). **(B)** Histograms illustrating the percentage of striatal projections in the three anatomo-functional territories of the striatum defined in

the text. Abbreviations: Cd, caudate; GPe, external globus pallidus; GPi, internal globus pallidus; ic, internal capsule; Put, putamen. Other conventions as in Figure 2.6.

Figure 2.8 summarizes the main anatomo-functional associations identified in the present study. The rostral part of F6 exhibits greater specificity than the caudal part in representing the position of objects relative to the monkey, with a clear-cut bias in favor of monkey's peripersonal space. These functional specificities are associated with stronger cortical connections with prefrontal, anterior cingulate and mesial parietal regions, as well as with efferences to the caudate nucleus and the anterior putamen in the basal ganglia. In contrast, the caudal part of F6 exhibits remarkable tuning for preparatory and executive aspects of monkey's own reaching-grasping action (i.e., go/no-go tuning, object/grip selectivity) as well as for observed action performed by others in the near and far space. These functional clusters appear to be based on a richer and stronger set of connections with all the lateral and dorsal premotor areas, the superior and inferior parietal lobule, as well as with efferences to the motor putamen in the basal ganglia.

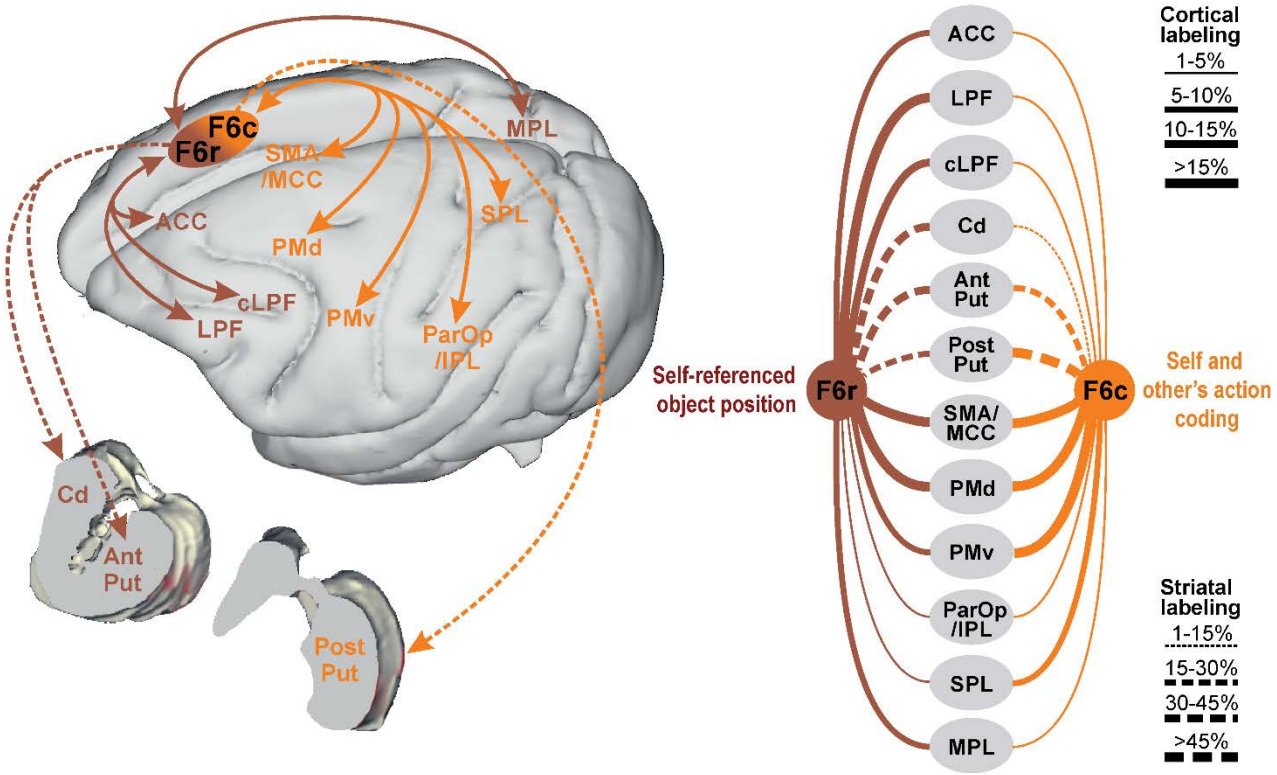

Figure 2.8. Schematic representation of the connectivity patterns of rostral and caudal part of area F6. The lines represent the stronger connections observed after the most rostral (injection 1, brown) and caudal (injection 4, orange) injection. The full lines represent the cortical connections, the dashed lines the striatal ones. Conventions and abbreviations as in Figure 2.6 and 2.7.

2.4 DISCUSSION

The agranular frontal cortex lying in the mesial wall of the primates' brain plays a role in a multiplicity of functional domains, such as the processing of spatial[4,21], contextual[31] and social information[32,35,49], and it has been hypothesized that this functional heterogeneity may derive from two possible organizational principles. The classical model[44] supports the existence of discrete anatomo-functional areas (i.e., SMA and pre-SMA), each endowed with its connectional and functional fingerprint, whereas a most recent alternative view[1] maintains that the manifold nature of mesial premotor cortex relies on a rostro-caudal continuum of graded anatomo-functional changes. In the present study, we provide direct anatomo-functional support to this latter view, by showing that the cytoarchitectonically defined pre-SMA F6 is not homogeneous neither from the functional nor from the connectional point of view. By systematically applying the same set of execution and observation tasks to test neural dynamics in different antero-posterior sites of F6, we found evidence of a variety of functional properties, from spatial information to self and other's action processing. These properties, in spite of the obvious inter-individual variability, appear to form increasing/decreasing gradients along the rostro-caudal axis highly consistent between the two monkeys, paralleled by changes in anatomical connectivity with frontal, parietal and basal ganglia regions. These findings support the view that gradual transitions in connectional and functional properties constitute the basic organizational principle underlying the mapping of functions in the mesial premotor cortex.

Most of the existing neurophysiological studies on mesial frontal regions focused on the identification of an anatomo-functional boundary between the so-called supplementary motor (caudally) and the pre-supplementary motor (rostrally) areas[3,4,68]. However, none of them focused on the possible uneven distribution of the investigated properties within each area. In fact, the findings of some of these studies support the presence of a smooth rostro-caudal change in electrical excitability[3,4], somatosensory and visual responses[4] and agent-specific signals related to motor planning and action execution[32,35]. In line with these data, our results show, in the most caudal probes, a stronger tuning for 1) actions executed by the monkey, 2) the type of object that will be grasped, 3) the agent who was expected to act before trial onset, and 4) overtly observed actions independently from the space sector (peri- or extrapersonal) in which these latter occurred. Previous studies also provide some evidence of spatial tuning for left/right location of visual cues and/or direction of arm movements[4], as well as the description of F6 neurons increasing their firing rate when graspable objects approached the monkey[21]. Nonetheless, possible uneven rostro-caudal

distribution of these spatially tuned neurons was unknown. Here, we found robust evidence of a clear-cut preference for objects located in the monkey's operative space in all the investigated sites of F6. Furthermore, we showed that a preference for the peripersonal space is prevalent in the most rostral probes. Altogether, the evidence of the present study supports the existence of functional gradients in area F6, with its rostral part more tuned to the encoding of distance of objects from the monkey relative to the caudal one, which in turn exhibits stronger tuning to self and other's (observed) action.

The distribution of neuronal properties along the rostro-caudal axis of F6 is paralleled by an even more clear-cut (and consistent between animals) gradient of cortical and striatal connectivity. Indeed, the prevalence of self and others' (observed) action representation and agent tuning prior to trial onset in the caudal part of F6 is paralleled by an increase, in the rostro-caudal direction, of the anatomical connectivity with hand/arm related visuomotor regions of the premotor (F2, F3, F4 and F5), cingulate and lateral parietal/opercular cortices, which host peripersonal[69–71], mirror[39,72,73]; see[40]) and object/grip selective[74–77] neurons. This set of connections may extend the well-established role of dorsolateral parieto-frontal regions in the motor representation of self and other's actions[13,40] and of the surrounding space[78]. In addition to the cortical targets, the caudal part of F6 is also linked with the sector of the so-called "motor" putamen, deemed to correspond to forelimb representation[64,79], where set-related activity has been demonstrated[22]. Along the opposite, caudo-rostral direction, increasing tuning for objects located in the monkey's operative space is associated with stronger connections with the dorsolateral prefrontal cortex, deemed to play a pivotal role in coding the spatial location of sensory stimuli[18,80], the anterior cingulate cortex, playing a role in social decision making processes[81], and the mesial posterior parietal cortex, hosting neurons involved in the coupling of visual and motor processing of targets located in the peripersonal space[82,83] and in the processing of potential target objects and other agent's actions[84]. The stronger link between rostral area F6 and the anterior striatum (caudate nucleus and the anterior putamen) may embed space-constrained representations of objects and agents into cortico-basal ganglia loops devoted to the processing of social context[85].

Note that space-constrained representations of objects relative to one's own and another's body are widespread along the entire F6. However, they most likely derive from different sources and, hence, different reference frames: the caudal F6, linked with motor-related areas of the lateral parieto-frontal network, may encode a body-centered representation of the peripersonal space,

whereas the rostral F6, by virtue of its link with dorsolateral prefrontal and medial parietal cortex, may subserve a more abstract processing of spatial context. Likewise, bimodal (somatosensory and visual) space tuning has been observed in a large territory of the putamen[86], which we have shown to be heavily (and unevenly) targeted by a large territory of area F6, spanning its rostral and caudal sectors. Hence, future studies may unravel differential rostro-caudal trends and tuning properties of striatal neurons devoted to context- or target-specific representations of the peripersonal space. In sum, we evidenced a rostro-caudal organization of cortico-cortical and cortico-basal ganglia connectivity of the monkey pre- that supports a rostro-caudal distribution of functional properties.

Although, to our knowledge, there is no study explicitly investigating local connectional and functional coupling in mesial frontal regions rostral or caudal to F6, separate lines of evidence in the monkey suggest that at least the connectional trends evidenced in the present study are maintained in mesial frontal territories adjacent to F6. Indeed, mesial frontal areas rostral to F6 (i.e. 8B and 9) exhibit increasingly strong connections with dorsolateral prefrontal, anterior striatal and mesial parietal regions[63,87,88], whereas the mesial cortex caudal to F6 (i.e. area F3) exhibits increasingly strong connections with somatomotor regions and the caudal putamen, as well as the emergence of direct projections to the spinal cord, which are virtually absent in F6[9,89,90]. From the functional point of view, nobody has ever mapped the mesial frontal cortex along the antero-posterior axis using the same task or set of tasks. Nonetheless, existing evidence suggest that area F3 exhibits more markedly motor and somatomotor responses[91] whereas mesial frontal cortex rostral to F6 operates multisensory integration at a more abstract level and contributes to complex cognitive and decision-making processes[92].

Neuroanatomical and neurophysiological data in non-human primates are often used to complement each other, but they are rarely collected in a truly integrated manner that enables the achievement of solid conclusions about anatomo-functional relationship. Consequently, non-human primate literature emphasizes the “discretization” of potentially continuous brain functions. Likewise, functional brain imaging studies in humans tend to produce inherently discretized pictures of brain activity, especially due to technical constraints. However, several recent models support the existence of a rostro-caudal organizational principle of the primates’ brain, with abstract cognitive processes mapped rostrally and sensori-motor behavioral control implemented by the most caudal regions[93–96]. These models often infer the existence of smooth anatomo-functional changes based on previous data, and this applies to the mesial frontal cortex as well[1]. Our study provides direct

support to this view, shedding new light on the intrinsic anatomo-functional organization of the pre-SMA F6 by demonstrating that anatomical and functional transitions smoothly occur in parallel gradients, from visuomotor processing of self and other's action, caudally, to spatially-committed representation of objects, rostrally. The well-established architectural homology between human and non-human primates' mesial frontal cortex[1,7,97,98] and the evidence of morphological and neurochemical smooth transitions in both species[8,99], suggest that the anatomo-functional gradients observed here likely represent the anatomo-functional organization principle of the human mesial premotor cortex as well.

3 LOCAL AND SYSTEM MECHANISMS FOR ACTION EXECUTION AND OBSERVATION IN PARIETAL AND PREMOTOR CORTICES

The action observation network (AON) includes a system of brain areas largely shared with action execution in both human and nonhuman primates. Yet, temporal and tuning specificities of distinct areas and of physiologically-identified neuronal classes in the encoding of self and others' action remain unknown. We recorded the activity of 355 single units from three crucial nodes of the AON, the anterior intraparietal area (AIP) and premotor areas F5 and F6, while monkeys performed a Go/No-Go grasping task and observed an experimenter performing it. At the system level, during task execution, F6 displays a prevalence of suppressed neurons and signals whether an action has to be performed, whereas AIP and F5 share a prevalence of facilitated neurons and remarkable target selectivity; during task observation, F5 stands out for its unique prevalence of facilitated neurons and its stronger and earlier modulation than AIP and F6. By applying unsupervised clustering of spike waveforms, we found distinct cell classes unevenly distributed across areas, with different firing properties and carrying specific visuomotor signals. Broadly spiking neurons exhibited a balanced amount of facilitated and suppressed activity during action execution and observation, whereas narrower spiking neurons showed more mutually facilitated responses during the execution of one's own and others' action, particularly in areas AIP and F5. Our findings elucidate the time course of activity and firing properties of neurons in the AON during one's own and others' action, from the system level of anatomically distinct areas to the local level of physiologically distinct cell classes.

3.1 INTRODUCTION

Action execution and observation recruit the same neural substrates in a wide set of brain regions in both human[100–102] and nonhuman primates[40,88,103]. Indeed, after the discovery of mirror neurons, a class of cells in the premotor area F5 of the macaque that become active during both the execution and observation of actions[39,104], similar neuronal properties have been found in a larger network of anatomically connected brain regions[59,105,106], which form the AON. The ventral premotor area F5 is thought to be the core of the AON and is certainly the most widely studied region[40,107]. More recently, two other AON areas have attracted increasing interest: the anterior intraparietal area AIP and the pre-supplementary area F6. AIP plays a role in routing to F5 visual information regarding manipulative actions of other[108–110] and area F6 hosts neurons that selectively encode actions and targets of self

and others[32,34,35,106,111]. Despite these recent advances in our understanding of the AON, two critical questions remain unanswered.

First, what are the temporal and neuronal tuning specificities of the different areas of the AON? fMRI studies in humans[101,112] and monkeys[105,113] provide a system-level view of some areal specificities but cannot address their activation dynamics.

Second, how are self and other's actions represented by different cell classes in the AON? The only available evidence comes from two previous studies demonstrating that a set of antidromically-identified pyramidal-tract neurons in F5[114] and F1[115] exhibit mirror properties, often showing suppressed activity during action observation. A recent study provides a new unsupervised methodology to identify extracellularly recorded neuronal classes[116], but their possible functional specificities across and within different nodes of the AON remain unknown.

To address these issues, we extracellularly recorded neuronal activity from AIP, F5 and F6 in the AON using the same execution (EXE) and observation (OBS) tasks, and we extracted single neuron action potentials by applying a fully automated spike-sorting approach[55]. Then, we compared single neuron and population codes among the three areas to obtain a functional fingerprint of the areal specificities in planning, execution, and observation of actions. Next, we pooled together all the recorded neurons and applied an unsupervised clustering of spike waveforms to identify distinct cell-classes regardless of the area of origin. We found that cell classes 1) showed different properties in the execution and observation tasks, 2) were unevenly distributed across the investigated areas and 3) made a substantial and differential contribution to areal functional specificities.

3.2 METHODS

Animal models

Experiments were performed on three purpose-bred, socially housed adult macaques, Mk1 (*M. nemestrina,* male, 9 kg), Mk2 (*M. mulatta,* male, 7 Kg) and Mk3 (*M. mulatta,* female, 4 Kg). Neuronal activity was recorded from two different monkeys per area (see Figure 3.1A). Before recordings, the monkeys were habituated to sitting in a primate chair and interacting with the experimenters. Then, they were trained to perform an execution (EXE) and an observation (OBS) task[117], as described below. When the training was completed, a head fixation system and different types of probes were implanted (during distinct surgeries) as previously described elsewhere[50,51,53]. All surgical procedures were carried out under general anaesthesia (ketamine hydrochloride, 5 mg/kg intramuscularly [i.m.]

and medetomidine hydrochloride, 0.1 mg/kg, i.m), followed by postsurgical pain medications. The experimental protocols complied with the European law on the humane care and use of laboratory animals (Directive 2010/63/EU), were authorised by the Italian Ministry of Health (D.M. 294/2012-C, 11/12/2012 and 48/2016-PR, 20/01/2016), and were approved by the Veterinarian Animal Care and Use Committee of the University of Parma (Prot. 78/12, 17/07/2012 and Prot. 91/OPBA/2015).

Apparatus and behavioural paradigm

The apparatus for the visuomotor (EXE) and observation (OBS) tasks (Figure 3.1B) is described in detail in a previous study[117]. Briefly, during EXE, the monkey was seated on a primate chair in front of a box, divided horizontally into two sectors by a half-mirror where a spot of light (fixation point) was projected in the exact position of the centre of mass of the not-yet-visible target object. The objects (a ring, a small cone, and a big cone) were presented randomly, one at a time, within reach of the monkey's hand starting position. The objects afforded three different grip types: hook grip (ring), precision grip (small cone) and whole-hand prehension (big cone). The task included two basic conditions, Go and No-Go, and each trial was preceded by a variable (from 1 to 1.5 s) intertrial period.

1. *Go condition.* The fixation point was presented, and the monkey was required to start fixating on it within 1.2 s. Fixation onset resulted in the presentation of a cue sound (high tone, 1200 Hz), which instructed the monkey to grasp the subsequently presented object (Go cue). After 0.8 s, one of the objects became visible. Then, after a variable time lag (0.8–1.2 s), the sound ceased (Go signal), and the monkey had to reach, grasp and pull (for 0.8 s) the object within 1.2 s to receive a fixed amount of juice reward (automatically delivered).
2. *No-Go condition.* The sequence of task events in this condition was the same as in the Go condition, but a different cue sound (low tone, 300 Hz) instructed the monkey to remain still and fixate on the object for 1.2 s after the end of the sound in order to receive the reward.

The same sequence of events described for EXE also applied to OBS, in which an experimenter performed the task in the monkey's extrapersonal space, seen by the monkey from a 90° visual perspective[57].

Contact-sensitive devices (Crist Instruments) were used to detect when the monkey (grounded) touched the metal surface of the starting position or one of the target objects. To signal the onset and tonic phase of object pulling, an additional device was connected to the switch located behind each object. Custom-made LabView-based software was used to monitor the monkey's

performance and to control the presentation of auditory and visual cues[57]. Eye position was monitored at 50 Hz with a camera-based eye tracking system and the monkey was required to maintain its gaze on the fixation point (with a tolerance radius of 5°) throughout the task. If the monkey broke fixation, made an incorrect movement or did not respect the task's temporal constraints, no reward was delivered and the incorrectly performed trials were put back in the randomised list to be subsequently repeated. We collected at least 10 correctly performed trials for each condition.

Recording techniques

Neuronal recordings were performed by means of multielectrode linear silicon probes in different single-shaft[53,54] or 3D[51] configurations, implanted chronically in AIP[56] and F6[16] and acutely in F5[117], based on MRI reconstruction of the target brain regions. The analog signal from all the recording electrodes was simultaneously amplified and sampled either at 30 kHz with an OpenEphys system (http://open-ephys.org/) or at 40 kHz with an Omniplex system (Plexon).

All formal signal analyses were performed offline. Spike sorting was performed with the fully automated software MountainSort[55] using -3.0 SDs of the signal of each channel as the threshold for detecting units. To discriminate single- from multi-units, we used the noise overlap parameter. This parameter, ranging between 0 and 1, estimates the fraction of "noise events" in a waveform cluster, i.e., above-threshold events not associated with well-isolated clusters. In most of the recording sessions, the noise overlap distribution is bimodal, with putative single-units associated with values below ~0.1 and putative multi-units with values above ~0.3. Thus, we considered as well-isolated single units only those with noise overlap values lower than 0.1. We then automatically inspected all waveforms of all isolated units and retained, for each unit, only those waveforms that did not exceed ±3 SD from the average waveform in all data points (approximately 10% of the waveforms in each unit were removed with this procedure), to reduce the random variability and improve the accuracy in the extraction of spike shape parameters. Single unit isolation was further verified using standard criteria (ISI distribution, refractory period > 1 ms, and absence of cross-correlated firing with time-lag of ≈ 0 relative to other isolated units, to avoid oversampling).

To obtain the average waveform for each individual unit we randomly selected 1000 of the filtered signal's spikes in a window of 2.5 ms centred on the spikes' absolute minimum. Each waveform was spline interpolated in order to achieve 1000 points in the 2.5-ms window, regardless of the original sampling rate, and realigned to the absolute minimum. This procedure produced the

average waveform for all units. Then, we obtained the final data set by excluding all units with 1) less than 1000 spikes (n = 15); 2) very noisy waveforms (multipeak, e.g. multiple local maxima between the main trough and the subsequent peak) (n = 35); 3) a main trough amplitude smaller than the subsequent peak or a peak before the trough greater than 20% the trough depth amplitude (n = 31), because they likely belong to axon fibres[118,119]. The final dataset included 355 single neurons fulfilling all these criteria.

Analysis of the neuronal activity

Clustering of single-neuron waveforms

To cluster neurons, we first explored the possibility to use a combination of waveform parameters and firing features, but the results (Figure S3.3A) did not outperform those obtained with the two most widely established waveform parameters, namely, trough-to-peak duration[120,121] and repolarisation time[116]. The trough-to-peak duration is the interval between the global minimum of the curve and the subsequent local maximum. Repolarisation time is the interval between the late positive peak and the subsequent inflection point (where the second derivative equals zero); although it does not clearly correspond to the actual full repolarization of the cell membrane post-spike, it is a reliable predictor of this parameter.

Then, to identify clusters of waveforms based on these two parameters, we followed a recently described procedure[116] in which the two-dimensional data points are fitted with a Gaussian mixture distribution (Matlab function: fitgmdist). The procedure optimizes the likelihood Gaussian mixture model using the iterative Expectation-Maximization (EM) algorithm. Each iteration implies two steps: first, EM algorithm estimates posterior probabilities of each data point given the current set of component means, covariance matrices and mixing proportions (E step); then, using these probabilities as weights, it estimates new component means, covariance matrices and mixing proportions (M step) and evaluates the log-likelihood with these new parameters' estimates. These steps are repeated until convergence or for a maximum of 100 iterations. To initialize the EM algorithm, we used k-means++ algorithm: 500 different replicates were run with different initializations and the model with the largest log-likelihood was adopted. For all the replicates, in order to reduce the number of free parameters, we imposed the covariance matrix of each component to be diagonal because even if trough-to-peak duration and repolarization time are generally correlated, this is not the case within individual clusters. We repeated this procedure by fitting the data with a different number of clusters (from 1 to 10), taking as the number of clusters

the one that minimise the Bayesian Information Criteria (BIC, Figure 3.3A). We obtained three clusters (cell classes) with a variable number of neurons attributed by hard assignment, that is, by assigning each neuron to the cluster associated with the highest posterior probability. For visualization purposes, 68% confidence ellipses, i.e., the bivariate analogue of the standard error, were shown for each cluster[122]. Previous studies adopted an additional outlier removal procedure, which led to the exclusion of approximately 11% of the neurons[116]; this procedure would have had a similar impact on our dataset, with 7% of the neurons excluded, more than 68% of them belonging to class 3, which includes the greatest number of neurons. Because in this study one of the main goals was to provide a comprehensive comparative picture of areal specificities, we decided not to remove otherwise fully valid physiological data by adding further exclusion criteria to those described above.

In order to look for additional support to the subdivision of neurons into functional classes and, more specifically, to further evaluate the possibility to functionally characterize some narrow spiking neurons as inhibitory interneurons, we applied cross-correlation analysis[123,124] but the results did not provide sufficiently robust evidence to reach a sound conclusion on this issue (Figure S3.3B).

Population analyses

For each neuron, we first computed its baseline firing rate (corresponding to the 500-ms time interval preceding cue-sound presentation) for EXE and OBS (objects and trials averaged), separately. We then computed the net normalised activity of each neuron. First, we subtracted its baseline activity in a given condition from the firing rate of each bin; then, we soft-normalised the resulting net activity vector by dividing each data point by the absolute maximum across all conditions + 5 spk/s (this latter constant factor reduces the overall net normalised activity of neurons a with very low firing rate). The resulting net normalised activities (ranging theoretically between -1 and 1) were used to produce the heat-maps in order to show individual neurons' firing rate in a comparable form during EXE and OBS task-unfolding periods.

Neurons were classified as facilitated or suppressed depending on the sign of the average modulation they showed during the movement period (action execution or observation in the time interval ranging from -300 ms before to 900 ms after the Go signal). To test whether the modulation of facilitated (red lines in Figure 3.2 and 3.5) and suppressed (blue lines in Figure 3.2 and 3.5) neurons was statistically significant, we compared their baseline activity with each bin of the movement period (one-tailed sliding t-test, window = 200 ms, step = 20 ms, $p < 0.05$, uncorrected) in the -300/+900-ms interval around the Go signal during the entire movement period of EXE and OBS. We

considered significantly facilitated or suppressed all those neurons with at least five consecutive significant bins, whereas neurons that did not meet this criterion were classified as non-significantly modulated. Note that this constitutes a very permissive statistical criterion relative to conventional epoch-based approaches[57]. This choice was motivated by the fact that we did not want to study very restrictive and specific functional categories of neurons, but rather to include all the available cells and provide an (as much as possible) unbiased comparison of the three studied areas. Because they are known to possess different firing/temporal pattern of activity[16] conventional epoch-based statistics would have strongly biased the results of the comparisons among areas.

The peak of activity times of facilitated neurons were calculated in the 100/500-ms time interval after object presentation and in 0/600-ms time interval after the Go-signal.

Decoding analyses

To compare how information about task parameters was represented in different areas, we employed the Neural Decoding Toolbox[125] used in our previous studies[34,56,109]. Specifically, we assessed the decoding accuracy of a Poisson naïve Bayes classifier trained and tested to classify different variables, that is, Go/No-Go or type of object (Figure 3.2 and S3.1).

Regardless of the decoded variable, for each neuron, data were first converted from raster format into binned format. Specifically, we created binned data that contained the average firing rate in 200-ms bins sampled at 20-ms intervals for each trial (data point). We obtained a population of binned data characterized by a number of data points corresponding to the number of trials per conditions (i.e. 30 x 2 = 60 data-points for Go/No-Go decoding; 10 x 3 = 30 data-points for object decoding) in an N-dimensional space (where N is the total number of neurons considered for each analysis). Next, we randomly grouped all the available data points into a number of splits corresponding to the number of data points per condition, with each split containing a "pseudo-population", that is, a population of neurons that could be partially recorded separately but treated as if they were recorded simultaneously. Before sending the data to the classifier, we pre-selected those features (neurons) that showed a difference between conditions with $p<0.5$. Subsequently, the classifier was trained using all but one of the splits of the data and then tested on the remaining one. This procedure was repeated as many times as the number of splits (i.e., 30 in the case of Go/No-Go decoding, 10 in the case of object decoding), leaving out a different test split each time.

As a measure of the performance of the classification, we used the mutual information (MI[126]), defined as the reduction of uncertainty (or gain of information) about the current condition

achieved by knowing the neuronal response. The greater the amount of information carried by the population, the smaller the uncertainty regarding the current condition. When the probability of presenting each of *K* different conditions is equal, MI can reach a theoretical maximum of $log_2 K$ (i.e. 1 for Go/No-Go decoding and 1.585 for object decoding); we used these values to normalise MI corresponding curves in Figure 3.2 and S3.1. Because, on average, the higher the number of neurons used in the decoding, the higher the performance of the classifier, we performed a number-matching procedure to make the results of different areas comparable. To this end, we performed the decoding analysis on randomly selected sets of 65 neurons from each area (with replacement), corresponding to 3/4 of the neurons in AIP (n = 86), which is the area with the lowest number of neurons. We repeated this procedure 50 times, averaging each iteration across 10 runs with different data in the training and test splits from the same set of neurons and smoothing it with a 40 ms Gaussian kernel, to increase the robustness of the results. Finally, we computed the mean and the standard deviation (shading in Figure 3.2) of the resulting distribution.

To assess statistically when each area starts to convey a given type of information (i.e. Go/No-Go or object/grip type), we calculated for each iteration of the procedure described above the time point where the mutual information exceeds 1/3 of its maximum theoretical value. This calculation was repeated with all iterations and the standard deviation of the resulting time point distribution (multiplied by $65/N_{area}$ in order to consider the different subsample size with respect to the reference population) was taken as standard error. We compared the mean onset among areas by performing multiple two-tailed two-sample z-tests (p-values uncorrected). We also compared how information about task parameters was represented among cell classes (Figure 3.4C-D). Since the investigated areas differently encode information about task events (Figure 3.2C-D), for each cell class we randomly sampled (with replacement) pseudo-populations including a fixed number (n = 20) of neurons of that class from each area. Decoding was performed on these 3 pseudo-populations (n = 60), and this procedure was repeated 50 times, averaging each iteration across 10 runs. Average mutual information curves and their significance were obtained as described above.

To assess the difference in mutual information about object type across areas (Figure 3.2C) and cell classes (Figure 3.4C), we used the same procedure described above on the average mutual information in the 200/700 ms interval after object presentation.

Index of Mutual Modulation Depth

For the purpose of comparing the dynamic (positive or negative) modulation of single-neuron discharge in corresponding time bins of EXE and OBS, we created an index quantifying the mutual modulation depth (MMD). For each neuron, in the interval -500/700 ms relative to the movement onset, we calculated the net soft-normalised activity (as described above) separately for EXE and OBS, and we smoothed it with 200-ms (centered at intermediate values) bins advanced in steps of 20 ms. The MMD index was then computed for each neuron as the product of EXE and OBS activity values, as follows:

$$MMD_n(t) = EXE_n(t) * OBS_n(t)$$

where $EXE_n(t)$ and $OBS_n(t)$ represent the net (500 ms prior to the Go signal) soft-normalised activity of neuron *n* during time bin *t* of EXE and OBS task, respectively. Neurons showing a similar discharge profile in both EXE and OBS (regardless of whether the neuron was jointly facilitated or suppressed) showed positive MMD values: the closer to 1 (theoretical value), the greater the (positive or negative) discharge modulation (Figure 3.6A, Neuron 1 and 2). In contrast, neurons showing large but opposite modulation in the two tasks (facilitated/suppressed or vice versa), showed negative MMD values: the closer to -1 (theoretical value), the greater the EXE and OBS opposite modulation (Figure 3.6A, Neuron 3 and 4). If in one condition the neuron does not modulate its discharge, the index tends to 0 regardless of the neuron's modulation in the other condition (Figure 3.6A, Neuron 5 and 6).

To assess possible significant changes in overall MMD values during the movement epoch of specific neuronal subpopulations, we compared bin-by-bin MMD values with a fixed value corresponding to the average of the first 5 bins (300 ms of activity) of each plot (one-tailed paired sample t-test, $p < 0.01$). We considered significant only series of at least five consecutive bins (black asterisks at the top of each plot of Figure 3.6B).

3.3 RESULTS

We isolated 436 units from three monkeys. All units with atypical features relative to a predefined set of criteria (see Methods) were excluded (n = 81, 18.6%), leading to a dataset of 355 well-isolated single neurons in three cortical areas (Figure 3.1A): AIP (n = 86), F5 (n = 106) and F6 (n = 163). During the recordings, monkeys performed an execution task (EXE, Figure 3.1B) and observed an experimenter performing the same task (OBS, Figure 3.1B). The temporal sequence of events was the same in both tasks (Figure 3.1C).

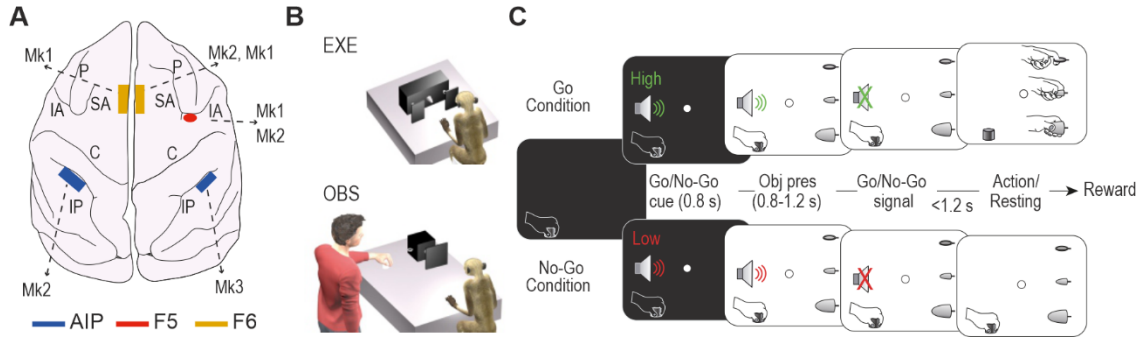

Figure 3.1. Recorded regions and behavioural task. (A) Schematic reconstruction of the recorded regions in the three animals reported on Mk2's brain. C, central sulcus; IA, inferior arcuate sulcus; IP, intraparietal sulcus; P, principal sulcus; SA, superior arcuate sulcus. **(B)** Behavioural setting for the execution (EXE) and observation (OBS) tasks, run in blocks (EXE first). **(C)** Temporal sequence of events of the Go/No-Go visuomotor task. The monkey starts with its hand in a fixed position. The onset of central fixation in the position where the object will be presented triggers a Go/No-Go auditory cue (high/low frequency sound, respectively). Following a variable delay after object presentation, the end of the sound (Go/No-Go signal) instructs the monkey to reach and grasp the visually presented object or to remain still until the end of the trial to obtain the reward. The different types of trials (Go/No-Go and object type) within EXE and OBS blocks were presented in a randomized order.

Functional fingerprint of parietal and frontal areas during task execution and observation

To investigate the time course and functional specificities of neuronal processing during the tasks in the three areas, we first classified each neuron as facilitated (red), suppressed (blue) or nonsignificant (white) depending on its modulation during action execution (Figure 3.2A) and observation (Figure 3.2B) relative to baseline (see Methods).

During EXE (Figure 3.2A), in AIP and F5 we found a similar proportion of facilitated and suppressed neurons (AIP vs F5: $\chi^2 = 0.04$, $p = 0.8354$), with an overall prevalence of facilitated ones, and both areas differed from F6 where, instead, cells with suppressed response prevailed (F6 vs AIP: $\chi^2 = 8.62$, $p = 0.0033$; F6 vs F5: $\chi^2 = 12.22$, $p = 0.0005$). Facilitated neurons exhibited clearly measurable peaks of activity already in relation to the visual presentation of the object, first in AIP (median, +230 ms) and F5 (+240 ms) and later on in F6 (+350 ms, Mann-Whitney test, F6 vs AIP: $Z = 2.91$, $p = 0.0036$; F6 vs F5: $Z = 2.20$, $p = 0.0276$; see Methods). In contrast, relative to the Go-signal, the facilitated neurons' peak of activity showed the opposite trend, occurring earlier in F6 (+230 ms) than in both F5 (+400 ms, $Z = 2.78$, $p = 0.0054$) and AIP (+390 ms, $Z = 2.49$, $p=0.0127$), which in turn did not significantly differ from each other ($Z = 0.19$, $p = 0.85$).

To better investigate the time course of different signals across the studied areas, we performed a neural decoding analysis[125] by training and testing a Poisson naïve Bayes classifier to discriminate between Go and No-Go conditions based on the population activity of each area (see

Methods). The results (Figure 3.2C) show that the mutual information distinguishing Go and No-Go trials became significant much earlier in area F6 (-280 ms from object presentation) than in F5 (+100 ms, z-test on subsampling repetitions, Z = 2.60, p = 0.0092) and AIP (+440 ms, Z = 6.59, p = $4.3 \cdot 10^{-11}$), with F5 significantly preceding AIP (Z = 2.46, p = 0.0138). Conversely, mutual information about the type of target object emerges first in AIP (at 180 ms after object presentation), shortly thereafter in F5 (200ms) and then in F6, significantly later (240ms) compared to AIP (Z = 2.25, p = 0.024) but not to F5 (Z = 1.68, p = 0.092). The object-selective signal was both stronger and earlier in AIP and F5 relative to F6, where the mutual information about object type remained smaller than in the other two areas for the entire duration of the trial (Figure 3.2C, lower part). Interestingly, a stronger and earlier contribution of AIP in signalling the type of object is also made evident by an analysis of the neuronal population response during No-Go trials (Figure S3.1), supporting a predominantly visual nature of AIP object-related signal relative to F5 and F6.

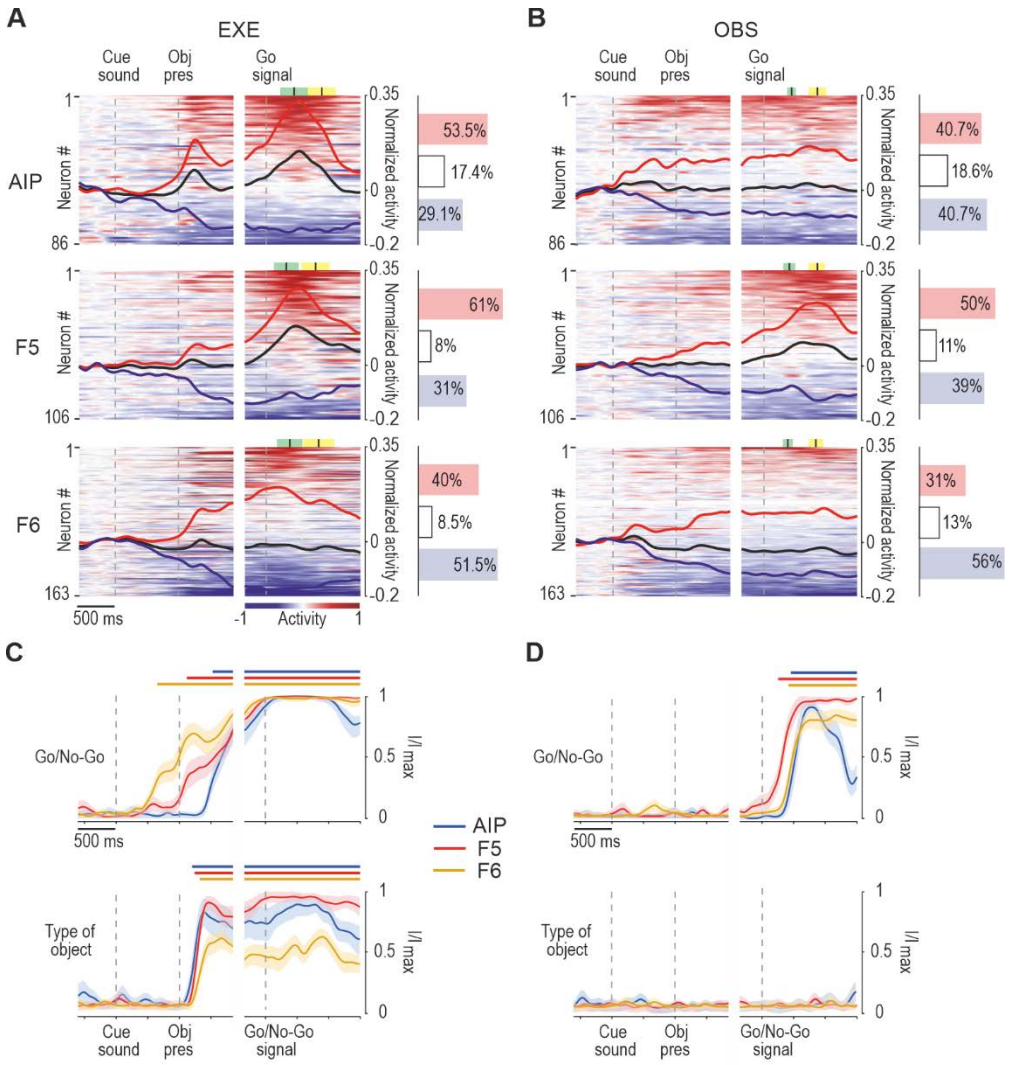

Figure 3.2. Functional fingerprint of parietal and frontal areas during task execution and observation. (A) Heat maps of all the recorded neurons in each area during EXE. Each line represents one cell (average activity of the responses to all the three objects). Cells are ordered (from top to bottom) based on the magnitude of their activity with respect to baseline (red = facilitated, blue = suppressed) in the interval between 300 ms before and 900 ms after the Go signal, independently for EXE and OBS. Black lines represent the averaged response of each population as a whole. The histograms on the right indicate the percentage of facilitated (red), suppressed (blue) and nonsignificant (white) neurons in each area (see Methods). Green and yellow marks represent average ± standard deviation of movement onset and pulling onset, respectively. No-Go condition of EXE is shown in Figure S3.1A. **(B)** Heat maps of all the neurons shown in A recorded during OBS. Data have been normalised together with EXE to facilitate comparisons. Note that the neurons have been ordered independently from panel A (see Figure S3.1E for OBS data plotted in the same order as in EXE). Other conventions as in A. No-Go condition of OBS is shown in Figure S3.1B. **(C)** Mutual information on Go/No-Go trials (top) and type of object (bottom) during EXE decoded from neuronal population activity of each area during the task-unfolding period. Continuous coloured bars above each plot indicate the period in which the mutual information is higher than 1/3 of its maximum theoretical value (see Methods). Mutual information about object during EXE is greater in both AIP and F5 relative to F6 ($p<0.05$ for both comparisons, see Methods). Object decoding in No-Go condition of EXE is shown in Figure S3.1C. **(D)** Mutual information about Go/No-Go (top) and type of object (bottom) during OBS. Conventions as in C. Object decoding in No-Go condition of OBS is shown Figure S3.1D.

Altogether, these findings highlight a greater similarity between the lateral convexity areas AIP and F5 than between either of those areas and F6, with the AIP-F5 circuit playing a major role in the processing of graspable objects and reaching-grasping actions by linking visual features of the target, encoded in AIP, with specific motor plans for grasping it, represented primarily in F5[127,128]. Area F6 differs strongly from both AIP and F5 in terms of the timing and strength of its object- and action-related response, showing earlier and predominantly suppressed activity signalling whether a forthcoming action will be performed or withheld.

During OBS (Figure 3.2B), the overall modulation of both facilitated and suppressed neurons was smaller than during EXE in all the investigated areas. The number of facilitated and suppressed neurons was perfectly balanced in AIP, similarly to F5 ($\chi^2 = 0.66$, $p = 0.4175$), where facilitated neurons were only slightly more numerous; in contrast, in F6, suppressed neurons clearly prevailed, especially relative to F5 (F6 vs F5: $\chi^2 = 10.31$, $p = 0.0013$; F6 vs AIP $\chi^2 = 4.27$, $p = 0.0388$). The proportion of nonsignificant cells slightly increased in OBS relative to EXE in all three areas; nonetheless, area F5 still exhibited a clear-cut modulation during the agent's reaching-grasping action due to the prevalence of facilitated neurons, which exhibited a measurable peak of activity corresponding to the observation of object pulling onset. Instead, areas AIP and F6, despite hosting some single neurons with transiently facilitated activity during reaching-grasping observation (see heat map in Figure 3.2B), did not show any phasic modulation of their population response.

By applying the neural decoding approach to OBS (Figure 3.2D), the classifier could detect significant mutual information discriminating between Go and No-Go trials only during the movement epoch, essentially revealing a robust signal related to action observation in all three areas. However, as compared to EXE (Figure 3.2C), we found no additional object or observed grip-type specificity during OBS. Significant mutual information about Go/No-Go raises earlier in F5 (+200 ms relative to the Go/No-Go signal) than in F6 (+360 ms, $Z = 2.90$, $p = 0.0038$) and AIP (+400 ms, $Z = 3.11$, $p = 0.0019$). Because neurons in different areas were not recorded simultaneously, hence being potentially subject to variation in the reaction time of the actor, we also repeated this analysis by aligning the activity of Go trials to reaching movement onset: the findings confirm the earlier activation of area F5 (-260 ms relative to movement onset) with respect to both AIP (-40 ms, $Z = 3.55$, $p = 3.8 \cdot 10^{-4}$) and F6 (0 ms, $Z = 3.23$, $p = 0.0012$).

These data lend strong support to the idea that, in the action observation network, area F5 does not necessarily need to be triggered by visual information about other's actions coming from the parietal cortex[40,129] but can also predictively represent upcoming actions of others[130] with inherently generative capacities[57,131,132].

Identification and functional properties of cell classes based on extracellular spike waveforms

Next, we wanted to investigate cell-class specificities of each of the areas described so far. To this end, we measured two parameters of spikes waveforms for all the neurons isolated in the three investigated areas, namely, trough-to-peak duration and repolarisation time[116]. The trough-to-peak duration defines the spike amplitude in terms of the interval between the global minimum of the spike shape and the following local maximum, whereas the repolarisation time is the interval between the local maximum following the global minimum and the subsequent inflection point of the curve (Figure 3.3A).

To identify two-dimensional clusters with the available parameters and waveforms, we adopted an unsupervised clustering procedure (Gaussian mixture model; see Methods). A Bayesian information criterion (BIC) indicated the optimal number of Gaussian components (i.e., three waveform classes) in our dataset (Figure 3.3A, inset). The overall representation of the clustering results revealed three well separated neuronal classes (Figure 3.3B) ranging from narrow spiking (class 1) to broad spiking (class 3) neurons, with a clear prevalence of broad spiking neurons (Figure 3.3C), in line with previous studies[120,121,133,134].

Representative examples of single neurons belonging to each of the three classes are shown in Figure 3.3D. Neuron 1 is an AIP cell belonging to class 1: during EXE, this neuron discharged vigorously during the presentation of the object and, subsequently, while it was being grasped, but it also fired during the experimenter's grasping in OBS. Neuron 2 was recorded from area F5 and belongs to class 2: it discharged during the grasping of the ring and of the big cone in EXE and even more strongly during the experimenter's grasping in OBS, but with no selectivity for the target object in this task. Finally, Neuron 3 is an F6 cell belonging to class 3: it reaches its peak of discharge during object pulling in EXE and shows no significant modulation during OBS.

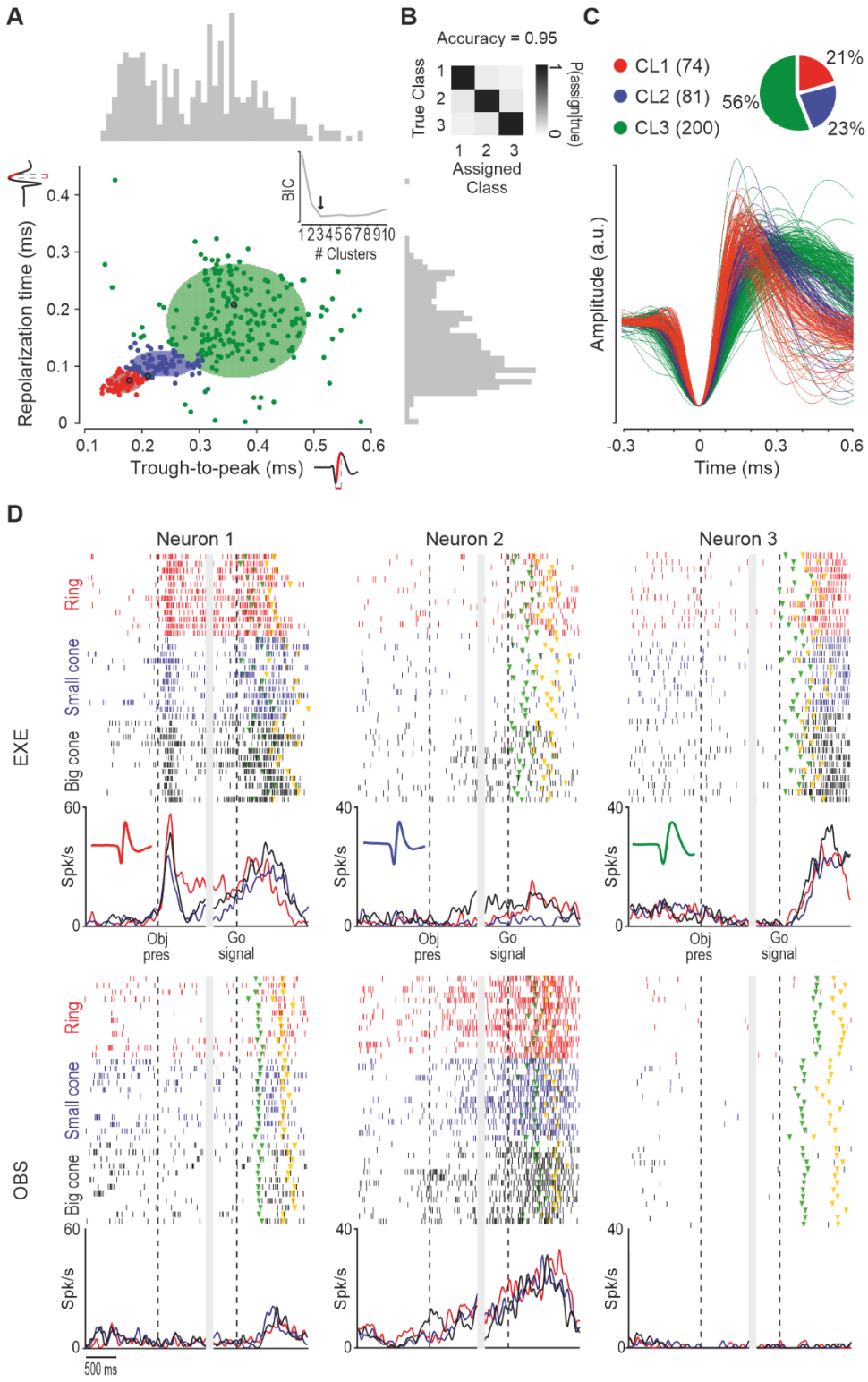

Figure 3.3. Identification and functional properties of cell classes based on extracellular spike waveforms. (A) Projection of each spike waveforms in the 2D space formed by trough-to-peak duration and repolarisation time. Colour codes identify the clusters (cell classes) resulting from the Gaussian mixture model applied with the number of components (n = 3) indicated by the Bayesian information criterion (BIC) shown in the inset (see Methods). The black dots in each cluster indicate the example neurons shown in panel D. Colored ellipses indicate, for each cluster, the 2D confidence interval. Trough-to-peak values range from 0.13 ms to 0.58 ms, and repolarization time values range from 0.0025 ms to 0.43 ms. Average variability in trough-to-peak

estimation is 3.1 µs (95th percentile = 7.9 µs); average variability in repolarization time estimation is 14.8 µs (95th percentile = 65.4 µs). See Figure S3.2 for clustering reliability within and across areas. Figure S3.3A shows alternative clustering results obtained using spiking and waveform features. **(B)** Separation among cell classes. For each of 10^4 data points randomly generated from the fitted Gaussian mixture distribution we compared the true class from which the point was drawn with the class to which it was assigned. The confusion matrix shows the classification results; accuracy is 0.95 and results from the mean of the three diagonal probabilities[116]. **(C)** Number of neurons in each cell class (in colour code) in the entire dataset and individual average spike waveforms belonging to each class. **(D)** Example neurons recorded in AIP, F5 and F6 (from Neuron 1 to 3, see black circles in panel A), belonging to each of the three classes (spike waveform is shown in the inset of each histogram, colour code as in B). Activity is aligned (vertical dashed lines) on object presentation (Obj pres) and then (after the gap) on the Go signal, in both tasks. Each colour refers to trials with one type of target object: a ring (red), a small cone (blue) and big cone (black). Triangular markers indicate the movement onset (green) and object pulling onset (yellow).

By comparing the firing properties of the cells in the three classes (regardless of the anatomical areas from which they were recorded), we reported several distinctive features. Although we generally found a greater number of facilitated than suppressed neurons (especially in class 1), their relative proportion did not differ significantly across classes in either EXE (Figure S3.4A) or OBS (Figure S3.4B); nonetheless, facilitated cells of classes 1 and 2 showed stronger average (Figure 3.4A) and peak (Figure 3.4B) activity during visual presentation of objects, executed and observed actions, relative to cells of class 3. In turn, neurons of class 3 exhibit an earlier and remarkably stronger tuning to the object during EXE relative to the other two classes (Figure 3.4C and 3.4D). Thus, neurons with narrower spikes exhibit stronger visual and visuomotor responses, but they show a weaker object-selectivity relative to broadly spiking neurons. In line with this latter observation, the firing statistics of the identified cell classes (Figure S3.4C) indicate that narrow spiking neurons exhibit a greater baseline firing rate, a shorter and more variable interspike interval (ISI), and a stronger tendency to fire in bursts than do broadly spiking neurons, which show a slower and more regular firing pattern.

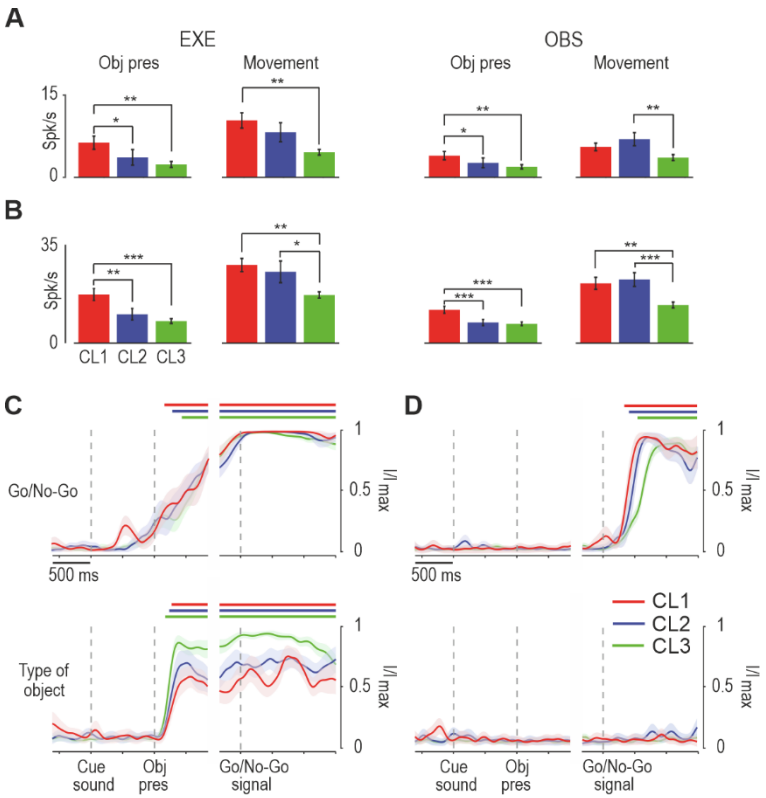

Figure 3.4. Cell-class response properties during EXE and OBS. (A) Average net firing rates of facilitated neurons of cell class 1 (red), 2 (blue) and 3 (green) during object presentation (0.1 to 0.3 sec relative to object presentations) and movement epoch (0.3 sec before to 0.9 sec after the Go-signal) in EXE (left) and OBS (right) tasks (one-way ANOVA with Newman-Keuls post-hoc test). Cell classes response is shown in Figure S3.4A and S4B. **(B)** Average peak of net firing rates of facilitated neurons of the three cell classes during object presentation (0.1 to 0.3 relative to object presentations) and movement epoch (0.3 sec before to 0.9 sec after the Go-signal) in EXE (left) and OBS (right). Conventions as in A. *$p < 0.05$; **$p < 0.01$; ***$p < 0.001$. Cell classes response is shown in Figure S3.4A and S3.4B. **(C)** Mutual information on Go/No-Go trials (top) and type of object (bottom) during EXE decoded from neuronal population activity of each area during the task-unfolding period. Mutual information about object during EXE conveyed by neurons of Class 3 is greater than that of neurons of Class 1 (z-test, $p = 0.046$) and 2 ($p = 0.090$). Conventions as in Figure 3.2C. **(D)** Mutual information about Go/No-Go (top) and type of object (bottom) during OBS. Conventions as in Figure 3.2C.

Functional specificities of cell classes in AIP, F5 and F6

Based on the findings presented thus far, we then asked whether the identified cell classes (Figure 3.5A) contribute differently to the functional specificities of the three investigated areas. By comparing the overall distribution of neurons in the three classes (see Figure 3.3C) with that obtained in each area (Figure 3.5B), we found no significant deviation in AIP ($\chi^2 = 1.19$, $p = 0.55$); furthermore, we found a greater proportion of neurons in the first two classes and a smaller number in class 3 in F5 ($\chi^2 = 18.27$, $p = 0.0001$), and the opposite trend in F6, which had a greater proportion of neurons in class 3 ($\chi^2 = 10.57$, $p = 0.005$). It is important to note that these results derive from a clustering applied to all the recorded neurons, pooled across areas, but we verified that they are extremely consistent and can be substantially reproduced even if clustering is performed within each area, independently (Figure S3.2).

Next, we asked how neuronal classes contributed to the overall output signal of the three areas during EXE (Figure 3.5C). To this purpose, we applied a 3 x 3 x 3 repeated measures ANOVA (within factor: Epoch), with Cell class and Area as grouping factors, followed by a Newman-Keuls post-hoc test where appropriate. The results (see Figure 3.5C and S3.5) indicate that neurons of area F5 showed an overall stronger firing rate than those of both AIP and F6 ($p < 0.001$ for both comparisons), regardless of the cell class and, in particular, during the movement epoch relative to both baseline ($p < 0.001$) and object presentation ($p < 0.001$). Among cell classes, neurons of class 1 showed the overall highest firing rate, particularly in area F6; furthermore, they made the strongest contribution to object presentation ($p < 0.005$). These findings do not only depend on overall facilitated responses but are also accounted for by the uneven distribution across cell classes and areas of suppressed neurons, which are particularly represented in F6 (Figure S3.5G).

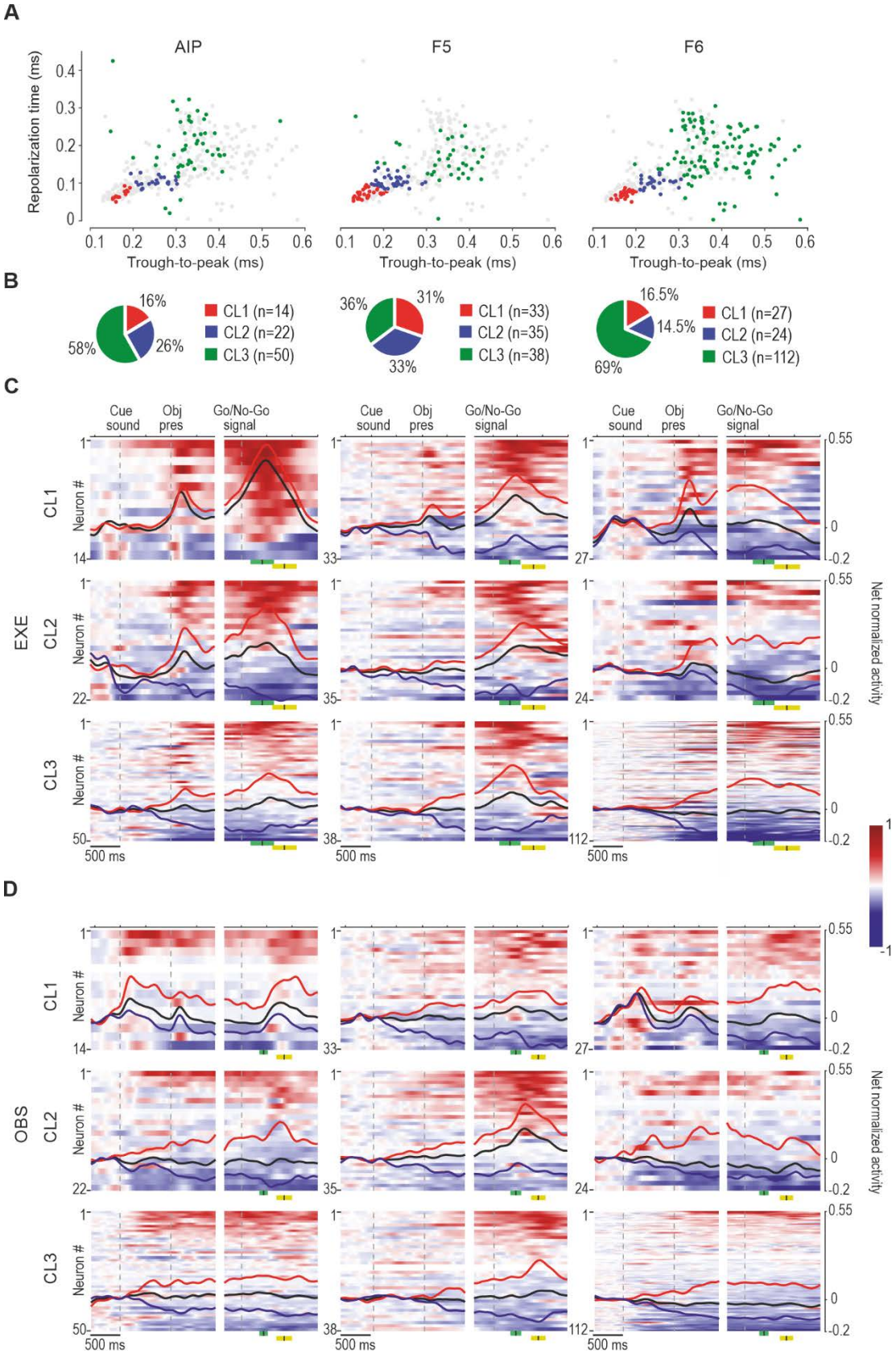

Figure 3.5. Functional specificities of cell classes in AIP, F5 and F6. (A) Projection of each spike waveform in the 2D space formed by trough-to-peak duration and repolarisation time. Colour codes identify the cell class to which each neuron of a given area has been attributed; grey dots in each plot correspond to the neurons that

do not belong to the corresponding area. Other conventions as in Figure 3.3A. **(B)** Number of neurons of each cell class (in colour code) in each area, expressed as a percentage of the total number of neurons recorded in each area. **(C)** Heat maps and population response of all the recorded neurons recorded in each area during EXE, subdivided into the cell classes to which they belong. Conventions as in Figure 3.2A. Note that there are only 2 suppressed neurons in CL1 of AIP, so their average population line has not been plotted. Green and yellow marks represent average ± standard deviation of movement onset and pull, respectively. See also Figure S3.5. **(D)** Heat maps and population response of all the neurons recorded in each area during OBS, subdivided into the cell classes to which they belong. Conventions as in Figure 3.2C. See also Figure S3.6.

The same analysis applied to OBS (Figure 3.5D and S3.6) confirmed the stronger activity of neurons in area F5 compared to those in AIP and F6 ($p < 0.001$ for both comparisons) regardless of the cell class and, in particular, during action observation relative to both baseline ($p < 0.001$) and object presentation epoch ($p < 0.001$), which in turn did not differ from each other ($p = 0.2$). Among cell classes, neurons of classes 1 and 2 showed greater firing rates during action observation relative to baseline and object presentation ($p < 0.05$); in particular, class 1 neurons of F6 exhibited a greater firing rate than neurons of classes 2 ($p < 0.05$) and 3 ($p < 0.05$) in the same area. The overall lower modulation of neuronal firing rate across epochs of OBS relative to EXE is likely due to a generally lower discharge of individual neurons during OBS than EXE and to the increased proportion of neurons (Figure S3.6F) showing unmodulated or suppressed response in this context. Suppressed neurons may play a role in balancing the overall motor output during action observation[135].

Mutual modulation of activity during action execution and observation: cell-class and areal specificities

As a final step, we asked whether and to what extent individual neurons' modulation during the movement epoch of EXE and OBS jointly varied depending on area and cell class. Indeed, the only available evidence so far concerns antidromically-identified pyramidal tract neurons of the ventral premotor[114] and primary motor[115] cortex, which often modulate their firing rate in an opposite manner during action execution and observation. Previous studies typically investigated this issue in individual areas and with an epoch-based approach[16,56,114,136,137], which cannot be equally adapted to the firing properties of neurons in the various areas here investigated, where individual neurons' activity has been tested with sliding t-tests (see Methods).

Thus, to address this issue within cell-classes and areas in our data set, we devised an index to measure in a time-resolved manner the mutual modulation depth (MMD) of individual neurons' discharge during EXE and OBS (see Methods). MMD values in the two tasks (Figure 3.6A) are closer to 1 the greater is the positive (Neuron 1) or negative (Neuron 2) mutual modulation of the neuron's activity in the two tasks, and are closer to -1 the greater is the opposite positive-negative (Neuron 3)

or negative-positive (Neuron 4) modulation of the neuron's activity in EXE and OBS. MMD values are close to zero whenever a neuron's discharge shows no modulation in any (Neuron 5 and 6) or both of the tasks. By looking at MMD changes of the different cell classes in each area (Figure 3.6B) during the task-unfolding period, we found increased MMD for cell class 1 and 2 following movement onset, particularly in AIP and F5, whereas neurons of cell class 3 did not show any relevant MMD change (with the exception of cells of class 3 in F5, which slightly increased their MMD later on, during object pulling). These findings indicate that neurons with narrow spikes exhibit stronger mutual modulation during action execution and observation.

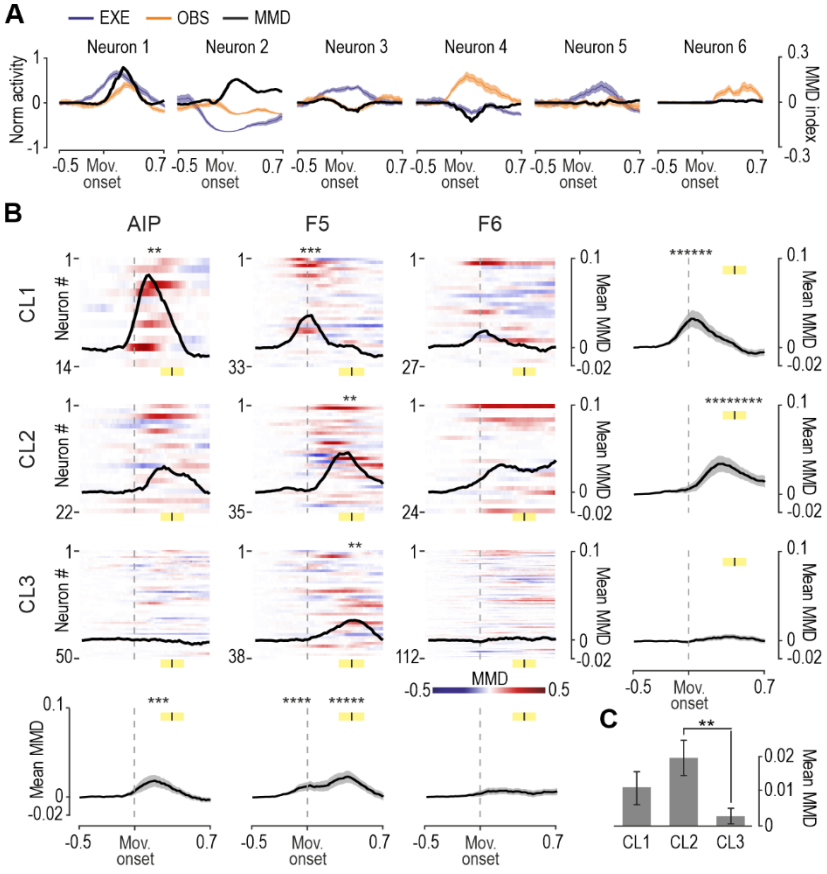

Figure 3.6. Mutual modulation of activity during action execution and observation: cell-class and areal specificities. (A) Example of neurons showing a positive (Neurons 1 and 2), negative (Neurons 3 and 4), or flat (Neurons 5 and 6) MMD index during the movement epoch (aligned to the movement onset). Black curves represent the MMD time course, and coloured trace represents the average ± standard error net soft-normalised firing rates aligned to movement onset for EXE and OBS. **(B)** Heatmaps show the MMD time course for each neuron within areas and cell class (see color scale bar on the bottom right corner); black curves represent the average MMD values. Yellow marks represent average ± standard deviation of object pulling time. Asterisks above each curve indicate sets of at least 5 consecutive time bins (200 ms in steps of 20 ms) of significantly increased MMD relative to the first 5 bins of the investigated period (one-tailed paired samples t-tests, $p<0.05$). Each panel in the last row and column represents the time course of MMD index averaged across cell classes and areas, respectively; grey shadings represent standard errors. Vertical black bars centred on the yellow shaded region represent average ± standard deviation of pulling onset. The distribution and properties of neurons in each class depending on their modulation in EXE and OBS is shown in Figure S3.7. **(C)** Histograms show the mean MMD index (± Std Error) for each Class. A 3 x 3 factorial ANOVA (factor: Class and Area) showed significant main effect of the factor Cell Class, and Newmann-Keuls post-hoc tests revealed greater MMD of Class 2 neurons relative to Class 3 ($p < 0.002$).

3.4 DISCUSSION

In this study, we recorded single-neuron activity from three crucial nodes of the AON, the intraparietal area AIP and the premotor areas F5 and F6, during the execution and observation of reaching-grasping actions in a Go/No-Go paradigm. By leveraging the same tasks in all areas, we provided comparative evidence of temporal and neuronal tuning specificities at the system-level and, at the same time, shed light on the cell-class coding principles that contribute to the AON functioning.

During action execution (Figure 3.2A), more than half of AIP and F5 neurons exhibit a facilitated response, whereas in F6 the majority of neurons showed suppressed discharge. During task unfolding (Figure 3.7), area F6 neurons become active after cue sound onset, allowing to decode whether an action will be performed earlier than in the other areas (Figure 3.2C); this information spread to F5 and finally to AIP (Figure 3.7A). When the target object is presented (Figure 3.7B), AIP generates an early and robust signal conveying object selectivity, closely coupled with that of F5: the object decoding accuracy obtained with the signal of these areas is followed by a lower and later object selective signal conveyed by area F6. This latter area reaches its peak of facilitated activity shortly after the Go signal, followed by that of F5 and AIP (Figure 3.7C), which are known to support proper execution of the visually-guided grasping[127,138]. These results favor a model in which F6 signals whether and when a forthcoming action has to be performed and receives feedback visuomotor information about graspable objects and ongoing actions from the AIP-F5 circuit[128,139].

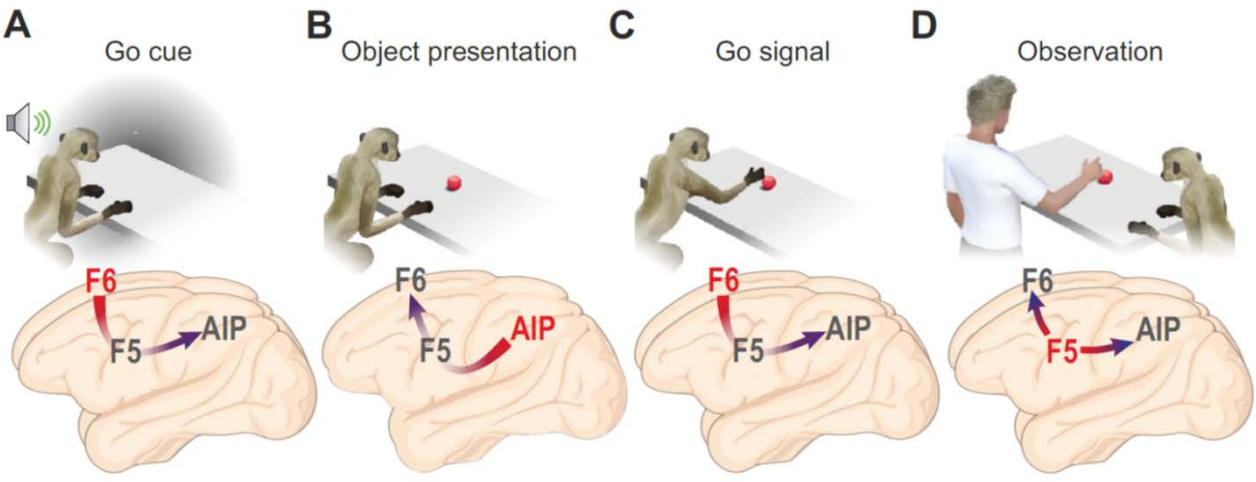

Figure 3.7. Schematic representation of the sequential contribution of AIP, F5 and F6 to tasks stages. (A-C) Sequence of epochs of the execution task and time course of the activation (from red to blue) of the investigated areas in each epoch. **(D)** Experimenter's movement epoch of the observation task.

As illustrated in Figure 3.7D, and in line with existing evidence from anatomo-functional tracing studies[56,59,106], area F5 plays a key role in this network even during action observation. All areas showed weaker modulation in their overall activity during action observation (Figure 3.2B), both because of a generally lower discharge of individual neurons and a greater number of neurons showing suppressed discharge than during action execution. This applies particularly to AIP and F6. Indeed, F5 has a prevalence of facilitated neurons during both action observation and execution and it is the only studied area with a cortico-spinal output[140–142] and robust, direct connections to M1[143,144]; furthermore, it shows a stronger and earlier modulation than do AIP and F6, consistently with recent neuronal population data emphasizing the representational similarity of executed and observed actions in F5[137,145]. Importantly, control analyses of the temporal priority of F5 over the other two areas confirmed its capacity to actively generate a signal that not only anticipates the onset of another's observed action[130] but is also independent from the signal coming (260 ms later) from AIP or F6. Previous studies have demonstrated that F5 neurons can internally generate representations of external events even with limited[131,145] or no[117] visual information, and with very modest selectivity for the visual features of the stimuli[132]. In line with previous works[56,57,84], we did not find object/grip type selectivity in the observation task in any of the investigated areas. This finding could be due to the fact that monkeys were not paying attention to the details of the experimenter's action because they were required to maintain fixation[146]; previous studies with free-gazing monkeys did actually reported object/grip selectivity in both parietal[108] and premotor[147] neurons recorded during observation of actions performed in the monkey's peripersonal space. In our study, observing the action in a completely extrapersonal space[148] may have further reduced object/grip selectivity. Thus, our findings support the idea that areas of the AON contribute to the temporal sequencing of motor events underlying others' observed actions[145] rather than their detailed perceptual analysis. Interestingly, in a predictive coding framework[149,150], the present findings suggest that among the tight reciprocal connections between F5, AIP and F6[56,59,106,151], the projections carrying predictive signals from area F5 may have an overriding functional relevance in triggering neuronal activity at all levels of the network relative to feedforward information coming from visual areas, at least in highly predictable contexts. This model has recently received direct support from simultaneous recordings and chemogenetic manipulations of neuronal activity in the F5-to-F6 neural circuit, demonstrating that coordinated activity along this pathway has a causal role in social action monitoring[152].

How do the key functional properties of the distinct nodes of the AON considered thus far map onto different cell classes? A null hypothesis would assume that distinct visuomotor functional properties are equally represented by different sets of neurons distinguished by their extracellular spike shape. The only attempt made so far for addressing this issue is constituted by studies that antidromically-identified as pyramidal tract cells a set of F5[114] and M1[115] neurons and showed that they can exhibit mirror properties: interestingly, more than half of them suppressed their spontaneous activity during action observation. In the present study, we applied recently validated methods to perform an unbiased clustering of single-neuron waveforms, blind to the area of origin[116]. In our dataset, we could distinguish three neuronal classes, varying in terms of their spike width from relatively narrow spiking (class 1 and 2) to broad spiking (class 3) neurons[120,121,153–155]. By assessing cell-class responses in the execution and observation tasks, we found that narrow spiking neurons fired stronger during baseline, object presentation and action execution/observation and showed a greater tendency to fire in bursts relative to broad spiking neurons. These latter, in turn, exhibited slower and more regular firing patterns, with greater selectivity for the target during both object presentation and grasping execution relative to narrow spiking neurons. These differences among neuronal classes are consistent with those reported by earlier studies that have examined different tasks in other cortical areas[156–158].

In terms of areal specificities, we found that F5 hosts a greater proportion of narrow spiking neurons, considering classes 1 and 2 together, whereas F6 exhibits the opposite trend, with a greater proportion of neurons belonging to class 3. Many previous studies suggested that neurons with narrow spikes correspond to putative interneurons[118,159–162] but a reliable association of class 1 (and at a certain extent, class 2) neurons with putative interneurons cannot be made as interneurons with broader spikes have been described as well[163]. Furthermore, there are many issues that can influence spike width even among interneurons[164,165]. Finally, there is evidence that in areas hosting big pyramidal cells, like F5[166], the bigger the pyramids the thinner the spike waveform[136]: this may be a likely explanation for the prevalence of neurons in classes 1 and 2 in F5 relative to AIP and F6, which have smaller pyramidal cells as directly verified in histological slices of the brain regions investigated in the present study (Figure S3.3C). The fact that F5 has been recorded with daily-inserted, movable linear probes[53] may have further biased the sampling of bigger pyramidal cells with respect to the other two areas.

Interestingly, in all areas, especially AIP and F5, shared motor and sensory coding of one's own and others' action (as revealed by the MMD) is predominantly operated by more narrowly spiking neurons (classes 1 and 2), whereas broad spiking neurons (class 3) mostly encode either self- or other-related (unimodal) information. According to a previous hypothesis[40], cortico-cortical and cortico-striatal neurons could receive efference copies of motor actions encoded by cortico-spinal (pyramidal) neurons, supporting an evolutionarily ancient mechanism of sensorimotor remapping, which was previously demonstrated directly in songbirds[167]. This mechanism has been shown to be optimized for shaping social responses and may also contribute to the previously observed overall suppression of discharge of pyramidal (especially corticospinal) neurons during action observation.

In summary, the present findings shed light on the temporal and network-level organization of self and others' action in three of the recently recognized nodes of the AON in the monkeys. Although solely based on our results we cannot conclusively determine the correspondence between physiologically-identified neuronal classes and their histological nature (e.g. pyramidal cell vs inhibitory interneurons), our findings suggest that visuomotor properties may be unevenly represented by distinct cell classes, possibly including inhibitory interneurons. However, cell-specific causal manipulations studies with optogenetic or neuropharmacological approaches[168] are needed to investigate the possible correspondence between functional- and morphologically-identified cell classes, whose elucidation would considerably advance our understanding of the mechanisms underlying the wide range of perceptual and socio-cognitive functions implemented by the cortical motor system.

4 LARGELY SHARED NEURAL CODES FOR BIOLOGICAL AND NONBIOLOGICAL OBSERVED MOVEMENTS BUT NOT FOR EXECUTED ACTIONS IN MONKEY PREMOTOR AREAS

The neural processing of others' observed actions recruits a large network of brain regions (the action observation network, AON), in which frontal motor areas are thought to play a crucial role. Since the discovery of mirror neurons (MNs) in the ventral premotor cortex, it has been assumed that their activation was conditional upon the presentation of biological rather than nonbiological motion stimuli, supporting a form of direct visuomotor matching. Nonetheless, nonbiological observed movements have rarely been used as control stimuli to evaluate visual specificity, thereby leaving the issue of similarity among neural codes for executed actions and biological or nonbiological observed movements unresolved. Here, we addressed this issue by recording from two nodes of the AON that are attracting increasing interest, namely the ventro-rostral part of the dorsal premotor area F2 and the mesial pre-SMA F6 of macaques while they 1) executed a reaching-grasping task, 2) observed an experimenter performing the task, and 3) observed a nonbiological effector moving in the same context. Our findings revealed stronger neuronal responses to the observation of biological than nonbiological movement, but biological and nonbiological visual stimuli produced highly similar neural dynamics and relied on largely shared neural codes, which in turn remarkably differed from those associated with executed actions. These results indicate that, in highly familiar contexts, visuo-motor remapping processes in premotor areas hosting MNs are more complex and flexible than predicted by a direct visuomotor matching hypothesis.

4.1 INTRODUCTION

Since the pioneering study on mirror neurons (MNs), a class of cells originally discovered in area F5 of the macaque discharging during both action execution and observation, it was reported that "responses to tools or to objects moved in such a way as to imitate the effective action were usually weak or absent altogether"[39]. These findings emphasized the similarity between the neural codes for observed and executed actions, that is, the visual and motor formats. Nonetheless, subsequent studies have shown that MNs in various nodes of the AON[40] can exhibit visual responses to actions performed with tools[169,170], actions implied by moving cues[132,171–175], or even withheld actions signaled by an instructive cue[117,130], suggesting a greater flexibility and broader relationship between the visual and motor codes.

Recent studies have shown that the population dynamics associated with action execution and observation exhibit similarities in area F5 but not in M1[137,145], but they have not tested nonbiological motion stimuli. Here, we recorded from two important nodes of the AON - the ventro-rostral part of the dorsal premotor area F2[147] and the mesial pre-SMA F6[106] - under two main alternative hypotheses: 1) an "action hypothesis" (Figure 4.1A), which predicts greater similarity in the representation of "actions", regardless of their visual or motor format, and 2) a "format hypothesis" (Figure 4.1A), which predicts greater similarity between the visual formats, regardless of the biological or nonbiological nature of the stimuli.

4.2 METHODS

Animal models

Two purpose-bred, socially housed male macaques (Mk1, Macaca nemestrina, 9 kg, and Mk2, Macaca mulatta, 7 kg) were used for the present study. Monkeys were first prepared for electrophysiological recordings as previously described[50] and trained to perform the tasks described below. All experimental protocols complied with the European law on the protection of animals used for scientific purposes (2010/63/EU), were approved by the Veterinarian Animal Care and Use Committee of the University of Parma (Prot. 78/12, 17/07/2012 and Prot. 91/OPBA/2015), and were authorized by the Italian Ministry of Health (D.M. 294/2012-C, 11/12/2012 and 48/2016-PR, 20/01/2016).

Apparatus and behavioral paradigm

Monkeys performed a reaching-grasping Go/No-Go task (Figure 4.1B, EXE) with three different objects (a ring, a small cone, and a big cone) as potential targets, to be grasped with three different grip types (hook grip, side grip, and whole-hand prehension, respectively). Furthermore, they observed the same task performed by an experimenter in their extrapersonal space (Figure 4.1B, OBSb)[16,34] and a variant of the observation task (Figure 4.1B, OBSnb) in which an elongated object (a metal cylinder) was moved with nonbiological kinematics along the trajectory followed by the experimenter's arm during OBSb (only the ring object in the Go trials was used in this task). The cylinder's movement was triggered by a light smack applied on its extremity (invisible to the monkey) by the experimenter, which activated an automatic drawer-like sliding mechanism producing a regular and perfectly linear (hence nonbiological) shift forward of the cylinder toward the target, where it stopped. Trials were separated by a variable (from 1 to 1.5 s) intertrial period. The temporal

sequence of task events was the same in the three tasks (EXE, OBSb, and OBSnb, Figure 4.1C), run in different blocks.

The task phases were automatically controlled by LabView-based software: error trials were discarded (no reward was delivered) and repeated until at least 10 trials were collected for each condition. Here, we compare Go trials of EXE, OBSb, and OBSnb, in addition to the No-Go trials of OBSb as a control (hereafter referred to as NOGO task).

Recording Techniques

Area F2 (Figure 4.1D) was studied with acutely inserted linear silicon probes[53,54] with 16 recording sites spaced by 250 µm apart along 3.75 mm of an 8-mm shank (80 µm wide x 100 µm thick). Area F6 (Figure 4.1D) was investigated with four chronically implanted multishaft 3D arrays of linear silicon probes with eight recording sites per shaft and two parallel modules of four shafts per probe (64 channels per probe). Previous studies have presented the reconstruction of the location of the recording sites[16,51]. The signal was amplified and sampled at 40 kHz with a 16-channel Omniplex recording system (Plexon). In the case of the chronic implants, different sets of 16 channels were recorded only once during separate sessions on different days.

Monkey had to maintain central fixation throughout the entire trial duration in all tasks, which was monitored with an eye-tracking system ([34]; the tolerance radius of the fixation window was set at 5°). Previous analyses of the electromyographic activity of proximal and distal forelimb muscles of these two monkeys during the tasks[34] allow us to exclude the possibility that preparatory motor activity is present during the No-Go and observation trials.

Analysis of the neuronal activity

Spike sorting was performed off-line with fully automated software[55]. Uniform and restrictive criteria were applied to the selection of single units in both areas[176], and nonseparable spikes were also considered as multiunit activity (altogether referred to as “units”). Units were preliminarily tested by comparing their baseline activity (500 ms before object presentation) with each bin in the interval from 600 ms before to 600 ms after movement onset (one-tailed sliding t-test, window = 200 ms, step = 20 ms, $p < 0.05$, uncorrected). We regarded as facilitated or suppressed all those neurons with at least five consecutive bins significantly greater or lower than baseline activity, respectively. Neurons that did not meet this criterion were considered unmodulated. Only units modulated during OBSb and/or OBSnb were included in subsequent analyses.

Population analysis

We computed the object-averaged net soft-normalized activity for all selected units and tasks[176] and used it to produce the heatmaps. In this study, we were not interested in the contextual effect of the cue sound, which has been described in previous studies[34,176]; therefore, we focused our analysis on the time period following object presentation, taking as baseline the 500-ms interval before this event. We grouped units into facilitated or suppressed, depending on the sign of their average modulation during the movement period within each task (± 600 ms relative to movement onset in EXE, OBSb, and OBSnb; ± 600 ms relative to the No-Go signal in OBSb). To test whether neurons were significantly facilitated/suppressed, we used the 10 trials with the ring object as a target, which was identical for all tasks.

A one-way repeated measures ANOVA was applied to the net soft-normalized activity (averaged in a movement epoch corresponding to the 500-ms interval after movement onset) taking the task as main factor (four levels: EXE, OBSb, OBSnb, and NOGO); a Tukey-Kramer test was used for post-hoc comparisons. The fraction of units exhibiting a significantly different modulation between OBSb and OBSnb was obtained by applying a two-tailed paired t-test between the net soft-normalized activity of the ring-object trials of the two tasks (averaged in the 500-ms interval following movement onset, $\alpha = 0.05$).

Neural subspace analysis

We quantified the similarity in the neural population codes among tasks by computing the residual variance obtained after projecting the neural trajectory of one task onto the neural subspace of another[177]. We first calculated the soft-normalized firing rates of each unit in the time interval -600/+800 ms around movement onset for each task (or in the same interval around the No-Go signal in the NOGO task). Specifically, the spiking activity of each neuron was binned in 20-ms time windows, trial averaged, smoothed with a 60-ms Gaussian kernel, and soft-normalized by its absolute maximum (across conditions and tasks, + 5 spk/s). We thus obtained 10 matrices, each of dimensions T x N (T being the number of time bins, N the number of units), as follows: one matrix for each object tested in EXE, OBSb, and NOGO, and one for the unique object used for OBSnb.

First, for any pair of tasks A and B, we applied principal component analysis (PCA) to the corresponding mean-centered data matrices X_A and X_B (two principal components typically captured > 60% of the total variance), obtaining the coefficients of the first two principal components V_A and V_B. Next, we evaluated the overlap or "alignment" of task A over task B by projecting the neural

activity of *A* onto the principal components V_B and computing the residual variance normalized by the variance captured by the first two principal components V_A, as follows[137]:

$$alignment_{AB} = \frac{tr(V_B^T cov(X_A) V_B)}{tr(V_A^T cov(X_A) V_A)}$$

The alignment ranges from 0 (if neural subspaces are orthogonal) to 1 (if neural subspaces are perfectly aligned). As an estimate of the between-tasks alignment, we took the average alignment across every pair of objects of two different tasks; similarly, to estimate the within-task alignment, we took the average alignment across every pair of objects within that task. Then, to quantify the difference between alignments, we randomly sampled with replacement from the considered population a number of units equal to the population size, and we calculated for that sampled population the between- and within-task alignments and the pairwise alignment differences among them. We repeated this procedure 2000 times and considered any two alignments significantly different from each other if their alignment difference was higher or lower than 0 (corresponding to a two-tails $\alpha = 0.05$) in at least 97.5% of the iterations.

The drawings of neural population trajectories were produced as follows. Given the neural activity matrices *X* of a given population (obtained as described above), we normalized each matrix for the number of units *N* contributing to it; this allowed us to visually compare the amplitude of neural trajectories of populations with a different number of units. Then, we normalized the resulting matrices for the square root of their corresponding total variances to make the amplitude of the projected population trajectories comparable across tasks (irrespective of the magnitude of their overall modulations), thereby reflecting the value of alignment. Finally, the resulting activity matrices were projected onto the first two PCs of EXE and OBSb (which explained the largest fraction of variance of object-averaged EXE and OBSb activity, respectively), and the resulting two-dimensional neural trajectories were averaged across objects to obtain a single trajectory for each task.

4.3 RESULTS

We tested 549 units (175 single units and 374 multiunits) from area F6 (N = 357; 178 from Mk1 and 179 from Mk2) and F2 (N = 192; 27 from Mk1 and 165 from Mk2) with all tasks. Of these, 155 became active only during EXE (N = 134) or were not significantly activated in any of the tasks (N = 21). The remaining 394 units (N = 164 from Mk1 and N = 230 from Mk2) were significantly modulated during

OBSb and/or OBSnb; of these, 267 were recorded from area F6 and 127 from area F2: these units constituted the data set of the present study.

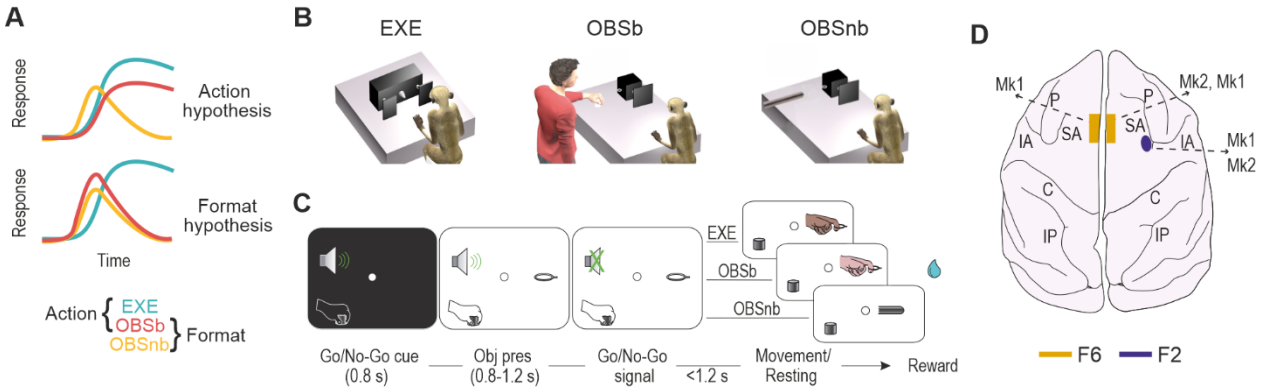

Figure 4.1. Experimental hypotheses, behavioral tasks, and recorded regions. (A) The action hypothesis predicts greater similarity between EXE and OBSb than between either and OBSnb; the format hypothesis predicts greater similarity between OBSb and OBSnb than between either and EXE. **(B)** Schematic representation of the setting for each task: execution (EXE), observation of a biological (OBSb) or nonbiological (OBSnb) movement in the monkey's extrapersonal space. **(C)** Temporal sequence of task events. Following the presentation of a central fixation point[57], fixation onset caused the presentation of a cue sound, either 1200 or 300Hz, which instructed the monkey to grasp (Go cue) or refrain from grasping (No-Go cue) the subsequently presented object, respectively. Following object presentation (Obj pres) the sound ceased and the monkey reached, grasped, and pulled (for 0.8 s) the object (or in the No-Go condition, remained still for 1.2 s) to receive a fixed amount of juice reward, automatically delivered after each correctly performed trial. In the No-Go trials of OBSb the monkey had to simply observe the experimenter remaining still until the end of the trial. **(D)** Recorded regions in the two monkeys reported on the schematic reconstruction of Mk2's brain. C, central sulcus; IA, inferior arcuate sulcus; IP, intraparietal sulcus; P, principal sulcus; SA, superior arcuate sulcus.

During EXE, the majority of the recorded units in both F6 (56.9%, Figure 4.2A) and F2 (76.4%, Figure 4.2B) exhibited facilitated responses, in contrast to the observation tasks, in which the modulation of activity was lower and characterized by a more balanced number of facilitated and suppressed units (Figure 4.2A and B, OBSb and OBSnb). During the No-Go condition of OBSb (NOGO), the unmodulated units prevailed (42.7%), in line with the essentially motor nature of the two areas. Figure 4.2C-D shows that, although most of the units in both F6 (64%) and F2 (67%) showed no significantly different activation between OBSb and OBSnb, the average modulation in both areas was stronger for OBSb than for OBSnb and NOGO, and units with a preference for OBSb were more numerous than those preferring OBSnb, especially in F6.

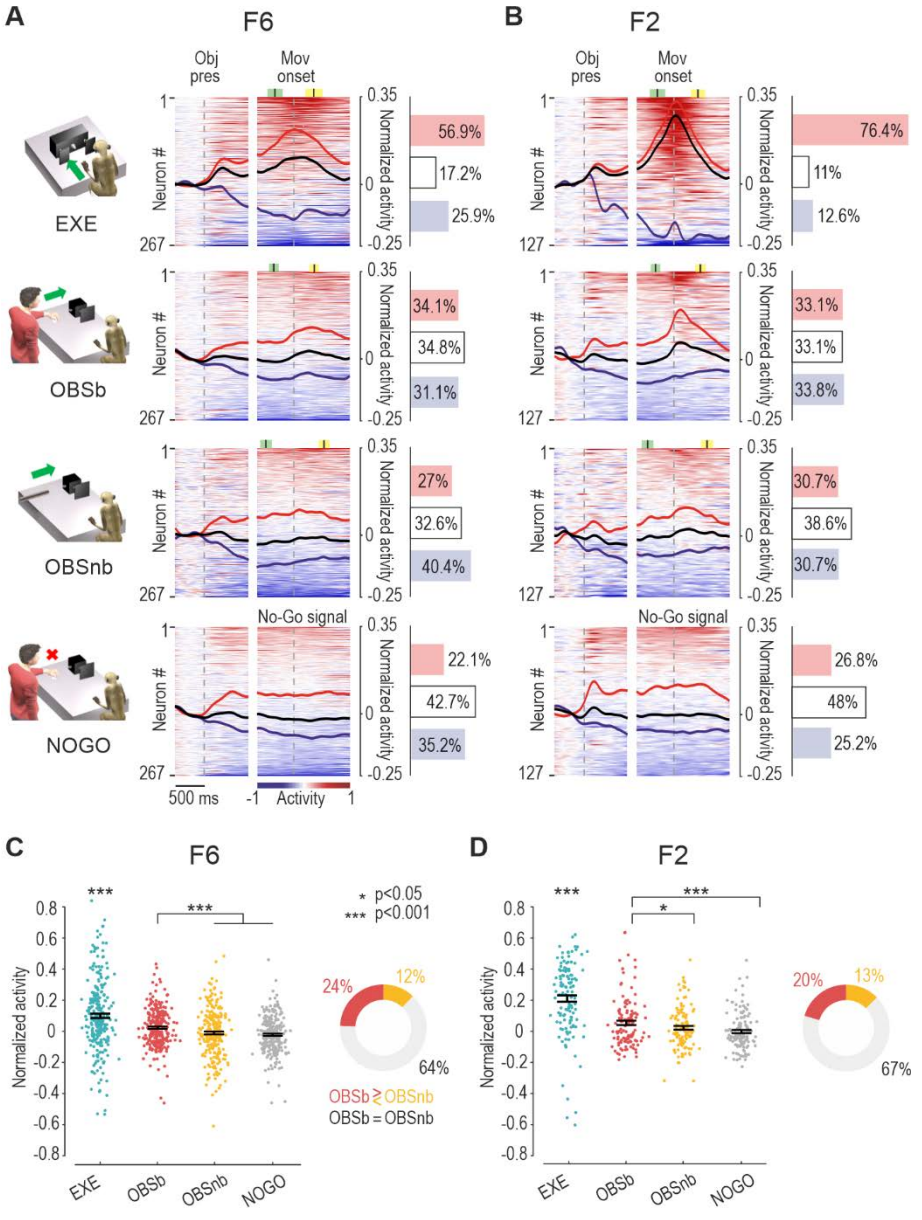

Figure 4.2. Neural-activity time course in the different tasks. **(A)** Heat maps of neural activity in area F6 during each task. Each line represents one unit. Units are ordered (from top to bottom) based on the magnitude of their activity with respect to baseline (red = facilitated, blue = suppressed) in the interval -600/+600 ms relative to movement onset (or in the case of NOGO, the No-Go signal), independently for each task. Black lines represent the averaged response of each population as a whole, whereas red and blue lines represent the averaged response of units with overall positive or negative modulation in the movement epoch, respectively (see Methods). The histograms on the right indicate the percentage of significantly facilitated (red), suppressed (blue), and nonsignificant (white) units ($p < 0.05$, see Methods) in each area. Colored markers represent the average ± 1 standard deviation of the Go/No-Go signal (green) and pulling onset (yellow). **(B)** Heat maps of neural activity in area F2. Conventions as in A. **(C)** Left: average net soft-normalized activity of F6 units during the overt movement epoch (500-ms after movement onset) of EXE, OBSb, OBSnb, and NOGO. Each dot represents one unit. One-way repeated measures ANOVA ($F(3,798) = 43.51$, $p = 4.8 \cdot 10\text{-}26$, $\eta 2 = 0.083$) followed by Tukey-Kramer post-hoc test indicates higher activity in EXE relative to all the other tasks and in OBSb relative to OBSnb and NOGO. Right: percentage of units with preference for OBSb vs OBSnb ($X2 = 11.23$, $p = 8.1 \cdot 10\text{-}4$). **(D)** Same as in C for F2 units. Left: One-way repeated measures ANOVA ($F(3,378) = 49.27$, $p = 6.7 \cdot 10\text{-}27$, $\eta 2 = 0.200$) followed by Tukey-Kramer post-hoc test indicates higher activity in EXE relative to all the other tasks and in OBSb relative to OBSnb and NOGO. Right: percentage of units with preference for OBSb vs OBSnb ($X2 = 2.38$, $p = 0.123$).

Next, we assessed the similarity in the neural codes of biological and nonbiological movements at the population level by applying recently proposed approaches[137,178]. For each task, we projected the activity during the epoch of interest (i.e., movement/No-Go epoch, depending on

the task) onto the plane defined by the first two principal components of EXE for both F6 (Figure 4.3A) and F2 (Figure 4.3B), and quantified the fraction of residual variance by computing the alignment index (see Methods). We found that the trajectories of OBSb and OBSnb were smaller than that of EXE but, more importantly, that their alignment with the neural plane of EXE did not differ significantly in either F6 (bootstrap procedure p = 0.087, see Methods) or F2 (p = 0.60), indicating that, contrary to the "action hypothesis" (Figure 4.1A), OBSb did not exhibit greater similarity with EXE than with OBSnb.

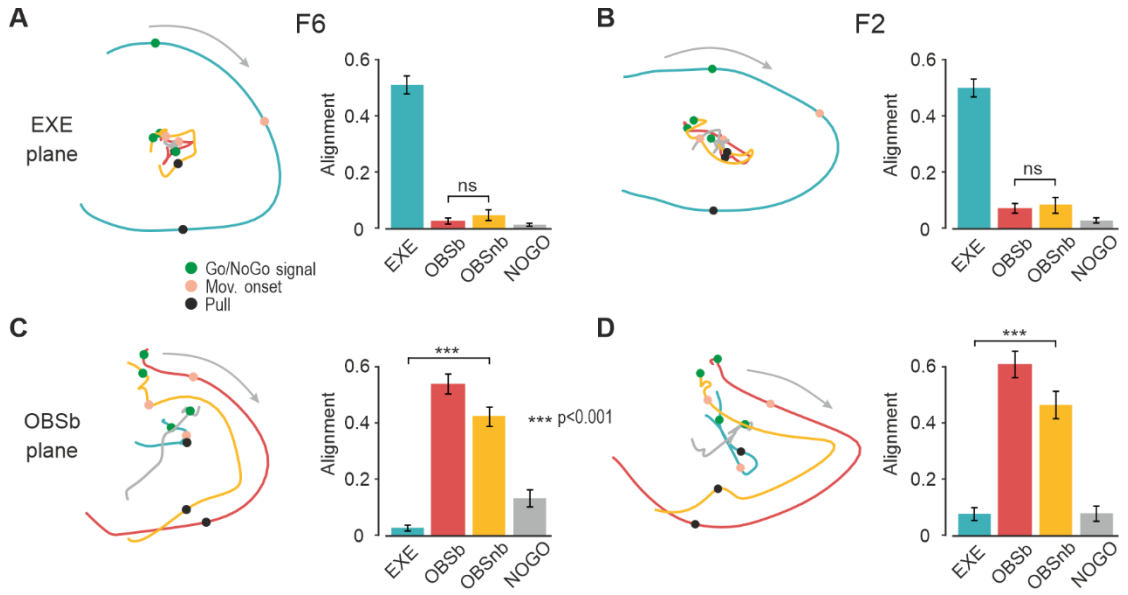

Figure 4.3. Neural similarity of population dynamics among tasks. (A) Left: projections of F6 neural population trajectories (trials and objects averaged) of different tasks onto the neural plane defined with reference to EXE (explained variance: PC1 = 33.5%, PC2 = 21.2%). Right: alignment index among tasks. Error bars were obtained using bootstrap repetitions by resampling units (see Methods). EXE showed the highest alignment (p ≈ 0 for all comparisons); NOGO showed the lowest (p = 0.163 vs OBSb; p = 0.035 vs OBSnb, which in turn did not differ from each other, p = 0.087). **(B)** Same as A for area F2 (explained variance: PC1 = 38.7%, PC2 = 17.8%). EXE showed the highest alignment (p ≈ 0); NOGO showed the lowest (p = 0.080 vs OBSb; p = 0.076 vs OBSnb, which in turn did not differ from each other, p = 0.60). **(C)** Population trajectories and alignment index as in A, but with reference to OBSb (explained variance: PC1 = 32.1%, PC2 = 13.2%). OBSb showed the highest alignment (p ≈ 0); for all other comparisons OBSnb > NOGO > EXE (p ≈ 0). D: same as C for area F2 (explained variance: PC1 = 28.8%, PC2 = 23.7%). OBSb showed the highest alignment (p ≈ 0); OBSnb > NOGO and EXE (p ≈ 0), which in turn did not differ from each other (p = 0.52). Note that the same results are obtained if the analyses are applied in individual monkeys, separately.

The same analysis was performed by taking OBSb as a reference. In both areas (Figure 4.3C and D), the neural trajectories of OBSb and OBSnb followed a similar evolution, strikingly different from that of EXE and NOGO. Importantly, the alignment of OBSnb with OBSb was significantly greater than that of EXE in both F6 (p ≈ 0) and F2 (p ≈ 0), in line with the prediction of the "format hypothesis".

4.4 DISCUSSION

In this study, we contrasted two main alternative hypotheses (Figure 4.1A): according to the "action hypothesis", one would expect greater similarity in the representation of "actions", regardless of their visual or motor format, as compared to nonbiological motion stimuli[39,104,179]; according to the "format hypothesis", by contrast, one would expect greater similarity between the visual format of biological and nonbiological stimuli than between either and executed actions[132,180,181]. Our findings indicate that although some neurons fired more strongly for observed actions than for nonbiological movements, in both areas F6 and F2 the neural representations of biological and nonbiological movements exhibit considerable similarity and strongly differed from the neural representations of executed actions, lending clear support to the format hypothesis.

It should be noted that the very low degree of overlap between the visual and motor codes reported here seems to contrast with the findings of previous studies[137,145,147]. However, some important differences may explain this discrepancy. First, in these studies, the target of the experimenter's action was closer to the monkey, which is known to exert a considerable effect on premotor neurons' visual responses[34,57,106,148,182]. Second, exploratory eye movements, which the monkey was allowed to perform in the aforementioned studies but not in our experiment, may have facilitated action observation responses[148], thereby increasing the visuomotor similarity. Nonetheless, even if the distance from the target and the fixation may have caused a reduced similarity between action observation and execution in our experiment, these constraints were the same for both observation tasks and hence cannot account for the remarkable similarity observed between biological and non-biological stimuli. A final possibility is that the discrepancy with the above mentioned previous studies may be due to the fact that they focused on F5 neurons whereas the present study dealt with F2 and F6; the remarkable similarity in the visuomotor properties of F5 and the ventro-rostral portion of F2 reported by previous studies[147] makes this interpretation less plausible (at least for F2), and suggest that similar result could be obtained in area F5 as well, in line with previous studies[132].

Future studies with longitudinal chronic recording approaches may address the issue of whether and how premotor neuronal activity becomes so similar for visual stimuli that are remarkably different from the physical and perceptual point of view. One possibility is that the highly predictable task context, in which the monkey was overtrained, had created a generalization between the biological action (which the monkey was used to seeing in that context for a very long time) and

the nonbiological stimulus, consistently with the fact that even neurons in the primary motor cortex can become active in similar conditions[173,174]. The findings of previous studies in both ventral[117,130], dorsal[175], and mesial[16] premotor cortices suggest that visually-triggered activity in highly predictable contexts has a considerable anticipatory capacity: the same activity could then be evoked by the sight of similar temporal sequence of events[145] despite perceptually different kinematics features. The hypothesis of an increased neural similarity caused by the repeated association between biological and nonbiological movements along the same spatial trajectory is supported by previous human fMRI data showing that areas of the human MN system can activate similarly for hand movements and meaningless artificial movements of objects in space, likely because an association of objects' movements with biological movements is evoked[180]. An additional, and not mutually exclusive, hypothesis is that greater neural similarity between (visual) formats is the result of the rehearsal of a shared motor representation afforded by both the visual stimuli[110]. This interpretation should lead to the hypothesis that, although apparently "visual" in nature, both observed actions and nonbiological motion stimuli produce much greater activation when presented within the monkey's operational space, especially when from a subjective viewpoint[106], thereby confirming their eminently pragmatic nature.

In summary, our findings show that in two key regions of the monkey AON, biological and nonbiological visual stimuli recruit highly overlapping neural substrates and dynamics, emphasizing the plasticity and the generalization capacities of the visual-to-motor mapping in premotor brain regions, whose functional role still needs to be explored with causal techniques[152].

5 GENERAL DISCUSSION

More than 30 years of neurophysiological studies on macaque monkeys suggest that area F6, the homologue of the human pre-SMA, plays a role in a variety of apparently well distinguished situations. Several studies assigned to F6 a role in motor preparation, emphasizing its contribution in the execution of reaching-grasping actions[4,16,20–22,34,47] or sequences of multiple actions[15,23,24]. Subsequent studies extended the range of functions ascribed to this area, including more cognitive ones such as the estimation of time intervals[25–30], the update of motor plans based on contextual changes[20,23,31], and the coordination of social interactions[32–35]. The classical studies on area F6[4,20,21], by stressing its specificity relative to neighboring areas, implicitly emphasized the existence of a discrete, essentially homogenous, area with a multiplicity of associated functions. However, it is hard to reconcile the variety of observed functions within a unique, specific, and indeed still undetermined computational principle. Instead, one may accept the idea that cytoarchitectonical, anatomical, and functional properties vary along a continuum so as close parts within the same area are as similar as equally close parts in neighbor areas, at least in the mesial frontal region[1].

Several evidence point toward this continuum hypothesis. The granularity of layer IV [6,7], the receptor-expression[8], the electrical excitability[3,16,19], the somatotopy[3,15,17,18] and the visual/somatosensory responses[4,19] of the mesial frontal areas all vary in a gradient-like fashion along the rostro-caudal direction. Unfortunately, despite some indirect evidence[32,35,47] the discrete nature of tracers' injections and neuronal recordings, normally localized at the putative center of target areas, have hindered the identification of possible gradual changes in connectivity and functional properties.

In the first of the presented studies[106], we addressed this issue and assessed the anatomo-functional heterogeneity of area F6. We found that caudal F6 showed higher tuning for executed actions and their target objects, for observed actions, and for the agent who will act before trial onset, in line with the closeness to the more motor-related area F3[3]. By contrast, rostral F6 showed a clearer distinction for object presented within vs outside the monkey reaching space, likely signaling whether the monkey can act on the object[34,183]. From the anatomical point of view, the caudal F6 resulted strongly linked with dorso-ventral premotor areas and motor putamen whereas the rostral F6 exhibited tighter connections with the lateral prefrontal cortex and associative putamen. The above anatomo-functional differences should not be interpreted as the existence of two anterior and posterior subregions within area F6, but rather as a smooth change in the anatomo-functional

properties along the rostro-caudal axis, likely encompassing the neighboring mesial frontal areas as well[1]. Thus, area F6 appears to be strictly inhomogeneous, crossed by multiple gradients in connectivity and functional properties that might in part account for the multiplicity of functions attributed to this area. Given the substantial homology between the mesial frontal cortex in human and non-human primates[97,98] and the evidence of smooth functional changes in both species[1], we suggest that this gradient-based organization principle likely holds in the human mesial premotor cortex as well.

We then focused on a different aspect: the specificity for area F6 of the functional roles ascribed to it. Since F6 appears to index several functions, it is critical to assess which of those functions pertain predominantly to it. We tackled this issue by devising a comparative study where, through the lens of our execution/observation task, the functional properties of area F6 were compared with those of F5 and AIP[176]. During action execution, the earliest selectivity of area F6 for the upcoming movement and the earliest peak of activity concomitantly with movement onset support its putative role in signaling whether and when to act[13], leveraging on information likely provided by lateral prefrontal areas[106]. Instead, the tuning for object type is weaker in area F6 than in the two other areas, considered to be crucial for visuomotor transformation for grasping[44,128,184]. Concerning action observation, F6 begins to encode other's action later and lesser than F5: indeed, area F5 appears to be the core of the AON[40,107], as recently supported with causal techniques[152]. Interestingly, the F5 anticipatory coding of other's action indicates that observation activity is not merely a reaction to the perceived visual stimulus. If that were the case, more visually responsive areas like AIP and F6 would have encoded the observed movement before F5. Thus, although we cannot exclude that the observation responses in F6 and AIP arise from feedforward signals coming from visual areas, in a predictable context they might instead represent predictive signals coming from area F5[149]. In sum, whether the observation activity in area F6 is predictive or visually triggered, its role in anticipating/processing other's action appears to be ancillary to that of area F5.

To explain the variety of situations in which F6 plays a role, we first demonstrated the functional heterogeneity of this area, and then tried to highlight its key functional roles relative to other areas. In a perspective of neural reuse[185], an additional and not mutually exclusive possibility to address the issue is to reconcile some apparently different functions into a single one[1]. This approach has indeed proven to be successful, for instance, in the identification of a common neural substrate for task switching and response inhibition/facilitation[31]. In the context of action

observation, a long-standing question pertains the evaluation of the biological specificity of action observation responses[39,132,152]. In the third of the presented studies[186], despite a quantitatively stronger activation for real actions, we found evidence for a large overlap between the neural representations of biological and nonbiological actions in area F6, in agreement with other monkey[132,152] and human[180,181,187] studies. A likely reason why other studies[39,179,188] reported a biological specificity of action observation response is that they only focused on the magnitude of the response that, as in our findings, appears to be higher for biological actions.

The similarity in the neural response patterns for the two types of observed movements suggests that a similar computation is ongoing in area F6. What is the role of this computation? The anticipatory and stronger encoding of other's action in area F5 suggest a motor, rather than visual, nature of action observation activity[176]. In the same line, the caudal part of F6, that exhibits a stronger action observation response, shows at the same time a stronger motor response[106]. A recent review tried to reconceptualize action observation responses of parieto-premotor areas within the framework of visuomotor transformations: as the visual properties of an object trigger the corresponding motor representation for grasping it, others' observed actions might elicit a motor representation to properly anticipate or react to them[110]. Extending this interpretation to area F6, the similarity of biological and nonbiological observed movements might reflect the similarity in the motor representation that those movements, occurring in the same space sector within a similar context, trigger.

In sum, the findings of this thesis indicates that in area F6 objects, contextual cues and observed actions might be encoded in motor terms, with some shared coding principles with other anatomically-connected areas of the extended cortical motor system. The recruitment of motor representations afforded by external stimuli, especially visual, is a general principle that may be shared by a variety of different processes, enabling to explain the manifold of functional roles attributed to F6.

REFERENCES

1. Nachev, P., Kennard, C. & Husain, M. Functional role of the supplementary and pre-supplementary motor areas. *Nat. Rev. Neurosci.* **9**, 856–869 (2008).
2. Behrens, T. E. J., Fox, P., Laird, A. & Smith, S. M. What is the most interesting part of the brain? *Trends Cogn. Sci.* **17**, 2–4 (2013).
3. Luppino, G., Matelli, M., Camarda, R. M., Gallese, V. & Rizzolatti, G. Multiple representations of body movements in mesial area 6 and the adjacent cingulate cortex: An intracortical microstimulation study in the macaque monkey. *J. Comp. Neurol.* **311**, 463–482 (1991).
4. Matsuzaka, Y., Aizawa, H. & Tanji, J. A motor area rostral to the supplementary motor area (presupplementary motor area) in the monkey: neuronal activity during a learned motor task. *J. Neurophysiol.* **68**, 653–662 (1992).
5. Picard, N. & Strick, P. L. Motor Areas of the Medial Wall: A Review of Their Location and Functional Activation. *Cereb. Cortex* **6**, 342–353 (1996).
6. Petrides, M. & Pandya, D. N. Dorsolateral prefrontal cortex: comparative cytoarchitectonic analysis in the human and the macaque brain and corticocortical connection patterns: Dorsolateral prefrontal cortex in human and monkey. *Eur. J. Neurosci.* **11**, 1011–1036 (1999).
7. Matelli, M., Luppino, G. & Rizzolatti, G. Architecture of superior and mesial area 6 and the adjacent cingulate cortex in the macaque monkey. *J. Comp. Neurol.* **311**, 445–462 (1991).
8. Geyer, S. *et al.* Receptor autoradiographic mapping of the mesial motor and premotor cortex of the macaque monkey. *J. Comp. Neurol.* **397**, 231–250 (1998).
9. Luppino, G., Matelli, M., Camarda, R. & Rizzolatti, G. Corticocortical connections of area F3 (SMA-proper) and area F6 (pre-SMA) in the macaque monkey. *J. Comp. Neurol.* **338**, 114–140 (1993).
10. Dum, R. & Strick, P. Motor areas in the frontal lobe of the primate. *Physiol. Behav.* **77**, 677–682 (2002).
11. Yeterian, E. H., Pandya, D. N., Tomaiuolo, F. & Petrides, M. The cortical connectivity of the prefrontal cortex in the monkey brain. *Cortex* **48**, 58–81 (2012).
12. Lu, M.-T., Preston, J. B. & Strick, P. L. Interconnections between the prefrontal cortex and the premotor areas in the frontal lobe. *J. Comp. Neurol.* **341**, 375–392 (1994).
13. Gerbella, M., Rozzi, S. & Rizzolatti, G. The extended object-grasping network. *Exp. Brain Res.* **235**, 2903–2916 (2017).
14. Mitz, A. R. & Wise, S. P. The Somatotopic Organization of the Supplementary Motor Area: Intracortical Microstimulation Mapping. *J. Neurosci.* 12.
15. Nakamura, K., Sakai, K. & Hikosaka, O. Neuronal Activity in Medial Frontal Cortex During Learning of Sequential Procedures. *J. Neurophysiol.* **80**, 2671–2687 (1998).
16. Lanzilotto, M. *et al.* Extending the Cortical Grasping Network: Pre-supplementary Motor Neuron Activity During Vision and Grasping of Objects. *Cereb. Cortex* **26**, 4435–4449 (2016).
17. Shima, K. & Tanji, J. Both Supplementary and Presupplementary Motor Areas Are Crucial for the Temporal Organization of Multiple Movements. *J. Neurophysiol.* **80**, 3247–3260 (1998).
18. Lanzilotto, M., Perciavalle, V. & Lucchetti, C. A new field in monkey's frontal cortex: Premotor ear-eye field (PEEF). *Neurosci. Biobehav. Rev.* **37**, 1434–1444 (2013).
19. Awan, M. A. H., Mushiake, H. & Matsuzaka, Y. Neuronal Representations of Tactic-Based Sensorimotor Transformations in the Primate Medial Prefrontal, Presupplementary, and Supplementary Motor Areas: A Comparative Study. *Front. Syst. Neurosci.* **14**, 536246 (2020).
20. Matsuzaka, Y. & Tanji, J. Changing directions of forthcoming arm movements: neuronal activity in the presupplementary and supplementary motor area of monkey cerebral cortex. *J. Neurophysiol.* **76**, 2327–2342 (1996).
21. Rizzolatti, G. *et al.* Neurons related to reaching-grasping arm movements in the rostral part of area 6 (area 6a/l). 14.
22. Alexander, G. E. & Crutcher, M. D. Preparation for movement: neural representations of intended direction in three motor areas of the monkey. *J. Neurophysiol.* **64**, 133–150 (1990).
23. Shima, K., Mushiake, H., Saito, N. & Tanji, J. Role for cells in the presupplementary motor area in updating motor plans. *Proc. Natl. Acad. Sci.* **93**, 8694–8698 (1996).
24. Shima, K. & Tanji, J. Neuronal Activity in the Supplementary and Presupplementary Motor Areas for Temporal Organization of Multiple Movements. *J. Neurophysiol.* **84**, 2148–2160 (2000).
25. Mita, A., Mushiake, H., Shima, K., Matsuzaka, Y. & Tanji, J. Interval time coding by neurons in the presupplementary and supplementary motor areas. *Nat. Neurosci.* **12**, 502–507 (2009).

26. Merchant, H., Zarco, W., Perez, O., Prado, L. & Bartolo, R. Measuring time with different neural chronometers during a synchronization-continuation task. *Proc. Natl. Acad. Sci.* **108**, 19784–19789 (2011).
27. Mendoza, G., Méndez, J. C., Pérez, O., Prado, L. & Merchant, H. Neural basis for categorical boundaries in the primate pre-SMA during relative categorization of time intervals. *Nat. Commun.* **9**, 1098 (2018).
28. Perez, O., Kass, R. E. & Merchant, H. Trial time warping to discriminate stimulus-related from movement-related neural activity. *J. Neurosci. Methods* **212**, 203–210 (2013).
29. Crowe, D. A., Zarco, W., Bartolo, R. & Merchant, H. Dynamic Representation of the Temporal and Sequential Structure of Rhythmic Movements in the Primate Medial Premotor Cortex. *J. Neurosci.* **34**, 11972–11983 (2014).
30. Merchant, H., Harrington, D. L. & Meck, W. H. Neural Basis of the Perception and Estimation of Time. *Annu. Rev. Neurosci.* **36**, 313–336 (2013).
31. Isoda, M. & Hikosaka, O. Switching from automatic to controlled action by monkey medial frontal cortex. *Nat. Neurosci.* **10**, 240–248 (2007).
32. Yoshida, K., Saito, N., Iriki, A. & Isoda, M. Representation of Others' Action by Neurons in Monkey Medial Frontal Cortex. *Curr. Biol.* **21**, 249–253 (2011).
33. Yoshida, K., Saito, N., Iriki, A. & Isoda, M. Social error monitoring in macaque frontal cortex. *Nat. Neurosci.* **15**, 1307–1312 (2012).
34. Livi, A. *et al.* Agent-based representations of objects and actions in the monkey pre-supplementary motor area. *Proc. Natl. Acad. Sci.* **116**, 2691–2700 (2019).
35. Falcone, R., Cirillo, R., Ferraina, S. & Genovesio, A. Neural activity in macaque medial frontal cortex represents others' choices. *Sci. Rep.* **7**, 12663 (2017).
36. Tanji, J. Sequential Organization of Multiple Movements: Involvement of Cortical Motor Areas. *Annu. Rev. Neurosci.* **24**, 631–651 (2001).
37. Zarco, W., Merchant, H., Prado, L. & Mendez, J. C. Subsecond Timing in Primates: Comparison of Interval Production Between Human Subjects and Rhesus Monkeys. *J. Neurophysiol.* **102**, 3191–3202 (2009).
38. Chen, Y.-C., Thaler, D., Nixon, P. D., Stern, C. E. & Passingham, R. E. The functions of the medial premotor cortex: II. The timing and selection of learned movements. *Exp. Brain Res.* **102**, (1995).
39. Gallese, V., Fadiga, L., Fogassi, L. & Rizzolatti, G. Action recognition in the premotor cortex. *Brain* **119**, 593–609 (1996).
40. Bonini, L. The Extended Mirror Neuron Network: Anatomy, Origin, and Functions. *The Neuroscientist* **23**, 56–67 (2017).
41. Orban, G. A., Sepe, A. & Bonini, L. Parietal maps of visual signals for bodily action planning. *Brain Struct. Funct.* **226**, 2967–2988 (2021).
42. Johansen-Berg, H. *et al.* Changes in connectivity profiles define functionally distinct regions in human medial frontal cortex. *Proc. Natl. Acad. Sci.* **101**, 13335–13340 (2004).
43. Morecraft, R. J. *et al.* Cytoarchitecture and cortical connections of the anterior cingulate and adjacent somatomotor fields in the rhesus monkey. *Brain Res. Bull.* **87**, 457–497 (2012).
44. Rizzolatti, G. & Luppino, G. The Cortical Motor System. *Neuron* **31**, 889–901 (2001).
45. Zapparoli, L. *et al.* Dissecting the neurofunctional bases of intentional action. *Proc. Natl. Acad. Sci.* **115**, 7440–7445 (2018).
46. Picard, N. & Strick, P. L. Imaging the premotor areas. *Curr. Opin. Neurobiol.* **11**, 663–672 (2001).
47. Fujii, N., Mushiake, H. & Tanji, J. Distribution of Eye- and Arm-Movement-Related Neuronal Activity in the SEF and in the SMA and Pre-SMA of Monkeys. *J. Neurophysiol.* **87**, 2158–2166 (2002).
48. Tanji, J. & Shima, K. Role for supplementary motor area cells in planning several movements ahead. *Nature* **371**, 413–416 (1994).
49. Sliwa, J. & Freiwald, W. A. A dedicated network for social interaction processing in the primate brain. *Science* **356**, 745–749 (2017).
50. Bruni, S., Giorgetti, V., Bonini, L. & Fogassi, L. Processing and Integration of Contextual Information in Monkey Ventrolateral Prefrontal Neurons during Selection and Execution of Goal-Directed Manipulative Actions. *J. Neurosci.* **35**, 11877–11890 (2015).
51. Barz, F. *et al.* Versatile, modular 3D microelectrode arrays for neuronal ensemble recordings: from design to fabrication, assembly, and functional validation in non-human primates. *J. Neural Eng.* **14**, 036010 (2017).
52. Barz, F., Paul, O. & Ruther, P. Modular assembly concept for 3D neural probe prototypes offering high freedom of design and alignment precision. in *2014 36th Annual International Conference of the IEEE Engineering in Medicine and Biology Society* 3977–3980 (IEEE, 2014). doi:10.1109/EMBC.2014.6944495.
53. Bonini, L. *et al.* Application of floating silicon-based linear multielectrode arrays for acute recording of single neuron activity in awake behaving monkeys. *Biomed. Eng. Biomed. Tech.* **59**, (2014).

54. Ferroni, C. G., Maranesi, M., Livi, A., Lanzilotto, M. & Bonini, L. Comparative Performance of Linear Multielectrode Probes and Single-Tip Electrodes for Intracortical Microstimulation and Single-Neuron Recording in Macaque Monkey. *Front. Syst. Neurosci.* **11**, 84 (2017).
55. Chung, J. E. *et al.* A Fully Automated Approach to Spike Sorting. *Neuron* **95**, 1381-1394.e6 (2017).
56. Lanzilotto, M. *et al.* Anterior Intraparietal Area: A Hub in the Observed Manipulative Action Network. *Cereb. Cortex* **29**, 1816–1833 (2019).
57. Bonini, L., Maranesi, M., Livi, A., Fogassi, L. & Rizzolatti, G. Space-Dependent Representation of Objects and Other's Action in Monkey Ventral Premotor Grasping Neurons. *J. Neurosci.* **34**, 4108–4119 (2014).
58. Anderssen, R. S., Brent, R. P., Daley, D. J. & Moran, P. A. P. Concerning ∫1 0 ⋯ ∫1 0 (x2 1 + ⋯ + x2 k)1/2 dx1 ⋯ dxk and a Taylor Series Method. *SIAM J. Appl. Math.* **30**, 22–30 (1976).
59. Bruni, S. *et al.* Cortical and subcortical connections of parietal and premotor nodes of the monkey hand mirror neuron network. *Brain Struct. Funct.* (2017) doi:10.1007/s00429-017-1582-0.
60. Haber, S. N., Kim, K.-S., Mailly, P. & Calzavara, R. Reward-Related Cortical Inputs Define a Large Striatal Region in Primates That Interface with Associative Cortical Connections, Providing a Substrate for Incentive-Based Learning. *J. Neurosci.* **26**, 8368–8376 (2006).
61. Gerbella, M., Borra, E., Mangiaracina, C., Rozzi, S. & Luppino, G. Corticostriate Projections from Areas of the "Lateral Grasping Network": Evidence for Multiple Hand-Related Input Channels. *Cereb. Cortex* **26**, 3096–3115 (2016).
62. Borra, E., Gerbella, M., Rozzi, S. & Luppino, G. Projections from Caudal Ventrolateral Prefrontal Areas to Brainstem Preoculomotor Structures and to Basal Ganglia and Cerebellar Oculomotor Loops in the Macaque. *Cereb. Cortex* **25**, 748–764 (2015).
63. Calzavara, R., Mailly, P. & Haber, S. N. Relationship between the corticostriatal terminals from areas 9 and 46, and those from area 8A, dorsal and rostral premotor cortex and area 24c: an anatomical substrate for cognition to action: The striatum of action planning. *Eur. J. Neurosci.* **26**, 2005–2024 (2007).
64. Alexander, G. E. & DeLong, M. R. Microstimulation of the primate neostriatum. II. Somatotopic organization of striatal microexcitable zones and their relation to neuronal response properties. *J. Neurophysiol.* **53**, 1417–1430 (1985).
65. Nambu, A. Somatotopic Organization of the Primate Basal Ganglia. *Front. Neuroanat.* **5**, (2011).
66. Alexander, G. E., DeLong, M. R. & Strick, P. L. Parallel Organization of Functionally Segregated Circuits Linking Basal Ganglia and Cortex. *Annu. Rev. Neurosci.* **9**, 357–381 (1986).
67. Tremblay, L., Worbe, Y., Thobois, S., Sgambato-Faure, V. & Féger, J. Selective dysfunction of basal ganglia subterritories: From movement to behavioral disorders: SELECTIVE DYSFUNCTION OF BG SUBTERRITORIES. *Mov. Disord.* **30**, 1155–1170 (2015).
68. Nakamura, K., Sakai, K. & Hikosaka, O. Effects of Local Inactivation of Monkey Medial Frontal Cortex in Learning of Sequential Procedures. *J. Neurophysiol.* **82**, 1063–1068 (1999).
69. Fogassi, L. *et al.* Coding of peripersonal space in inferior premotor cortex (area F4). *J. Neurophysiol.* **76**, 141–157 (1996).
70. Graziano, M. S. A., Yap, G. S. & Gross, C. G. Coding of Visual Space by Premotor Neurons. *Science* **266**, 1054–1057 (1994).
71. Graziano, M. S. A. & Cooke, D. F. Parieto-frontal interactions, personal space, and defensive behavior. *Neuropsychologia* **44**, 845–859 (2006).
72. Hihara, S., Taoka, M., Tanaka, M. & Iriki, A. Visual Responsiveness of Neurons in the Secondary Somatosensory Area and its Surrounding Parietal Operculum Regions in Awake Macaque Monkeys. *Cereb. Cortex* **25**, 4535–4550 (2015).
73. Rozzi, S., Ferrari, P. F., Bonini, L., Rizzolatti, G. & Fogassi, L. Functional organization of inferior parietal lobule convexity in the macaque monkey: electrophysiological characterization of motor, sensory and mirror responses and their correlation with cytoarchitectonic areas. *Eur. J. Neurosci.* **28**, 1569–1588 (2008).
74. Bonini, L. *et al.* Selectivity for grip type and action goal in macaque inferior parietal and ventral premotor grasping neurons. *J. Neurophysiol.* **108**, 1607–1619 (2012).
75. Maranesi, M., Bonini, L. & Fogassi, L. Cortical processing of object affordances for self and others' action. *Front. Psychol.* **5**, (2014).
76. Murata, A. *et al.* Object Representation in the Ventral Premotor Cortex (Area F5) of the Monkey. *J. Neurophysiol.* **78**, 2226–2230 (1997).
77. Raos, V., Umiltá, M.-A., Murata, A., Fogassi, L. & Gallese, V. Functional Properties of Grasping-Related Neurons in the Ventral Premotor Area F5 of the Macaque Monkey. *J. Neurophysiol.* **95**, 709–729 (2006).

78. Cléry, J., Guipponi, O., Wardak, C. & Ben Hamed, S. Neuronal bases of peripersonal and extrapersonal spaces, their plasticity and their dynamics: Knowns and unknowns. *Neuropsychologia* **70**, 313–326 (2015).
79. Liles, S. L. Activity of neurons in the putamen associated with wrist movements in the monkey. *Brain Res.* **263**, 156–161 (1983).
80. Romanski, L. M. Domain specificity in the primate prefrontal cortex. *Cogn. Affect. Behav. Neurosci.* **4**, 421–429 (2004).
81. Haroush, K. & Williams, Z. M. Neuronal Prediction of Opponent's Behavior during Cooperative Social Interchange in Primates. *Cell* **160**, 1233–1245 (2015).
82. Hadjidimitrakis, K. *et al.* Fix Your Eyes in the Space You Could Reach: Neurons in the Macaque Medial Parietal Cortex Prefer Gaze Positions in Peripersonal Space. *PLoS ONE* **6**, e23335 (2011).
83. Hadjidimitrakis, K., Breveglieri, R., Bosco, A. & Fattori, P. Three-dimensional eye position signals shape both peripersonal space and arm movement activity in the medial posterior parietal cortex. *Front. Integr. Neurosci.* **6**, (2012).
84. Breveglieri, R. *et al.* Neurons Modulated by Action Execution and Observation in the Macaque Medial Parietal Cortex. *Curr. Biol.* **29**, 1218-1225.e3 (2019).
85. Klein, J. T. & Platt, M. L. Social Information Signaling by Neurons in Primate Striatum. *Curr. Biol.* **23**, 691–696 (2013).
86. Graziano, MichaelS. A. & Gross, CharlesG. A bimodal map of space: somatosensory receptive fields in the macaque putamen with corresponding visual receptive fields. *Exp. Brain Res.* **97**, (1993).
87. Eradath, M. K. *et al.* Anatomical inputs to sulcal portions of areas 9m and 8Bm in the macaque monkey. *Front. Neuroanat.* **9**, (2015).
88. Lanzilotto, M., Gerbella, M., Perciavalle, V. & Lucchetti, C. Neuronal Encoding of Self and Others' Head Rotation in the Macaque Dorsal Prefrontal Cortex. *Sci. Rep.* **7**, 8571 (2017).
89. He, S., Dum, R. & Strick, P. Topographic organization of corticospinal projections from the frontal lobe: motor areas on the medial surface of the hemisphere. *J. Neurosci.* **15**, 3284–3306 (1995).
90. Inase, M., Tokuno, H., Nambu, A., Akazawa, T. & Takada, M. Corticostriatal and corticosubthalamic input zones from the presupplementary motor area in the macaque monkey: comparison with the input zones from the supplementary motor area. *Brain Res.* **833**, 191–201 (1999).
91. Picard, N. Activation of the Supplementary Motor Area (SMA) during Performance of Visually Guided Movements. *Cereb. Cortex* **13**, 977–986 (2003).
92. Matsuzaka, Y., Tanji, J. & Mushiake, H. Representation of Behavioral Tactics and Tactics-Action Transformation in the Primate Medial Prefrontal Cortex. *J. Neurosci.* **36**, 5974–5987 (2016).
93. Badre, D. & D'Esposito, M. Is the rostro-caudal axis of the frontal lobe hierarchical? *Nat. Rev. Neurosci.* **10**, 659–669 (2009).
94. Battaglia-Mayer, A., Babicola, L. & Satta, E. Parieto-frontal gradients and domains underlying eye and hand operations in the action space. *Neuroscience* **334**, 76–92 (2016).
95. Koechlin, E. & Summerfield, C. An information theoretical approach to prefrontal executive function. *Trends Cogn. Sci.* **11**, 229–235 (2007).
96. Petrides, M. Lateral prefrontal cortex: architectonic and functional organization. *Philos. Trans. R. Soc. B Biol. Sci.* **360**, 781–795 (2005).
97. Ruan, J. *et al.* Cytoarchitecture, probability maps, and functions of the human supplementary and pre-supplementary motor areas. *Brain Struct. Funct.* **223**, 4169–4186 (2018).
98. Vorobiev, V., Govoni, P., Rizzolatti, G., Matelli, M. & Luppino, G. Parcellation of human mesial area 6: cytoarchitectonic evidence for three separate areas: Human mesial area 6. *Eur. J. Neurosci.* **10**, 2199–2203 (1998).
99. Belmalih, A. *et al.* A multiarchitectonic approach for the definition of functionally distinct areas and domains in the monkey frontal lobe. *J. Anat.* **211**, 199–211 (2007).
100. Gazzola, V. & Keysers, C. The Observation and Execution of Actions Share Motor and Somatosensory Voxels in all Tested Subjects: Single-Subject Analyses of Unsmoothed fMRI Data. *Cereb. Cortex* **19**, 1239–1255 (2009).
101. Molenberghs, P., Cunnington, R. & Mattingley, J. B. Brain regions with mirror properties: A meta-analysis of 125 human fMRI studies. *Neurosci. Biobehav. Rev.* **36**, 341–349 (2012).
102. Rizzolatti, G. & Sinigaglia, C. The mirror mechanism: a basic principle of brain function. *Nat. Rev. Neurosci.* **17**, 757–765 (2016).
103. Fiave, P. A., Sharma, S., Jastorff, J. & Nelissen, K. Investigating common coding of observed and executed actions in the monkey brain using cross-modal multi-variate fMRI classification. *NeuroImage* **178**, 306–317 (2018).

104. di Pellegrino, G., Fadiga, L., Fogassi, L., Gallese, V. & Rizzolatti, G. Understanding motor events: a neurophysiological study. *Exp. Brain Res.* **91**, 176–180 (1992).
105. Nelissen, K. *et al.* Action Observation Circuits in the Macaque Monkey Cortex. *J. Neurosci.* **31**, 3743–3756 (2011).
106. Albertini, D. *et al.* Connectional gradients underlie functional transitions in monkey pre-supplementary motor area. *Prog. Neurobiol.* **184**, 101699 (2020).
107. Kilner, J. M. & Lemon, R. N. What We Know Currently about Mirror Neurons. *Curr. Biol.* **23**, R1057–R1062 (2013).
108. Maeda, K., Ishida, H., Nakajima, K., Inase, M. & Murata, A. Functional Properties of Parietal Hand Manipulation–related Neurons and Mirror Neurons Responding to Vision of Own Hand Action. *J. Cogn. Neurosci.* **27**, 560–572 (2015).
109. Lanzilotto, M. *et al.* Stable readout of observed actions from format-dependent activity of monkey's anterior intraparietal neurons. *Proc. Natl. Acad. Sci.* **117**, 16596–16605 (2020).
110. Orban, G. A., Lanzilotto, M. & Bonini, L. From Observed Action Identity to Social Affordances. *Trends Cogn. Sci.* **25**, 493–505 (2021).
111. Isoda, M. The Role of the Medial Prefrontal Cortex in Moderating Neural Representations of Self and Other in Primates. *Annu. Rev. Neurosci.* **44**, 295–313 (2021).
112. Caspers, S., Zilles, K., Laird, A. R. & Eickhoff, S. B. ALE meta-analysis of action observation and imitation in the human brain. *NeuroImage* **50**, 1148–1167 (2010).
113. Fiave, P. A. & Nelissen, K. Motor resonance in monkey parietal and premotor cortex during action observation: Influence of viewing perspective and effector identity. *NeuroImage* **224**, 117398 (2021).
114. Kraskov, A., Dancause, N., Quallo, M. M., Shepherd, S. & Lemon, R. N. Corticospinal Neurons in Macaque Ventral Premotor Cortex with Mirror Properties: A Potential Mechanism for Action Suppression? *Neuron* **64**, 922–930 (2009).
115. Vigneswaran, G., Philipp, R., Lemon, R. N. & Kraskov, A. M1 Corticospinal Mirror Neurons and Their Role in Movement Suppression during Action Observation. *Curr. Biol.* **23**, 236–243 (2013).
116. Trainito, C., von Nicolai, C., Miller, E. K. & Siegel, M. Extracellular Spike Waveform Dissociates Four Functionally Distinct Cell Classes in Primate Cortex. *Curr. Biol.* **29**, 2973-2982.e5 (2019).
117. Bonini, L., Maranesi, M., Livi, A., Fogassi, L. & Rizzolatti, G. Ventral Premotor Neurons Encoding Representations of Action during Self and Others' Inaction. *Curr. Biol.* **24**, 1611–1614 (2014).
118. Gold, C., Henze, D. A., Koch, C. & Buzsáki, G. On the Origin of the Extracellular Action Potential Waveform: A Modeling Study. *J. Neurophysiol.* **95**, 3113–3128 (2006).
119. Robbins, A. A., Fox, S. E., Holmes, G. L., Scott, R. C. & Barry, J. M. Short duration waveforms recorded extracellularly from freely moving rats are representative of axonal activity. *Front. Neural Circuits* **7**, (2013).
120. Kaufman, M. T. *et al.* Roles of Monkey Premotor Neuron Classes in Movement Preparation and Execution. *J. Neurophysiol.* **104**, 799–810 (2010).
121. Mitchell, J. F., Sundberg, K. A. & Reynolds, J. H. Differential Attention-Dependent Response Modulation across Cell Classes in Macaque Visual Area V4. *Neuron* **55**, 131–141 (2007).
122. Friendly, M., Monette, G. & Fox, J. Elliptical Insights: Understanding Statistical Methods through Elliptical Geometry. *Stat. Sci.* **28**, (2013).
123. Merchant, H., Naselaris, T. & Georgopoulos, A. P. Dynamic Sculpting of Directional Tuning in the Primate Motor Cortex during Three-Dimensional Reaching. *J. Neurosci.* **28**, 9164–9172 (2008).
124. Barthó, P. *et al.* Characterization of Neocortical Principal Cells and Interneurons by Network Interactions and Extracellular Features. *J. Neurophysiol.* **92**, 600–608 (2004).
125. Meyers, E. M. The neural decoding toolbox. *Front. Neuroinformatics* **7**, (2013).
126. Quian Quiroga, R. & Panzeri, S. Extracting information from neuronal populations: information theory and decoding approaches. *Nat. Rev. Neurosci.* **10**, 173–185 (2009).
127. Fogassi, L. Cortical mechanism for the visual guidance of hand grasping movements in the monkey: A reversible inactivation study. *Brain* **124**, 571–586 (2001).
128. Schaffelhofer, S. & Scherberger, H. Object vision to hand action in macaque parietal, premotor, and motor cortices. *eLife* **5**, e15278 (2016).
129. Ferrari, P. F., Bonini, L. & Fogassi, L. From monkey mirror neurons to primate behaviours: possible 'direct' and 'indirect' pathways. *Philos. Trans. R. Soc. B Biol. Sci.* **364**, 2311–2323 (2009).
130. Maranesi, M., Livi, A., Fogassi, L., Rizzolatti, G. & Bonini, L. Mirror Neuron Activation Prior to Action Observation in a Predictable Context. *J. Neurosci.* **34**, 14827–14832 (2014).
131. Umiltà, M. A. *et al.* I Know What You Are Doing. *Neuron* **31**, 155–165 (2001).
132. Caggiano, V., Fleischer, F., Pomper, J. K., Giese, M. A. & Thier, P. Mirror Neurons in Monkey Premotor Area F5 Show Tuning for Critical Features of Visual Causality Perception. *Curr. Biol.* **26**, 3077–3082 (2016).

133. Kaufman, M. T., Churchland, M. M. & Shenoy, K. V. The roles of monkey M1 neuron classes in movement preparation and execution. *J. Neurophysiol.* **110**, 817–825 (2013).
134. Hussar, C. R. & Pasternak, T. Flexibility of Sensory Representations in Prefrontal Cortex Depends on Cell Type. *Neuron* **64**, 730–743 (2009).
135. Kraskov, A. *et al.* Corticospinal mirror neurons. *Philos. Trans. R. Soc. B Biol. Sci.* **369**, 20130174 (2014).
136. Vigneswaran, G., Kraskov, A. & Lemon, R. N. Large Identified Pyramidal Cells in Macaque Motor and Premotor Cortex Exhibit 'Thin Spikes': Implications for Cell Type Classification. *J. Neurosci.* **31**, 14235–14242 (2011).
137. Jerjian, S. J., Sahani, M. & Kraskov, A. Movement initiation and grasp representation in premotor and primary motor cortex mirror neurons. *eLife* **9**, e54139 (2020).
138. Gallese, V., Murata, A., Kaseda, M., Niki, N. & Sakata, H. Deficit of hand preshaping after muscimol injection in monkey parietal cortex: *NeuroReport* **5**, 1525–1529 (1994).
139. Dann, B., Michaels, J. A., Schaffelhofer, S. & Scherberger, H. Uniting functional network topology and oscillations in the fronto-parietal single unit network of behaving primates. *eLife* **5**, e15719 (2016).
140. Dum, R. & Strick, P. The origin of corticospinal projections from the premotor areas in the frontal lobe. *J. Neurosci.* **11**, 667–689 (1991).
141. Savaki, H., Kennedy, C., Sokoloff, L. & Mishkin, M. Visually guided reaching with the forelimb contralateral to a 'blind' hemisphere: a metabolic mapping study in monkeys. *J. Neurosci.* **13**, 2772–2789 (1993).
142. Borra, E., Belmalih, A., Gerbella, M., Rozzi, S. & Luppino, G. Projections of the hand field of the macaque ventral premotor area F5 to the brainstem and spinal cord. *J. Comp. Neurol.* NA-NA (2010) doi:10.1002/cne.22353.
143. Muakkassa, K. F. & Strick, P. L. Frontal lobe inputs to primate motor cortex: evidence for four somatotopically organized 'premotor' areas. *Brain Res.* **177**, 176–182 (1979).
144. Matelli, M., Camarda, R., Glickstein, M. & Rizzolatti, G. Afferent and efferent projections of the inferior area 6 in the macaque monkey. *J. Comp. Neurol.* **251**, 281–298 (1986).
145. Mazurek, K. A., Rouse, A. G. & Schieber, M. H. Mirror Neuron Populations Represent Sequences of Behavioral Epochs During Both Execution and Observation. *J. Neurosci.* **38**, 4441–4455 (2018).
146. Maranesi, M. *et al.* Monkey gaze behaviour during action observation and its relationship to mirror neuron activity. *Eur. J. Neurosci.* **38**, 3721–3730 (2013).
147. Papadourakis, V. & Raos, V. Neurons in the Macaque Dorsal Premotor Cortex Respond to Execution and Observation of Actions. *Cereb. Cortex* **29**, 4223–4237 (2019).
148. Maranesi, M., Livi, A. & Bonini, L. Spatial and viewpoint selectivity for others' observed actions in monkey ventral premotor mirror neurons. *Sci. Rep.* **7**, 8231 (2017).
149. Kilner, J. M., Friston, K. J. & Frith, C. D. Predictive coding: an account of the mirror neuron system. *Cogn. Process.* **8**, 159–166 (2007).
150. Shipp, S., Adams, R. A. & Friston, K. J. Reflections on agranular architecture: predictive coding in the motor cortex. *Trends Neurosci.* **36**, 706–716 (2013).
151. Borra, E. *et al.* Cortical Connections of the Macaque Anterior Intraparietal (AIP) Area. *Cereb. Cortex* **18**, 1094–1111 (2008).
152. Ninomiya, T., Noritake, A., Kobayashi, K. & Isoda, M. A causal role for frontal cortico-cortical coordination in social action monitoring. *Nat. Commun.* **11**, 5233 (2020).
153. Diester, I. & Nieder, A. Complementary Contributions of Prefrontal Neuron Classes in Abstract Numerical Categorization. *J. Neurosci.* **28**, 7737–7747 (2008).
154. Song, J.-H. & McPeek, R. M. Roles of Narrow- and Broad-Spiking Dorsal Premotor Area Neurons in Reach Target Selection and Movement Production. *J. Neurophysiol.* **103**, 2124–2138 (2010).
155. Torres-Gomez, S. *et al.* Changes in the Proportion of Inhibitory Interneuron Types from Sensory to Executive Areas of the Primate Neocortex: Implications for the Origins of Working Memory Representations. *Cereb. Cortex* **30**, 4544–4562 (2020).
156. Katai, S. *et al.* Classification of extracellularly recorded neurons by their discharge patterns and their correlates with intracellularly identified neuronal types in the frontal cortex of behaving monkeys. *Eur. J. Neurosci.* **31**, 1322–1338 (2010).
157. Zhang, Y., Li, S., Jiang, D. & Chen, A. Response Properties of Interneurons and Pyramidal Neurons in Macaque MSTd and VPS Areas During Self-Motion. *Front. Neural Circuits* **12**, 105 (2018).
158. Thiele, A. *et al.* Attention Induced Gain Stabilization in Broad and Narrow-Spiking Cells in the Frontal Eye-Field of Macaque Monkeys. *J. Neurosci.* **36**, 7601–7612 (2016).
159. McCormick, D. A., Connors, B. W., Lighthall, J. W. & Prince, D. A. Comparative electrophysiology of pyramidal and sparsely spiny stellate neurons of the neocortex. *J. Neurophysiol.* **54**, 782–806 (1985).

160. Connors, B. W. & Gutnick, M. J. Intrinsic firing patterns of diverse neocortical neurons. *Trends Neurosci.* **13**, 99–104 (1990).
161. Henze, D. A. *et al.* Intracellular Features Predicted by Extracellular Recordings in the Hippocampus In Vivo. *J. Neurophysiol.* **84**, 390–400 (2000).
162. González-Burgos, G., Krimer, L. S., Povysheva, N. V., Barrionuevo, G. & Lewis, D. A. Functional Properties of Fast Spiking Interneurons and Their Synaptic Connections With Pyramidal Cells in Primate Dorsolateral Prefrontal Cortex. *J. Neurophysiol.* **93**, 942–953 (2005).
163. Zaitsev, A. V. *et al.* Interneuron Diversity in Layers 2–3 of Monkey Prefrontal Cortex. *Cereb. Cortex* **19**, 1597–1615 (2009).
164. Xu, W. & Baker, S. N. In vitro characterization of intrinsic properties and local synaptic inputs to pyramidal neurons in macaque primary motor cortex. *Eur. J. Neurosci.* **48**, 2071–2083 (2018).
165. Casale, A. E., Foust, A. J., Bal, T. & McCormick, D. A. Cortical Interneuron Subtypes Vary in Their Axonal Action Potential Properties. *J. Neurosci.* **35**, 15555–15567 (2015).
166. Belmalih, A. *et al.* Multimodal architectonic subdivision of the rostral part (area F5) of the macaque ventral premotor cortex. *J. Comp. Neurol.* **512**, 183–217 (2009).
167. Prather, J. F., Peters, S., Nowicki, S. & Mooney, R. Precise auditory–vocal mirroring in neurons for learned vocal communication. *Nature* **451**, 305–310 (2008).
168. Mondoloni, S., Durand-de Cuttoli, R. & Mourot, A. Cell-Specific Neuropharmacology. *Trends Pharmacol. Sci.* **40**, 696–710 (2019).
169. Ferrari, P. F., Rozzi, S. & Fogassi, L. Mirror Neurons Responding to Observation of Actions Made with Tools in Monkey Ventral Premotor Cortex. *J. Cogn. Neurosci.* **17**, 212–226 (2005).
170. Rochat, M. J. *et al.* Responses of mirror neurons in area F5 to hand and tool grasping observation. *Exp. Brain Res.* **204**, 605–616 (2010).
171. Jiang, X., Saggar, H., Ryu, S. I., Shenoy, K. V. & Kao, J. C. Structure in Neural Activity during Observed and Executed Movements Is Shared at the Neural Population Level, Not in Single Neurons. *Cell Rep.* **32**, 108006 (2020).
172. Pani, P., Theys, T., Romero, M. C. & Janssen, P. Grasping Execution and Grasping Observation Activity of Single Neurons in the Macaque Anterior Intraparietal Area. *J. Cogn. Neurosci.* **26**, 2342–2355 (2014).
173. Tkach, D., Reimer, J. & Hatsopoulos, N. G. Congruent Activity during Action and Action Observation in Motor Cortex. *J. Neurosci.* **27**, 13241–13250 (2007).
174. Dushanova, J. & Donoghue, J. Neurons in primary motor cortex engaged during action observation. *Eur. J. Neurosci.* **31**, 386–398 (2010).
175. Cisek, P. & Kalaska, J. F. Neural correlates of mental rehearsal in dorsal premotor cortex. *Nature* **431**, 993–996 (2004).
176. Ferroni, C. G. *et al.* Local and system mechanisms for action execution and observation in parietal and premotor cortices. *Curr. Biol.* **31**, 2819-2830.e4 (2021).
177. Gallego, J. A. *et al.* Cortical population activity within a preserved neural manifold underlies multiple motor behaviors. *Nat. Commun.* **9**, 4233 (2018).
178. Elsayed, G. F., Lara, A. H., Kaufman, M. T., Churchland, M. M. & Cunningham, J. P. Reorganization between preparatory and movement population responses in motor cortex. *Nat. Commun.* **7**, 13239 (2016).
179. Tai, Y. F., Scherfler, C., Brooks, D. J., Sawamoto, N. & Castiello, U. The Human Premotor Cortex Is 'Mirror' Only for Biological Actions. *Curr. Biol.* **14**, 117–120 (2004).
180. Engel, A., Burke, M., Fiehler, K., Bien, S. & Rösler, F. How moving objects become animated: The human mirror neuron system assimilates non-biological movement patterns. *Soc. Neurosci.* **3**, 368–387 (2008).
181. Gazzola, V., Rizzolatti, G., Wicker, B. & Keysers, C. The anthropomorphic brain: The mirror neuron system responds to human and robotic actions. *NeuroImage* **35**, 1674–1684 (2007).
182. Caggiano, V., Fogassi, L., Rizzolatti, G., Thier, P. & Casile, A. Mirror Neurons Differentially Encode the Peripersonal and Extrapersonal Space of Monkeys. *Science* **324**, 403–406 (2009).
183. Rizzolatti, G., Cattaneo, L., Fabbri-Destro, M. & Rozzi, S. Cortical Mechanisms Underlying the Organization of Goal-Directed Actions and Mirror Neuron-Based Action Understanding. *Physiol. Rev.* **94**, 655–706 (2014).
184. Jeannerod, M., Arbib, M. A., Rizzolatti, G. & Sakata, H. Grasping objects: the cortical of visuomotor transformation. 7.
185. Anderson, M. L. Neural reuse: A fundamental organizational principle of the brain. *Behav. Brain Sci.* **33**, 245–266 (2010).
186. Albertini, D., Lanzilotto, M., Maranesi, M. & Bonini, L. Largely shared neural codes for biological and nonbiological observed movements but not for executed actions in monkey premotor areas. *J. Neurophysiol.* **126**, 906–912 (2021).

187. Oberman, L. M., McCleery, J. P., Ramachandran, V. S. & Pineda, J. A. EEG evidence for mirror neuron activity during the observation of human and robot actions: Toward an analysis of the human qualities of interactive robots. *Neurocomputing* **70**, 2194–2203 (2007).
188. Frenkel-Toledo, S., Bentin, S., Perry, A., Liebermann, D. G. & Soroker, N. Mirror-neuron system recruitment by action observation: Effects of focal brain damage on mu suppression. *NeuroImage* **87**, 127–137 (2014).

APPENDIX

"Connectional gradients underlie functional transitions in monkey pre-supplementary motor area"

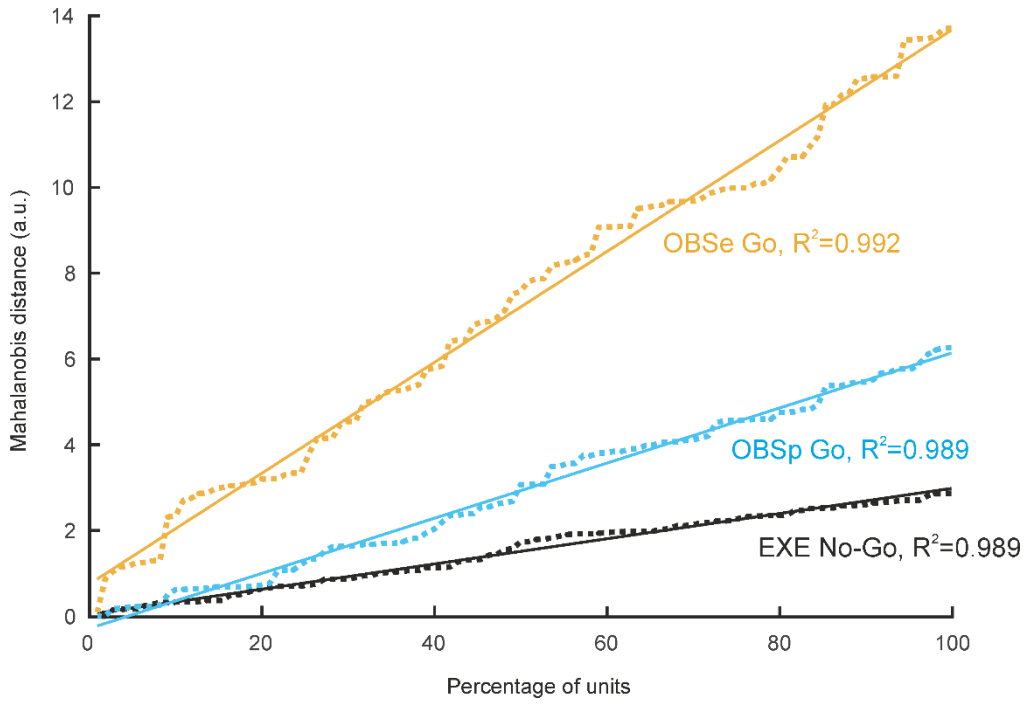

Figure S2.1. Linkage distance increases linearly as function of the number of units. The dotted curves represent the Mahalanobis distances between EXE Go and EXE No-Go (black), OBSp Go (cyan) and OBSe Go (yellow) as a function of the percentage of units considered for the computation. They have been calculated in the neural state space of units of Probe 1 during the Object presentation epoch (the result is pretty the same in any other Probe, epoch, and condition): the linkage distances increase linearly (continuous lines) with the percentage of considered units.

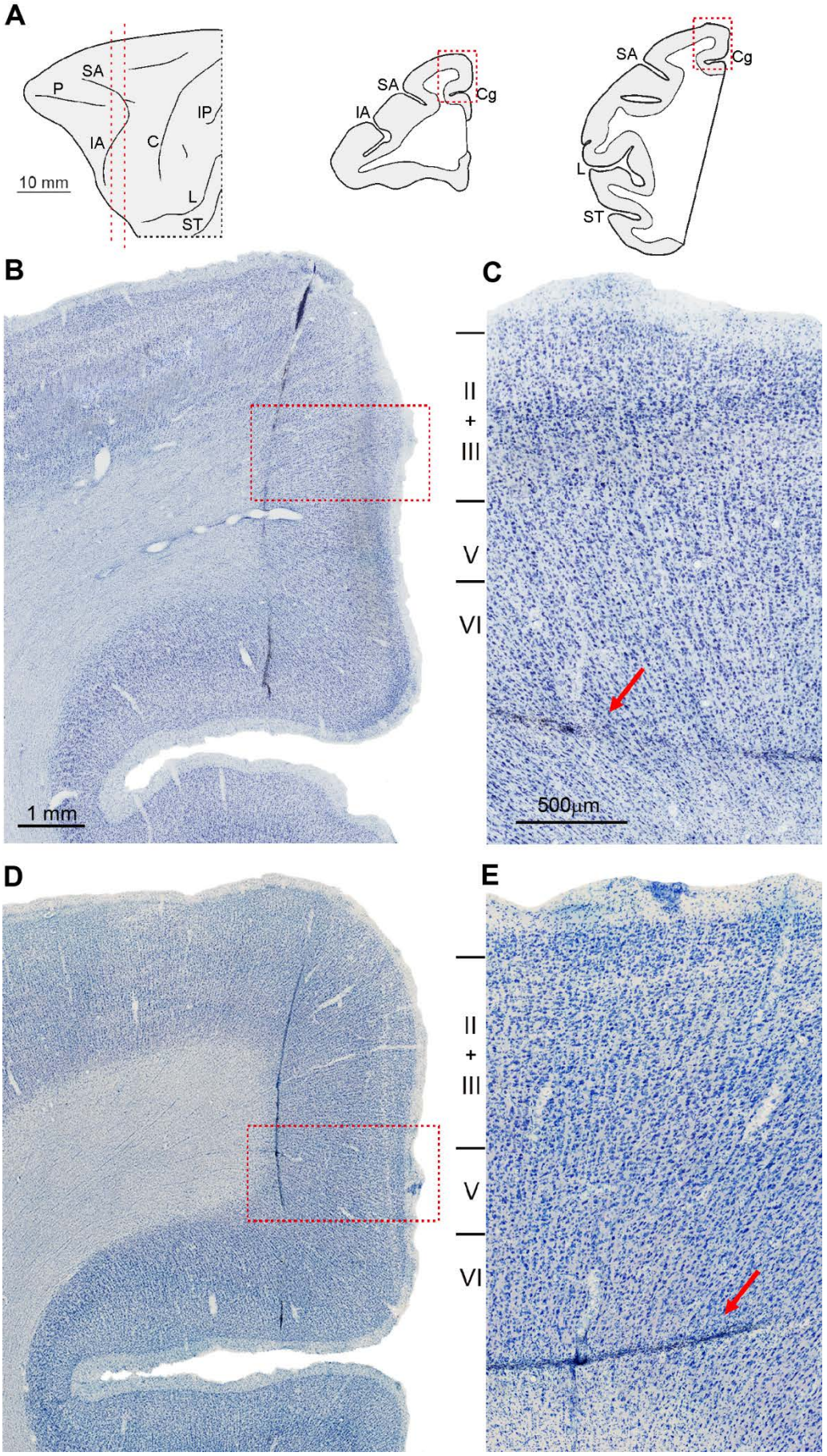
A
SA
P
IP
IA
C
L
ST
10 mm
SA
Cg
IA
SA
Cg
L
ST
B
1 mm
C
II
+
III
V
VI
500µm
D
E
II
+
III
V
VI

Figure S2.2. Architectonic features of the recorded region and histological identification of the position of the Probe 2 and 4 in Mk1. (A) Left: dorsolateral view of the recorded hemisphere (left). The dashed red lines indicate the positions of the coronal sections shown on the right where a track of the rostral probe (Probe 2, B and C) and a track of the caudal probe (Probe 4, D and E) were identified. Dashed red boxes in each coronal section indicate the location of the photomicrograph in (B) and (C). (B-D) Photomicrographs of Nissl-stained sections. The dashed red boxes in (B) and (D) indicate the cortical sector magnified in (C) and (E). Scale bar in (B) applies also to (D). (C-E) High magnification views of the cortical sector included in the red boxes of panels (B) and (D) rotated by 90°. Red arrows indicate the probe tracks. Note that the typical architectonic features of area F6 (Luppino et al. 1991) are evident, namely: a uniform layer III composed by small pyramids and a relatively prominent layer V populated by larger pyramids. Scale bar in (C) applies also to (E). Abbreviations: C, central sulcus; Cg, cingulate sulcus; IA, inferior arcuate sulcus; IP, Intraparietal sulcus; L, lateral sulcus; P, principal sulcus; SA, superior arcuate sulcus; ST, superior temporal sulcus.

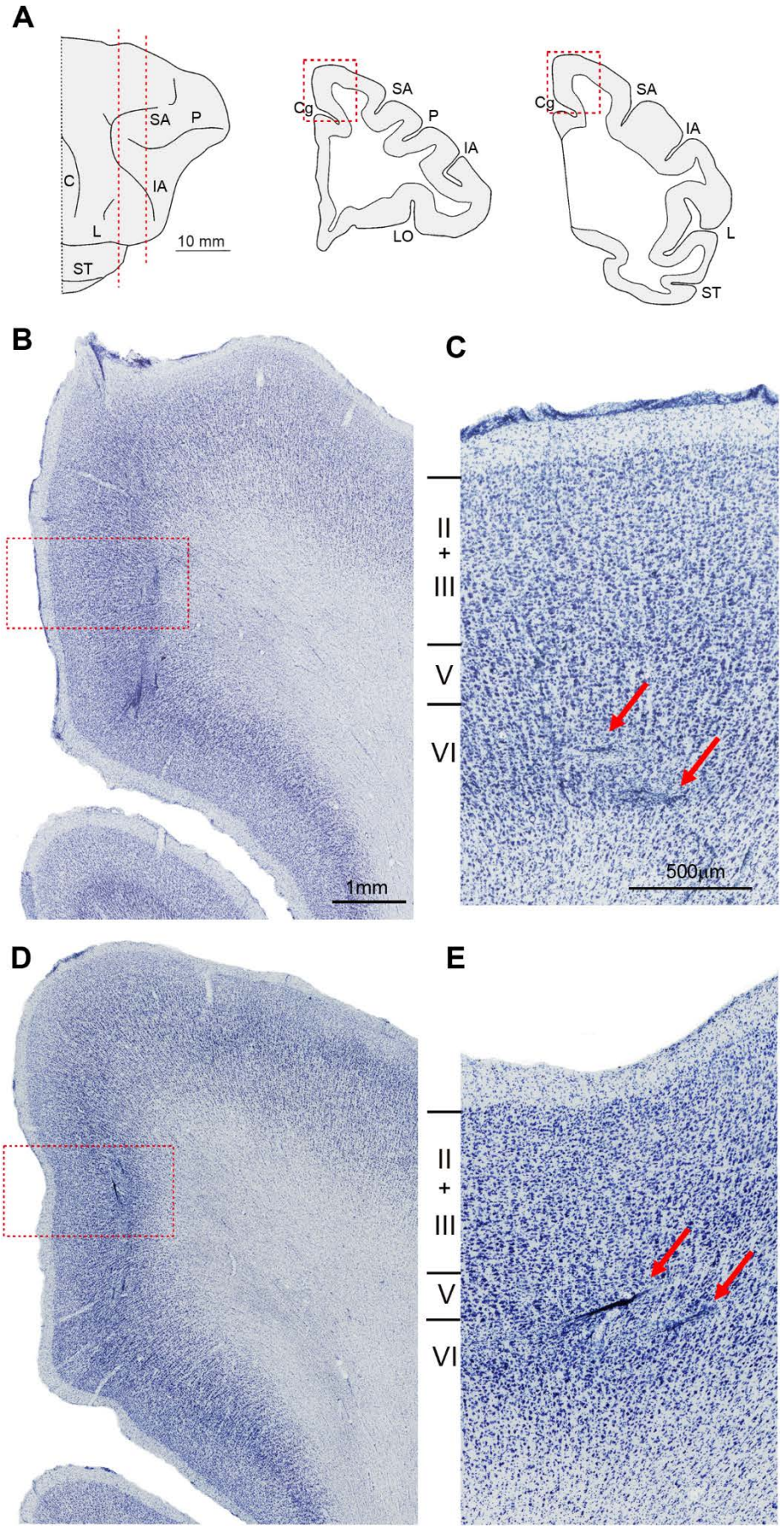
A
SA
P
C
IA
L
ST
10 mm
Cg
SA
P
IA
LO
Cg
SA
IA
L
ST
B
1mm
C
II
+
III
V
VI
500µm
D
E
II
+
III
V
VI

Figure S2.3. Architectonic features of the recorded region and histological identification of the position of the Probe 1 and 3 in Mk2. (A) Left: dorsolateral view of the recorded hemisphere (left). The dashed red lines indicate the positions of the coronal sections shown on the right where a track of the rostral probe (Probe 1, B and C) and a track of the caudal probe (Probe 3, D and E) were identified. Dashed red boxes in each coronal section indicate the location of the photomicrograph in (B) and (C). (B-D) Photomicrographs of Nissl-stained sections. The dashed red boxes in (B) and (D) indicate the cortical sector magnified in (C) and (E). Scale bar in (B) applies also to (D). (C-E) High magnification views of the cortical sector included in the red boxes of panels (B) and (D) rotated by 90°. Red arrows indicate the probe tracks. Note that the typical architectonic features of area F6 (Luppino et al. 1991) are evident, namely: a uniform layer III composed by small pyramids and a relatively prominent layer V populated by larger pyramids. Scale bar in (C) applies also to (E). Abbreviations as in Figure S2.2.

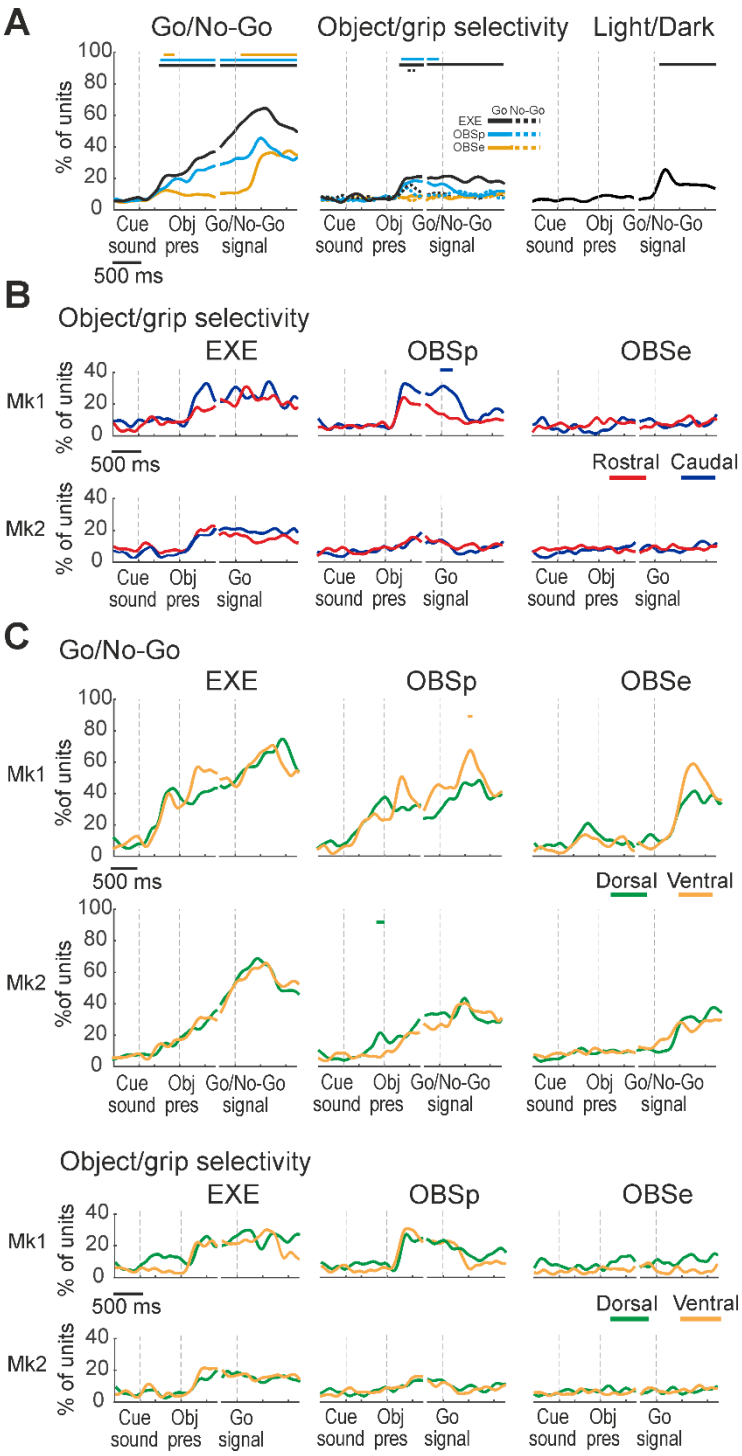

Figure S2.4. Tuning properties of F6 units. **(A)** Percentage of all F6 units with significant tuning for Go/No-Go condition and type of object across tasks and conditions (in color and line-style code) and for Light/Dark condition (in EXE). The colored lines above each plot indicate the time bins where the fraction of tuned units is significantly greater than that during the first 500 ms (baseline epoch, χ^2 $p < 0.01$). **(B)** Percentage of units with significant tuning for the type of Object/grip in (from left to right) EXE, OBSp and OBSe (Go conditions). Colored lines above each plot indicate the time bins where the fraction of tuned units is significantly different between the rostral and the caudal probe (χ^2 $p < 0.05$, uncorrected). **(C)** Upper part, comparison of the percentage of units with significant Go/No-Go tuning in (from left to right) EXE, OBSp and OBSe in each monkey's dorsal (51 in Mk1 and 109 in Mk2) and ventral (46 in Mk1 and 85 in Mk2) part of the implanted probes (see Methods). Lower part, same as B but comparing the tuning properties of units recorded in the more dorsal and more ventral parts of area F6 of the two monkeys. Other conventions as in panel B.

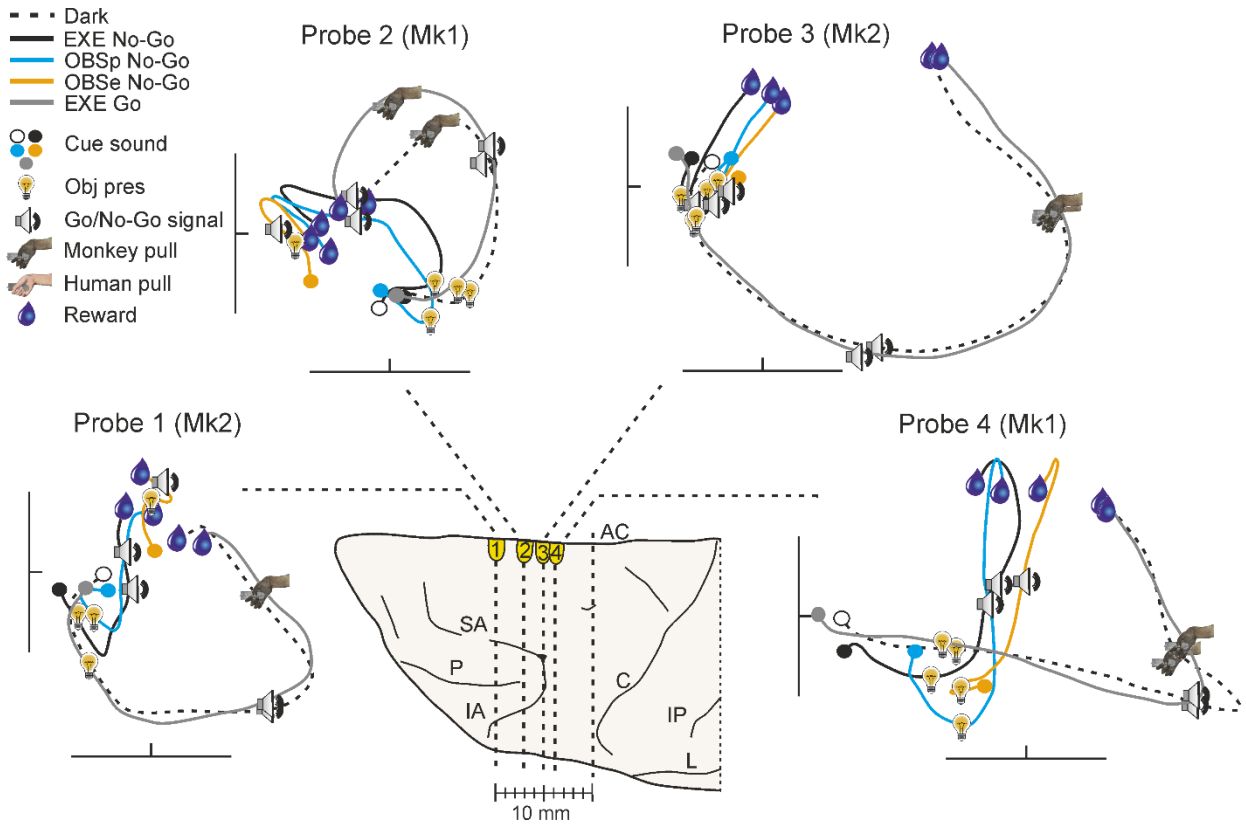

Figure S2.5. Local population dynamics along the rostro-caudal extent of area F6. Projection of each probe's neural population response (object averaged) in the plane defined by the first two principal components during tasks unfolding in the Dark condition of EXE and No-Go conditions of EXE, OBSp and OBSe. The trajectories of EXE in the Light condition, the same of Figure 2.3, are reported for comparison. Each trace (object averaged) represents the projection of the full trial-length activity aligned to Go/No-Go signal. Symbols identify the task events along the trial. Abbreviations as in Figure 2.1.

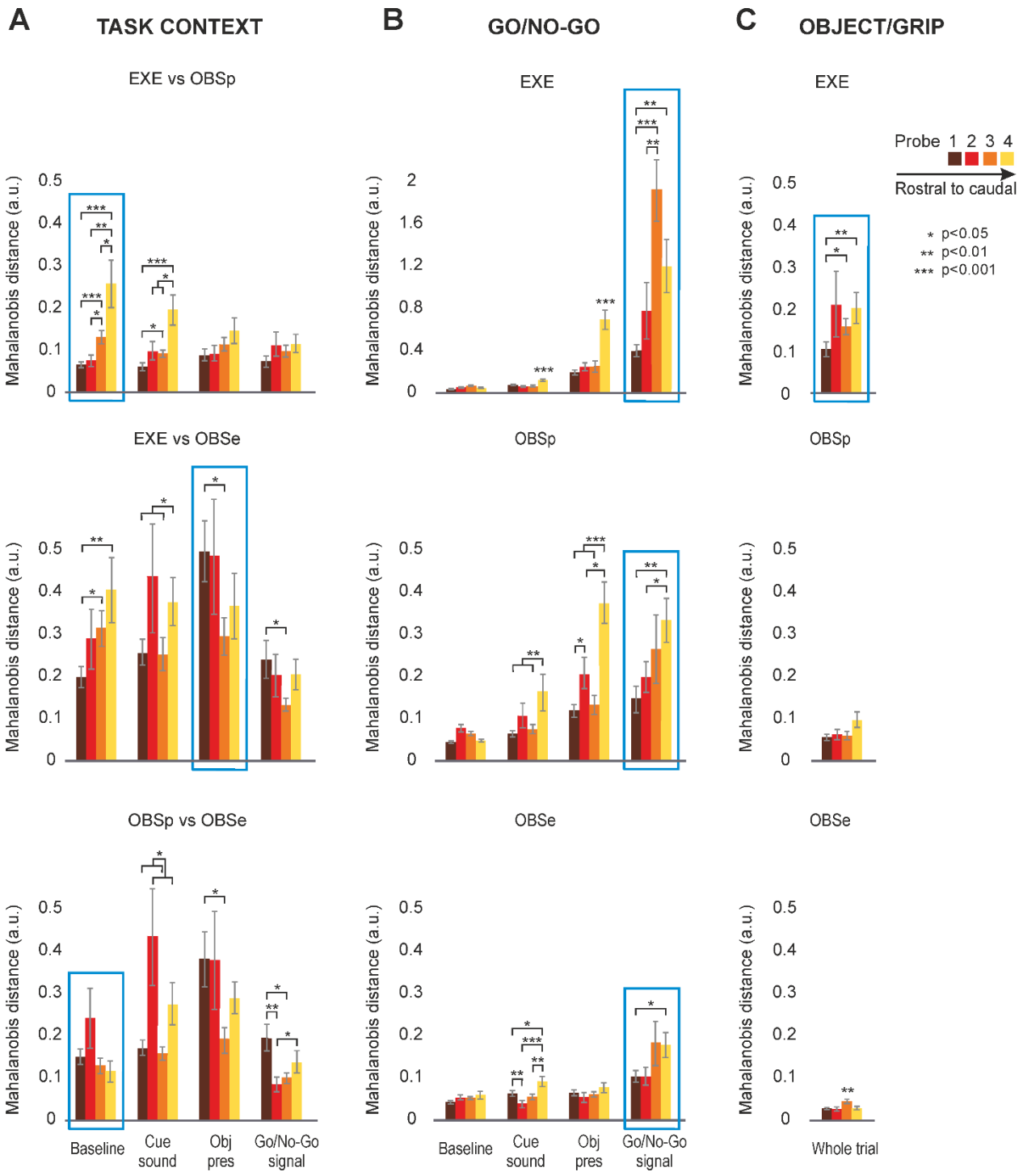

Figure S2.6. Full set of combination between specific factors and epochs (functional dimensions). (A) Histograms representing the combination of all possible contrasts between EXE, OBSp and OBSe in the four task epochs (baseline, Cue sound presentation, Object presentation, Go/No-Go signal). Trials with different objects as target and Go/No-Go conditions have been pooled together. **(B)** Histograms representing the contrast between Go and No-go conditions in the four task epochs defined in A in each task context. Trials with different objects as target have been pooled together. **(C)** Histograms representing the contrast between object/grip type in the task period ranging from object presentation to the end of the trial in the Go condition of each task context. Functional dimensions presented in Figure 2.5 here are shown within the blue boxes. Other conventions as in Figure 2.5.

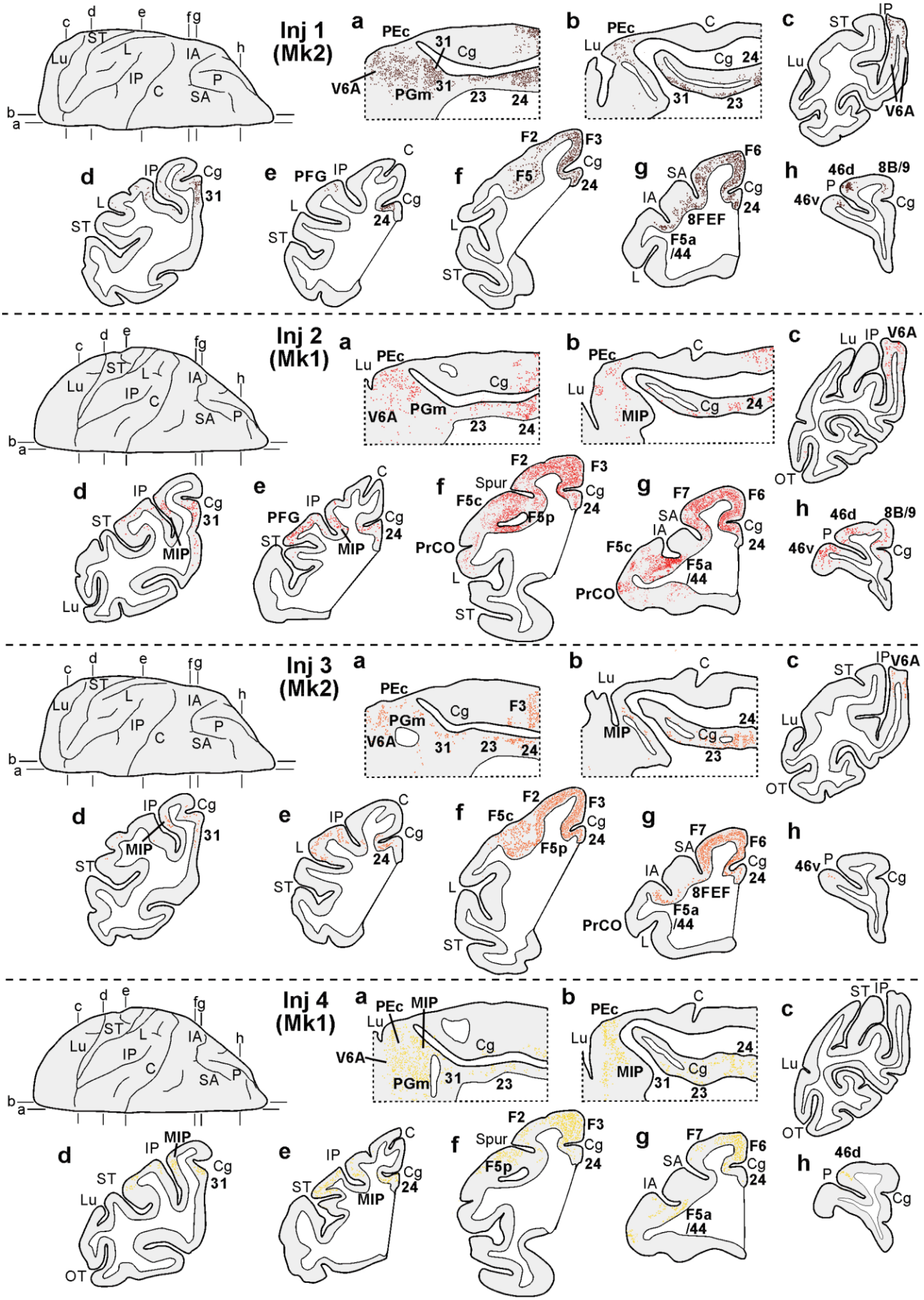
Inj 1 (Mk2)
Inj 2 (Mk1)
Inj 3 (Mk2)
Inj 4 (Mk1)
PEc
V6A
PGm
MIP
PFG
PrCO
F5
F5c
F5p
Spur
8FEF
F5a /44
46d
46v
8B/9
Lu
IP
ST
IA
SA
OT
Cg
C
L
P

Figure S2.7. Distribution of the cortical labeled cells shown in drawings of representative parasagittal and coronal sections. The parasagittal sections (a-b) are showed in a medio-lateral order, the coronal sections in a rostro-caudal order (c-g). The dorsolateral views top left of each panel show the levels at which the sections were taken (a-g).

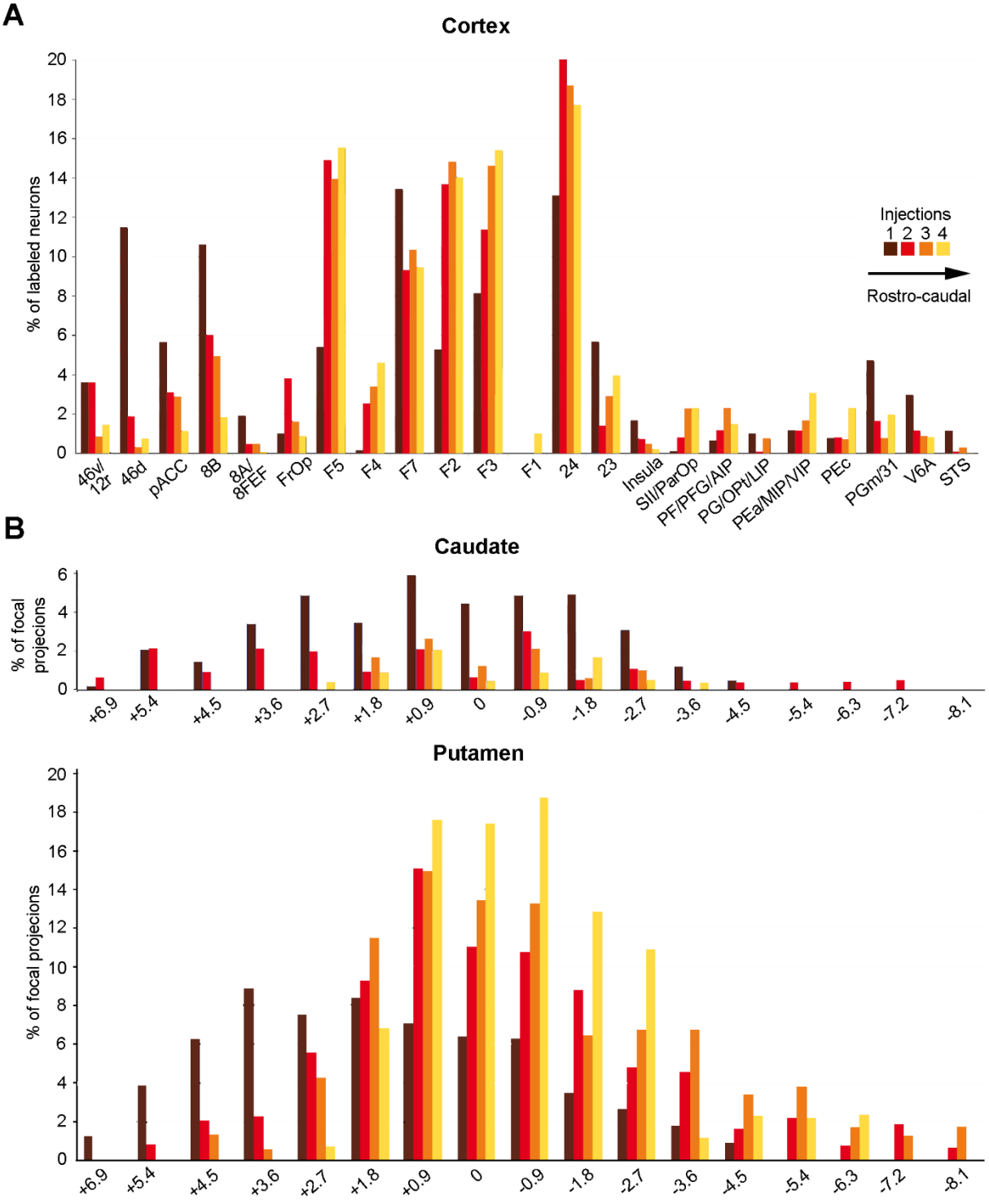

Figure S2.8. Anatomical connectivity of F6 sectors at different rostro-caudal locations. (A) Histograms illustrating the percentage of labeled cells in the various cortical areas following each injection (in color code). **(B)** Histograms illustrating the percentage of caudate and putamen projections along the rostro-caudal extension of the two nuclei. Color code and abbreviations as in Figure 2.6.

	LPF/ FrOp	cLPF	pACC	PMv	PMd	MCC/ SMA	ParOp /IPL	SPL	MPL	STS/ Insula	Total cells
Inj 1 LYD Mk2	4438 *(50.89)**	3868 *(56.04)**	1528 *(25.02)**	1464 *(-45.95)**	4516 *(-20.14)**	7282 *(-18.5)**	734 *(-2.39)*	520 *(-8.31)**	1881 *(39.1)**	747 *(43.99)**	26978
Inj 2 CTBg Mk1	8281 *(8.99)**	5710 *(-3.81)*	2759 *(-0.54)*	15532 *(12.73)**	20464 *(3.39)*	29228 *(-2.93)*	1854 *(-15.71)**	2032 *(-8.6)**	2373 *(-9.6)**	665 *(-7.11)*	88898
Inj 3 FR Mk2	646 *(-31.84)**	1284 *(-7.85)**	682 (-2.17)	4104 *(6.13)**	5963 *(8.93)**	8591 *(7.73)**	1278 *(23.06)**	512 *(-5.53)**	392 *(-13.82)**	184 *(-3.15)*	23636
Inj 4 FR Mk1	925 *(-33.41)**	572 *(-34.22)**	339 *(-20.31)**	5616 *(13.49)**	7112 *(5.15)**	11514 *(15.74)**	1163 *(9.47)**	1610 *(30.42)**	846 *(-3.85)*	64 *(-14.16)**	29761

Table S1. Distribution of cortical labeled cells across the different anatomical territories. The table indicates the absolute number of labeled cells in each anatomically defined territory. The areas are grouped based on anatomo-functional similarity as in histograms of Figure 2.6B. Each value indicates the number of labeled cells found in each anatomical territory. Statistical analysis was performed with a chi-square test, comparing the number in each cell with the value expected if the proportion of observed neurons was uniform across injections at different antero-posterior positions. In addition, to identify the injections-territory combinations mostly contributing to the effect, we computed the adjusted standardized cell residuals (value in comma). The asterisks indicate the significant adjusted standardized cell residuals exceeded an absolute value of 3.84, thus indicating an effect specificity for each territory ($p < 0.00125$, Bonferroni corrected for multiple comparison).

"Local and system mechanisms for action execution and observation in parietal and premotor cortices"

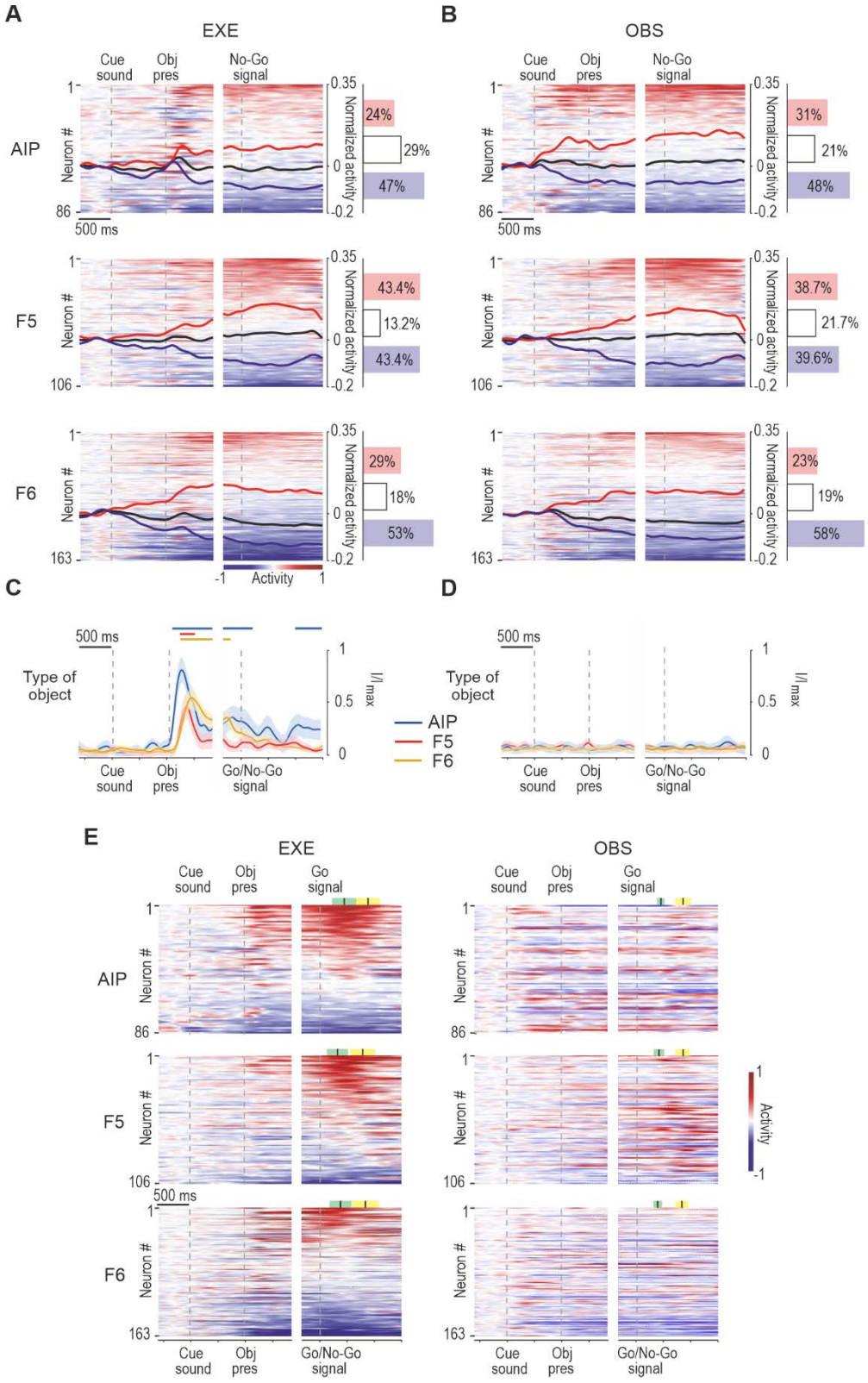

Figure S3.1. Functional properties of AIP, F5 and F6 neurons during No-Go trials of EXE and OBS. (A) Heat maps of all the recorded neurons in each area during No-Go trials of EXE. Each line represents one cell, and cells are ordered (from top to bottom) based on the magnitude of their activity with respect to baseline (red = facilitated, blue = suppressed) in the interval between 300 ms before, until 900 ms after, the No-Go signal. Black lines represent the averaged response of each population as a whole. The histograms on the right indicate the percentage of facilitated, suppressed and non-significant neurons in each area (see Methods). **(B)** Heat maps and population response of all the recorded neurons in each area during OBS. All conventions as in (A). Note that the neurons have been ordered independently from panel (A). **(C)** Mutual information on type of object in EXE No-Go trials decoded from neuronal population activity of each area along the task unfolding period. Continuous colored bars on top of each plot indicate the period in which the decoding accuracy is significantly higher than chance (z-test on real versus shuffled data, see Methods). **(D)** Mutual information on type of object (bottom) of OBS. Conventions as in (C). **(E)** Heat maps of all the recorded neurons in each area during EXE and OBS, using in both tasks the same arrangement of the neurons applied in EXE (for comparison see Figure 3.2).

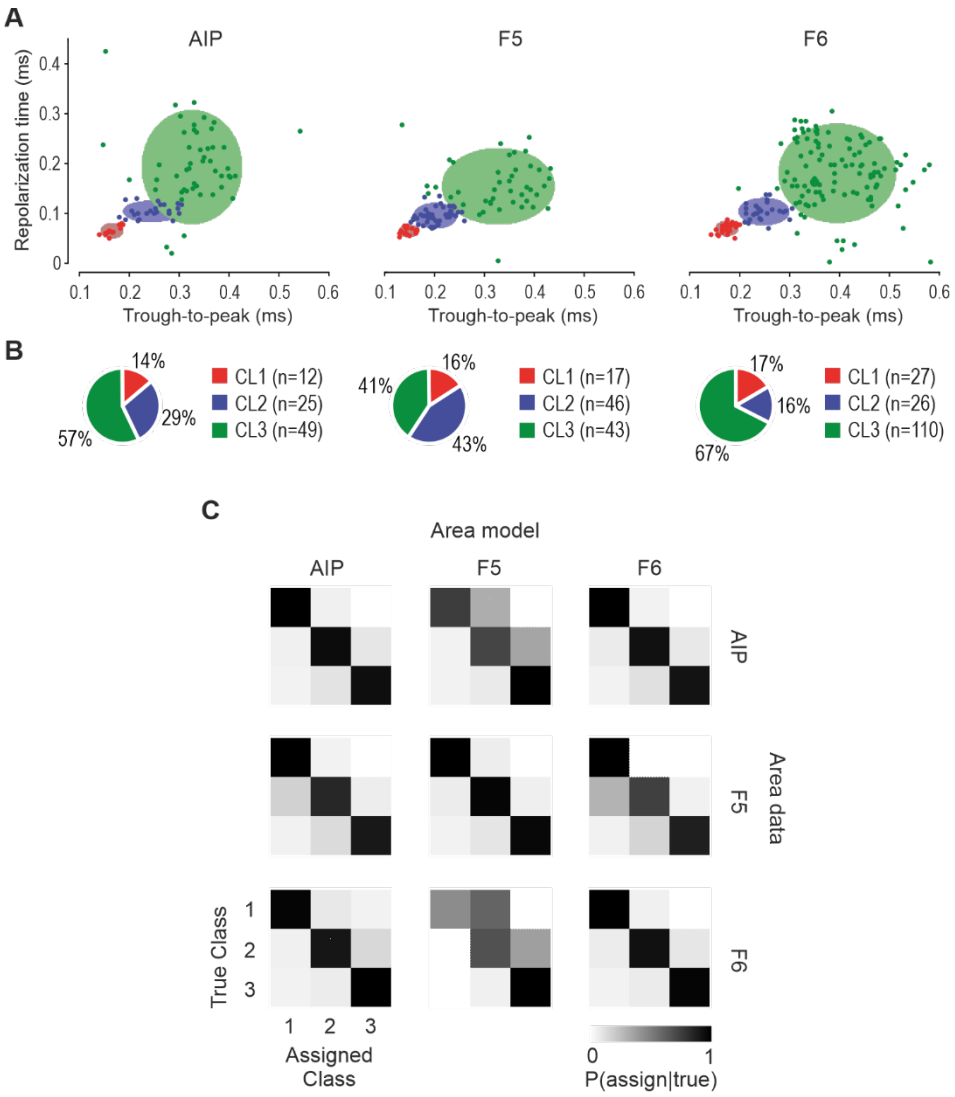

Figure S3.2. Reliability of waveform clustering within and across areas. (A) Projection of each spike waveforms in the 2D space formed by trough-to-peak duration and repolarization time: the clustering has been performed within each area, separately. Conventions as in main Figure 3.3A. **(B)** Number of neurons in each cell class (in colour code) obtained from within-area clustering procedure illustrated in (A). Neurons in each class are expressed as a percentage of the total number of neurons recorded in that area. The distribution of neurons across cell classes is not significantly different from that obtained following clustering applied to the whole data set combined across areas (see Figure 3.5B) in AIP (χ^2 =0.71, p= 0.7) and F6 (χ^2=0.19, p=0.9), whereas it differs in area F5 (χ^2 =18.27, p=0.0001), mostly because of a difference in the attribution of neurons to cell class 1 and 2. **(C)** Estimation of cluster separation within each area and across areas. We extended the procedure used to estimate the cluster separation in the whole dataset (Figure 3.3B, and see Methods) to assess whether and to what extent the clustering performed within individual areas generalizes to the other areas. For each pair of areas, 10^4 data points were randomly generated from the Gaussian mixture distribution of one area and assigned to classes based on the Gaussian mixture distribution of the other area. Thus, the diagonal plots of the resulting confusion matrix represent the cluster separation within each area, the off-diagonal plots represent how much the distribution of clusters is consistent across areas.

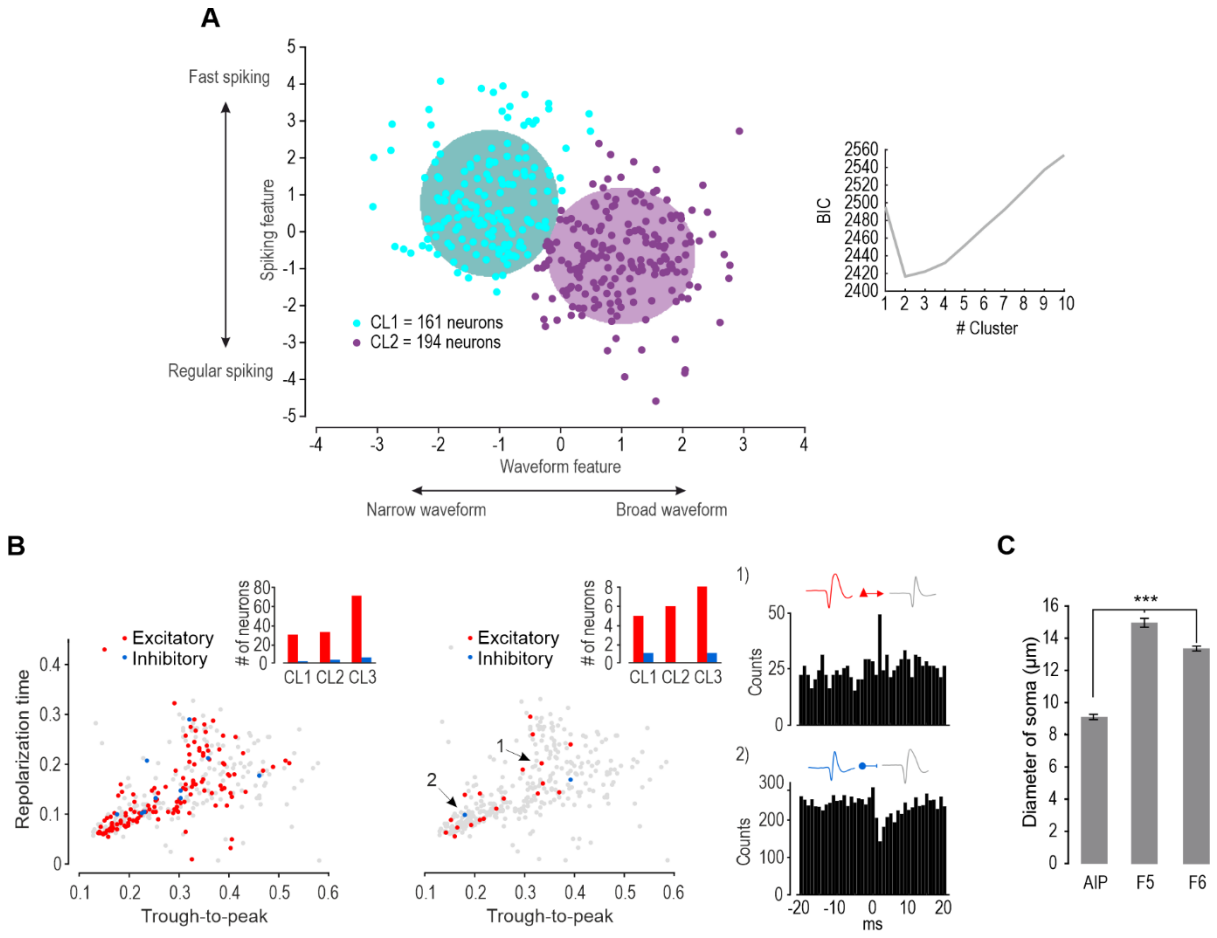

Figure S3.3. Clustering with spiking and waveform features, cross-correlograms and size of the cell soma in the three investigated areas. (A) Clustering of neurons based on combined waveform and spiking features. The clustering was performed by using a set of 6 dimensions: 3 spike shape features (Trough-to-peak, Repolarization time and Trough-amplitude ratio) and 3 neuronal firing features (Position of ISI's maximum, ISI's Coefficient of Variation, and Burst Index[S1]). We then reduced the dimensionality of the feature space by selecting a single "Waveform" and a single "Spiking" dimension by applying PCA within both set of features. Specifically, each feature was z-scored, PCA was performed within each set, and the projection onto the first principal component was selected as the score for the "Waveform" and "Spiking" features (the first PCs explained alone ~60% and ~70% of their total variance, respectively). Gaussian Mixture Model clustering was performed as in Figure 3.3A of the main text and Bayesian Information Criterion analysis revealed that the optimal number of clusters is 2. **(B)** Cross-correlograms of all possible pairs of neurons. To investigate causal relationships among spikes of different neurons we calculated cross-correlogram histograms (CCHs) for all pairs of simultaneously recorded neurons with the criteria applied by Merchant et al. (2008)[S2]. Since significant 1 ms-lag suppression between neurons recorded from the same channel are likely an epiphenomenon of their close proximity[S3] we excluded CCHs between neurons recorded from the same channel. 5654 CCHs fulfilled the above criteria and were examined, and 314 of them were significant. Since some neurons appeared to trigger in an opposite way (excitatory vs inhibitory) multiple cells (n = 76 pairs including one of such neurons), they have been excluded. We obtained 238 significant pairs, including 143 distinct triggering neurons. Of them, 133 (red dots in left panel) were associated to excitatory effect whereas 10 (blue dots) to inhibitory effects. We then reasoned that the high number of excluded pairs because of unreliable, opposite (facilitatory vs inhibitory) effects exerted on different neurons makes plausible to consider that the criteria was too permissive. Thus, we also tried to apply more restrictive criteria, that is, 1) ± 4 SD threshold, 2) exclusion of all those pairs in which the CCH peak was higher than 1 SD from the second-highest bin in the 40 ms time window, 3) inhibition accepted as valid only when it lasted for at least two consecutive bins. Within the 24 pairs fulfilling

these restrictive criteria, 21 different triggering neurons were identified (central panel). Among them, 19 showed excitatory interactions and 2 showed inhibitory interactions (right panel). These findings suggest that in our data set triggering neurons with facilitatory effects can exhibit thin spikes and neurons with inhibitory effects can exhibit broad spikes. **(C)** Each bar represents the average diameter of somata in each area (one-way ANOVA F=977.65, p<0.001). To measure each cell soma diameter, we used the measure function of the Nis-element software (Nikon Instruments Inc.). The histological material, prepared and processed as previously described[S4], was constituted by 3 sections digitized and photographed with a × 20 objective taken from the recorded regions of each area; from each section we sampled three 250 µm columns in order to have a uniform representation of cells from all the cortical layers. For each column, we plotted all the surface of the soma of each neuron for which the nucleus could be identified (AIP, n = 847; F5, n = 295; F6, n = 943).

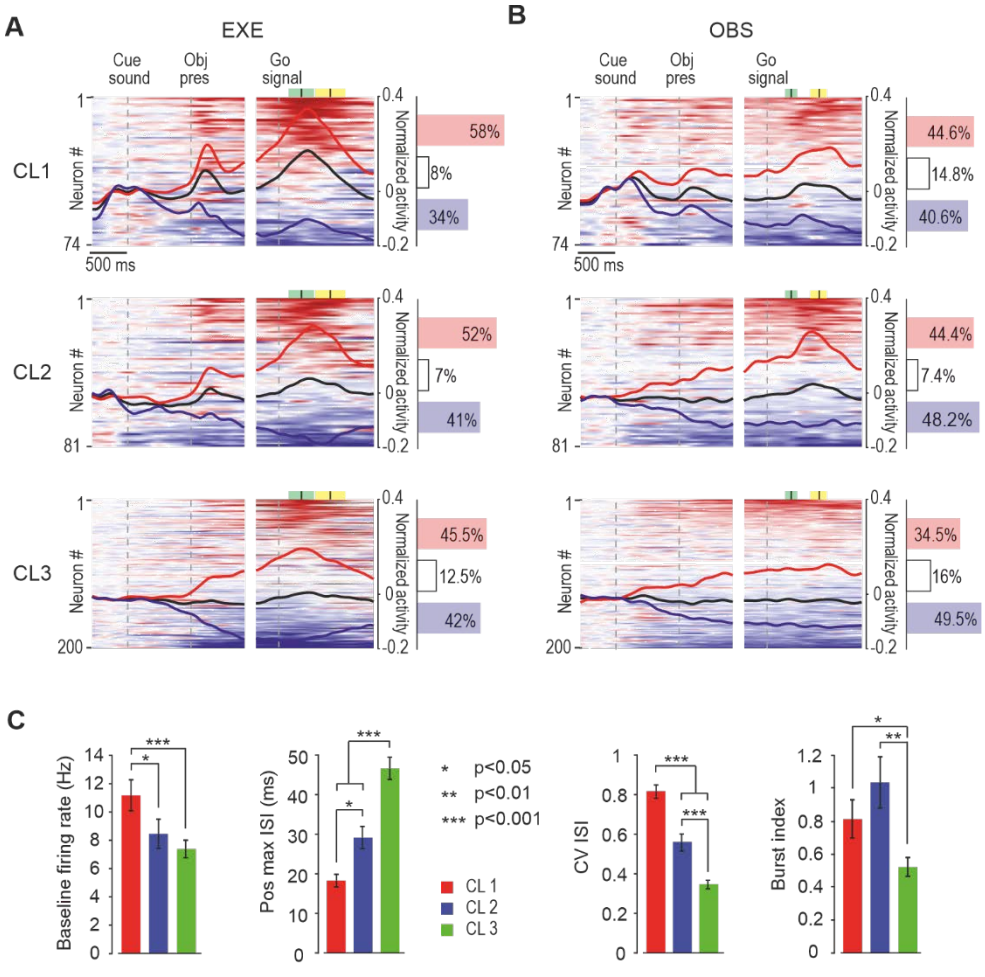

Figure S3.4. Tuning and firing properties of neurons in different cell classes. **(A)** Heat maps and population response of all the recorded neurons in each cell class during EXE. All conventions as in Figure S3.1A (all χ^2 comparisons between pairs of cell classes, p>0.11). **(B)** Heat maps and population response of all the recorded neurons in each class during OBS. All conventions as in Figure S3.1A (all χ^2 comparisons between pairs of cell classes, p>0.12). **(C)** From left to right: average baseline firing rate of each cell class during EXE (Mann-Whitney test); average position of the maximum of the ISI distribution (Mann-Whitney test); coefficient of variation of the ISI distribution (one-way ANOVA p<0.001, Tukey-Kramer post-hoc); average Burst index, calculated as the ratio of ISI intervals < 5ms divided by all intervals < 100ms, normalized by the same ratio that would be expected by a Poisson process of equal mean rate (Mann-Whitney test, [S1]). Error bars within each plot indicate standard errors.

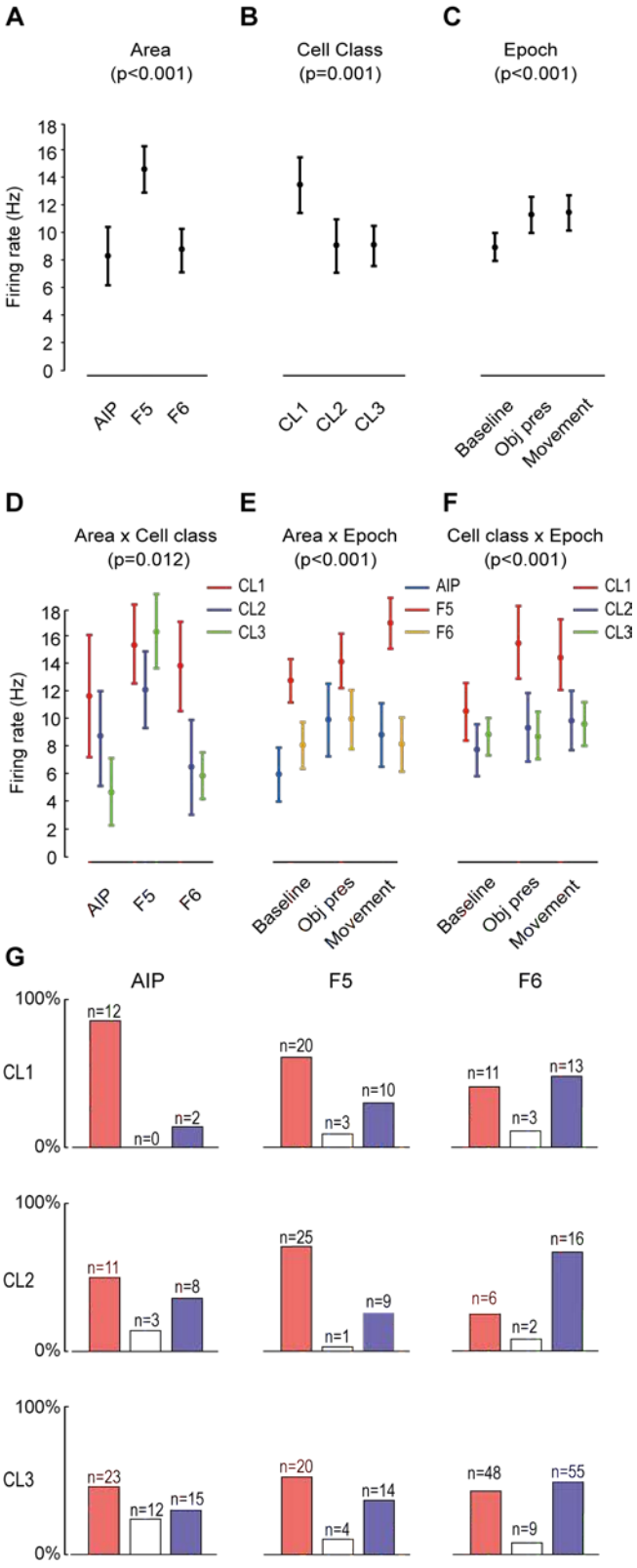

Figure S3.5. Tuning of different cell classes in different areas during EXE. (A) Main effect of Area ($F=15.44$, $df=2$, $p<0.001$) indicates that neurons of area F5 display greater firing rate than those of the other two areas (F5-AIP, $p<0.001$; F5-F6, $p<0.001$), which in turn did not differ from each other ($p=0.64$). **(B)** Main effect of Cell class ($F=6.75$, $df=2$, $p=0.001$) indicates that neurons of cell class 1 have greater firing rate than those of the other two classes (CL1 vs CL2, $p<0.001$; CL1 vs CL3, $p<0.001$), which in turn did not differ from each other ($p=0.18$). **(C)** Main effect of Epoch ($F=17.08$, $df=2$, $p<0.001$) indicates that, relative to baseline, the firing rate is greater during object presentation ($p=0.001$) and movement ($p<0.001$), which in turn did not differ from each other ($p=0.2$). **(D)** Interaction between Cell class and Area ($F=3.26$, $df=4$, $p=0.012$) shows that class 1 neurons exhibit greater firing rate than those of the other two classes in F6 ($p<0.05$ for both comparisons) and of class 3 neurons in AIP ($p=0.026$). Furthermore, neurons in class 3 of F5 has a greater firing rate than class 3 neurons of the other areas ($p<0.001$ for both comparisons), which in turn did not differ from each other ($p=0.57$). **(E)** Interaction between Area and Epoch ($F=8.58$, $df=4$, $p<0.001$) indicates that area F5 neurons discharge stronger than those of the other areas in all epochs, including baseline; their firing rate during movement is higher than during both baseline ($p<0.001$) and object presentation ($p<0.001$), which in turn did not differ from each other ($p=0.07$). AIP neurons significantly increase their firing rate relative to baseline during both object presentation epoch ($p=0.005$) and movement ($p=0.03$), which in turn did not differ from each other. Area F6 neurons did not show any overall modulation of their firing rate across epochs ($p>0.81$ for all comparisons). **(F)** Interaction between Cell class and Epoch ($F=5.27$, $df=4$, $p<0.001$) indicates that during baseline epoch all cell classes exhibit similar firing rates ($p>0.1$ for all comparisons). In contrast, neurons of class 1 showed greater firing rate relative to baseline during object presentation and movement epochs ($p<0.001$ for both comparisons) and greater firing rate relative to neurons in cell class 2 and 3, in all epochs ($p<0.005$ for all comparisons). **(G)** Percentage of facilitated (red), suppressed (blue) and non-significant (white) neurons within areas and cell classes in EXE.

Figure S3.6. Tuning of different cell classes in different areas during OBS. (A) Main effect of Area (F=26.42, df=2, p<0.001) indicates that neurons of area F5 display greater firing rate than those of the other two areas (F5-AIP, p<0.001; F5-F6, p<0.001), which in turn did not differ from each other (p=0.28). **(B)** Main effect of Epoch (F=4.63, df=2, p=0.01) indicates that the firing rate during movement epoch was greater than baseline (p=0.007) and object presentation epoch (p=0.02), which in turn did not differ from each other (p=0.45). **(C)** Interaction between Area and Epoch (F=8.56, df=4, p<0.001) indicates that area F5 neurons discharge stronger than those of the other areas in all epochs, including baseline; their firing rate during movement is higher than during both baseline (p<0.001) and object presentation (p<0.001), which in turn did not differ from each other (p=0.20). Area F6 and AIP neurons did not show any overall modulation of their firing rate across epochs (p>0.28 for all comparisons). **(D)** Interaction between Cell class and Epoch (F=2.44, df=4, p=0.046) indicates that during baseline all cell classes exhibit similar firing rates (p>0.09 for all comparisons). In contrast, neurons of class 1 showed greater firing rate relative to baseline during object presentation and movement epochs (p<0.05 for both comparisons), which in turn did not differ from each other (p=0.27), and neurons of class 2 showed greater firing rate during movement relative to baseline and object presentation (p<0.005), which in turn did not differ from each other (p=0.67). **(E)** Interaction between Cell class and Area (F=3.11, df=4, p=0.015) shows that, in F6, class 1 neurons exhibit greater firing rate than those of the other two classes (p<0.05 for both comparisons), whereas in AIP and F5 no significant difference between cell classes emerge (p>0.20). **(F)** Percentage of facilitated (red), suppressed (blue) and non-significant (white) neurons within areas and cell classes in OBS.

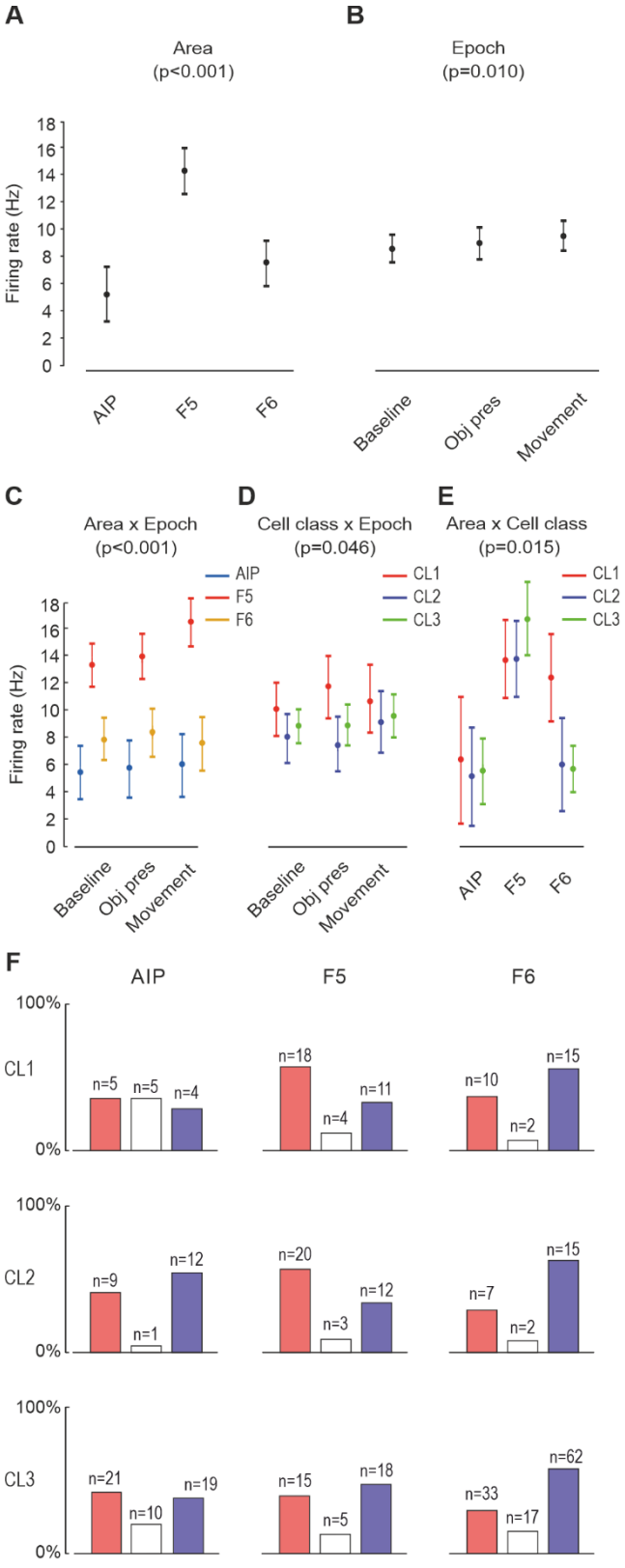

Figure S3.7. Distribution and properties of neurons in each class depending on their modulation in EXE and OBS. (A) Number of neurons with facilitated (F), suppressed (S) or non-significant (NS) response during EXE and OBS, across cell classes. Note that unselective neurons in both EXE and OBS are n = 8. **(B)** Number of F-F, S-S, F-S and S-F neurons across cell classes (the first letter refers to EXE, the second one to OBS). Percentages are relative to the sum of these four paired classes. **(C)** Firing rate maxima across paired classes. Maxima were obtained by taking the firing rate (trial- and object-averaged and smoothed with a 60 ms Gaussian kernel) of each neuron aligned to the object presentation (in the interval -1.3/0.7 s relative to this event) and Go/No-Go signal (in the interval -0.3/1.2 s relative to this event). The absolute maximum in this entire recording period within or across EXE and OBS is shown. **(D)** Number of neurons with average MMD > 0 across paired classed, cell classes and areas. The average was taken within the movement epoch (0/0.7 s after movement onset). **(E)** Number of F-F, S-S and Others neurons subdivided in areas and animals they were recorded from.

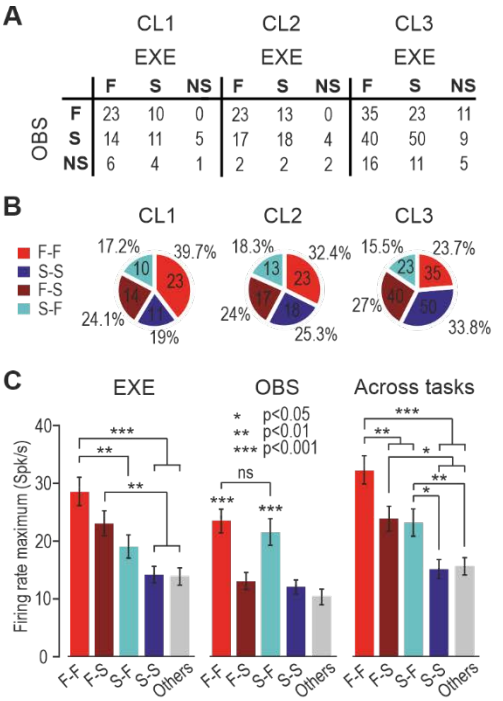

D

	AIP			F5			F6			
	CL1	CL2	CL3	CL1	CL2	CL3	CL1	CL2	CL3	TOT
FF	4	4	7	12	12	5	2	3	9	58
SS	0	3	3	2	2	6	3	7	14	40
TOT AREA	21 (24.4%)			39 (36.8%)			38 (23.3%)			

E

	AIP			F5			F6			
	FF	SS	OTs	FF	SS	OTs	FF	SS	OTs	TOT
Mk1	/	/	/	17	7	28	4	10	20	86
Mk2	3	5	10	19	9	26	19	42	68	201
Mk3	19	6	43	/	/	/	/	/	/	68
TOT AREA	22	11	53	36	16	54	23	52	88	

Appendix references

S1. Constantinidis, C., and Goldman-Rakic, P.S. Correlated Discharges Among Putative Pyramidal Neurons and Interneurons in the Primate Prefrontal Cortex. J. Neurophysiol. **88**, 3487–3497 (2002).

S2. Merchant, H., Naselaris, T., and Georgopoulos, A.P. Dynamic Sculpting of Directional Tuning in the Primate Motor Cortex during Three-Dimensional Reaching. J. Neurosci. **28**, 9164 LP – 9172 (2008).

S3. Barthó, P., Hirase, H., Monconduit, L., Zugaro, M., Harris, K.D., and Buzsáki, G. Characterization of Neocortical Principal Cells and Interneurons by Network Interactions and Extracellular Features. J. Neurophysiol. **92**, 600–608 (2004).

S4. Albertini, D. *et al.* Connectional gradients underlie functional transitions in monkey pre-supplementary motor area. *Prog. Neurobiol.* **184**, 101699 (2020).